NASA-CR-199447

NAGW-4290

Project Number: ME-HJ-9402

P-208

IN-12-CR

GASCAN II PAYLOAD INTEGRATION

A Major Qualifying Project Submitted to the Faculty of Worcester Polytechnic Institute

Department of Mechanical Engineering and the NASA Advanced Space Design Program

in Partial Fulfillment of the Requirements for the Degree of Bachelor of Science.

May 1, 1995

by:

Dennis J. Cody

Allan G. Concepcion

Edward C. Watras III

Approved By:

Prof. Hamid Johari, Advisor

ABSTRACT

This project, conducted in cooperation with the NASA Advanced Space Design Program, is part of an ongoing effort to place an experiment package into space. The goal of this project is to build and test flight ready hardware that can be launched aboard the Space Shuttle. Get Away Special Canister II (GASCan II) consists of three separate experiments. The Ionospheric Properties and Propagation Experiment (IPPE) determines effects of the ionosphere on radio wave propagation. The Micro-gravity Ignition experiment (MGI) tests the effects of combustion in a micro-gravity environment. The Rotation Fluid Flow experiment (RFF) examines fluid behavior under varying levels of gravity. This year the following tasks were completed: Design of the IPPE antenna, X- and J-cell battery boxes, J-cell battery box enclosure, and structural bumpers was completed. Construction of the MGI canisters, MGI mounting brackets, IPPE antenna, and battery boxes was completed. The selection of the RFF's operating fluid and the analysis of the fluid behavior under micro-gravity test conditions were also completed.

EXECUTIVE SUMMARY

GASCan is an acronym for the Get-Away Special Canister program, which is part of NASA's Advanced Space Design program. It was created by NASA to provide universities and industry with a means to conduct experiments in space. A university or company participates in the program by purchasing a canister from NASA. This canister provides five cubic feet of space for the purpose of experiments, the hardware necessary to interface the canister with the space shuttle, a 200 pound weight allowance, and a slot for launch aboard the space shuttle.

The GASCan II is the second GASCan experiment package to be launched by Worcester Polytechnic Institute. It consists of three experiments and an integrated support structure on which the experiments will be mounted. The three experiments are: the Ionospheric Properties and Propagation Experiment (IPPE) which will try to correlate the propagation of radio waves and the electron density in the ionosphere, the Micro-Gravity Ignition experiment (MGI) which will investigate the effects of micro-gravity on the ignition of combustible materials, and the Rotational Fluid Flow Experiment (RFF) which will measure the effect of gravity on the formation of free surface vorticies.

The goals of this year's project were to produce working designs from the conceptual designs for each experiment, and fabricate flight ready hardware from the working designs.

The Ionospheric Properties and Propagation Experiment's main concern from a mechanical standpoint was the completion of an acceptable design for the antenna that is

to be placed outside the GASCan. Safety considerations outlined by NASA have a set of strict guidelines that had to be met to insure the safety of the shuttle and its crew.

This includes the proof by analysis that the resonant frequency of the antenna, classified as a secondary structure, was above 35 Hz. Using IMAGES 3-D, a finite element package, the fundamental resonant frequency of the antenna using the most conservative model was found to be 64.15 Hz. The safety of all of the connections of the antenna also had to be found using a bolted joint analysis. The lowest acceptable Margin of Safety allowed for testing done by analysis is a positive Margin of Safety for an ultimate load case that is 2.0 times greater than the highest expected load. This load case is a fail safe load case, which assumes that the most critical connection has failed. The lowest Margin of Safety for the most extreme load case of any of the connections was found to be 5.9.

The designs for the Micro-gravity Ignition experiment were finalized. From these drawings, the components of the four canisters were manufactured. This included welding the canisters, manufacturing of the canister mounting brackets, manufacturing of the Teflon backplates and thermocouple tree, and re-machining of the canister endplates to allow correct mounting check and purge valves. In addition an analysis of the worst-case scenario, postulated by the 1994 MGI team, was conducted. This worst-case would occur if all the power from the packages batter supply was routed to one canister and did not shut off. Pressures of 4.75 atm and temperatures of up to 600 K could be expected. Positive margins of safety were noted, and the current design is considered safe. Also, conducted was a fail-safe bolt analysis under this worst case scenario. The MGI

experiment is completed. What remains is purchase of the infrared heat lamps, pressure transducers, heat flux gauge and holding block, and aluminum oxide ceramic plates.

The Rotational Fluid Flow's concerns were about the performance of the experiment. Silicon oil was chosen as the operating fluid. It demonstrates almost all of the desirable physical traits, except that it has a low flashpoint. This problem can be addressed by filling the vortex chamber with an inert gas. The flowrates and vortex behavior were estimated, a fluid filling procedure was developed, and the effects of Coriolis acceleration were investigated. A mirror assembly was designed to give the camera the best view of the vortex chamber in the limited space available. However the image will be distorted due to the viewing angle.

Several advances were made toward the completion of the Integrated Support Structure. The tri-wall structure was stripped of its old welds and was re-welded by a certified welder, as NASA requires. Design and manufacturing of the x-and j-cell battery boxes was completed. Design of the battery enclosure and lateral bumpers was completed, however, these parts must still be manufactured. Analysis of the ISS mounting brackets was conducted using the ANSYS finite element package. Under a fail-safe ultimate case of 40gs the legs will have a margin of safety of 2.1. In addition, bolt analyses of each battery box and the lateral bumpers was completed. Manufacturing of the ISS mounting brackets must still be completed.

This year's team accomplished the design of the x- and j- cell battery boxes, the IPPE antenna and baseplate, the mirror assembly, the battery enclosure, and the lateral bumpers. This year's team also fabricated the x and j cell battery boxes, the IPPE

antenna and baseplate, the MGI canisters, the MGI mounting brackets, and the tri-wall welding.

The experimental hardware for the IPPE antenna and MGI experiments is complete from the mechanical standpoint. The only thing that is required is integration with the electrical hardware for these experiments. The working fluid for the rotational fluid flow experiment has been chosen, and the performance envelope has been plotted. The tri-wall structure for the integrated support structure has been rewelded and the X and J cell battery boxes have been made.

The remaining work consists of the fabrication of remaining parts, the mounting of the components on the integrated support structure, integrating the experiments with the data collection hardware, and testing to prove that the hardware is flight ready.

ACKNOWLEDGMENTS

AUTHORSHIP

All three authors participated in the research, writing and editing of the material contained in this project. Principle authors for each section are listed below.

- Background

IPPE:	Dennis Cody
MGI:	Edward Watras
RFF:	Allan Concepcion

- Design and Implementation

IPPE:	Dennis Cody
MGI:	Edward Watras
RFF:	Allan Concepcion
ISS:	Edward Watras

- Appendices

Written by author to which the material pertains.

Nomenclature

MGI-	Micro-gravity Ignition
RFF-	Rotational Fluid Flow
ISS-	Integrated Support Structure
IPPE-	Ionospheric Properties and Propagation Experiment
UNC-	Unified National Course Thread
UNF-	Unified National Fine Thread
NPS-	National Pipe Straight Thread
NPT-	National Pipe Tapered Thread

TABLE OF CONTENTS

LIST OF FIGURES

LIST OF TABLES

Introduction

GASCan is an acronym for the Get-Away Special Canister program, which is part of NASA's Advanced Space Design program. It was created by NASA to provide universities and industry with a means to conduct experiments in space. A university or company participates in the program by purchasing a canister from NASA. This canister provides five cubic feet of space for the purpose of experiments, the hardware necessary to interface the canister with the space shuttle, a 200 pound weight allowance, and a slot for launch aboard the space shuttle.

The GASCan II is the second GASCan experiment package to be launched by Worcester Polytechnic Institute. It consists of three experiments and an integrated support structure on which the experiments will be mounted. The three experiments are: the Ionospheric Properties and Propagation Experiment (IPPE), the Micro-Gravity Ignition experiment (MGI), and the Rotational Fluid Flow Experiment (RFF).

The goals of this year's project were to produce working designs from the conceptual designs for each experiment, and fabricate flight ready hardware from the working designs.

2.0 BACKGROUND

2.1 IPPE

The purpose of the Ionospheric Properties and Propagation Experiment is to study ionospheric ducting, which is when a radio wave propagating through the atmosphere is trapped between two layers of high electron concentration. The ionospheric ducting to be studied by IPPE was to be done by measuring the propagation of radio waves with an antenna and the electron density with an ion density probe (Coolidge and Daigle, 1992). The antenna measures radio waves propagating from frequencies of 11.00MHz and 14.67MHz broadcast from Beijing, China and Ottawa, Canada, respectively (Kyaw and Wu, 1993).   The electron density probe was to measure the potential difference across the two surfaces of the probes and measuring the current in order to determine the concentration of ions in the immediate area of the probe. Both the antenna and the probe were to measure radio waves and the electron density of electrons in the F2 region of the ionosphere. However, it has been realized that NASA will not allow the Electrostatic Analyzer (ESA) Probe on the shuttle payload. It has been resolved that data on the strength of radio waves will be correlated with data on the strength of ions in the ionosphere from a NOAA (National Oceanic and Atmospheric Administration) satellite.

2.2   Micro-gravity Ignition Experiment (MGI)

This section concentrates on explanation of experiment apparatus, procedure and significance. It contains references to previous MQPs, citing information necessary for testing and completion of each experiment.

Motivation

The MGI experiment is of great scientific value. Presently, there is little conclusive data of the effect of micro-gravity on ignition. Ignition is affected by micro-gravity due to the lack of convection currents in space. This will have two possible effects on ignition. The first is the speeding up of the ignition process. The lack of convection currents causes a cloud of heated air and pyrolysis products to form around the specimen, increasing the specimen temperature and decreasing ignition time. The second effect is the possible smothering of the specimen, eliminating the possibility of ignition. This is because the convection currents that would normally provide the specimen with oxygen-rich air are no longer present. The MGI experiment seeks to define the process of ignition in a 0-g environment and compare it with earth based ignition information.

2.2.1   Experiment Layout and Procedure

The MGI experiment consists of four canisters. The first canister is a control chamber containing an Argus Model 44 Infrared heat lamp with gold plated reflector and quartz window, and Medtherm Corp. gardon gauge heat flux transducer (absorptivity =

.92). This canister is run first and last in the experiment timeline to establish initial and final levels of lamp output. The remaining three canisters are identical, containing the paper samples and measuring equipment. These canisters each contain: the Argus heat lamp, reflector and quartz window, a stainless steel SS-4C-VCR-10 Nupro "C" series check valve (nominal cracking pressure 10 psi), a SS-4P-4M Nupro "P" series purge valve, a miniature pressure transducer, a Teflon back plate to which is attached the ion sensor and thermocouple tree, a 12-pin Omega sealed electrical pass-through, and appropriate thermocouples (Omega K-type, Teflon insulated, shielded chromel-alumel thermocouples with gold plated connector pins).

The chambers themselves are constructed from 6061 - T6 aluminum and are nearly identical in construction. A chamber consists of a top plate and top middle plate which hold the Argus lamp in place. The top middle plate is fillet welded to the canister which is an aluminum cylinder. The top plate is secured via a nut and bolt fastener to the top middle plate. A bottom middle plate is fillet welded to the bottom the cylinder. The bottom plate is fastened to the bottom middle plate in the same manner as the top plate is attached to the top middle plate. The bottom plate has threaded holes machined in it to allow for the check and purge valves, the pressure transducer and electrical pass-through. In addition, the Teflon back plate and thermocouple tree assembly are attached to the bottom plate. All chambers are designed to be airtight and contain dry air at atmospheric pressure.

The experiment sequence is as follows: 3-10 hours after launch the experiment will be powered up. The MGI is the first experiment run in the GASCan II. The control

canister will be run for five seconds during which lamp, battery voltage, and current will be measured. After a five second battery recovery period, the second canister will be powered up. The lamp will run for 30 seconds or until ignition of the α - cellulose paper sample is detected. If ignition is detected, the lamp will shut off and the computer will sample data for the full thirty seconds. Next, there is again a five second battery recovery period. The third and fourth canisters proceed in the same fashion as the second canister. Finally, the control canister is run again to determine any changes that may appear in lamp output, battery voltage or current.

2.2.2 Critical Experiment Information and Areas of Concern

The following sections discuss areas of concern in the final construction of the MGI.

Ion Sensor

Listed here are the current specifications for the ion sensor:

- Threshold voltage = 0.0244V.

- Equidistant spacing (1/8") between wires - stainless steel

- Height of wires above the sample - (1mm) was found effective

Some of the present concerns regarding the ion sensor are now discussed:

The ion sensor fastenings were found to be susceptible to vibrations by the 1991 MGI team (Maranghides, et al, 1991). This problem was not addressed by the 1994-1995

integration team. Vibration testing equipment was dismantled during the Higgins Labs renovations. However, use of a chemical application such as "Liquid Nut" should keep ion sensor screws in place under vibration.

In addition, Mitre has concerns that pyrolysis may become a more important factor in low-g conditions and prematurely shut off the lamp. A second concern is that the lamp may remain on longer than necessary if combustion products do not reach the ion sensor soon enough. Alternate solutions to detection include use of the back plate thermocouple. Because it is in contact with the sample, it registers a spike at the time of ignition. A second alternative is the use of the pressure transducer. The ignition is marked by the formation of a pressure wave. This in conjunction with the back plate thermocouple could provide an adequate means of measuring the time of ignition. This option is further discussed in the design section of the report.

Despite Mitre's concern, Belliveau and Chase (1994) claimed the ion sensor is working properly and there is no need to examine secondary ignition detectors. These issues need to be investigated now that fabrication of the MGI canisters and experiment apparatus has been completed.

Teflon Back plate

The Teflon back plate has slit cut below the ion sensor so the paper sample may be replaced easily. An aluminum oxide ceramic plate is located below the paper sample (Teflon cannot withstand the necessary temperatures in the canister). One of the principle reasons for this choice of material is its insulating properties. The ceramic

plate is secured with Omegabond 100 epoxy. A thermocouple is located through center of plate for use in measuring sample temperature. The Teflon back plates (quantity = 4) were manufactured by Steve Derosier for the 1994-1995 Payload Integration Team.

Paper Sample Thermocouple

The paper sample's thermocouple needs to achieve a consistent means of contact with the sample. Smaller diameter wire with precision welded joints should be examined during the final test phase of the MGI.

Lamp Alignment Apparatus

In order to determine the focal point of maximum heat intensity, an aligning apparatus was designed by the 1991 project team (Maranghides, et al, p. 7 -29). The alignment procedure is carefully outlined in this document and the results of several test alignments have been provided. Possession of the alignment stand has been verified and cataloged by the 1994-95 Payload Integration Team. The 1991 project team found that the height of the α - cellulose paper sample in the container was critical. Raising or lowering the sample as little as 1mm could change ignition by as much as 1.5 seconds (in the 6.75-7.15 cm distance from the quartz window). In addition, finding the distance from the lamp to the point of maximum heat flux could conserve battery power. Procedures for lamp alignment, focal length testing, as well as other procedures and troubleshooting guidelines, are given in the Appendices of Maranghides' report.

The 1993 MGI team (Parker, pp. 14-15) also gives a similar procedure for lamp alignment (See also 1994, Belliveau et al, pp. 14-15). Heat flux testing is completed in the 1994 Belliveau and Chase MQP (pp. 43 - 46) and was determined to be approximately 104 kW / m^2. These issues may have to be considered in the final baseline tests of the MGI and the completion of the ISS.

Paper Drying Process and Ground Testing

Moisture in the α - cellulose paper was found to significantly effect ignition time. The drying procedure and storage of dried samples is outlined in the 1994 MGI MQP (Belliveau, et al, pp. 63-66). Also included here is the procedure for conducting the experiment and running a computer test (See Belliveau et al, 1994, pp. 15 - 17). In addition, Belliveau and Chase provide extensive baseline testing results. (see pp. 47 - 59)

Low Temperature Testing

The 1991 MGI team (Maranghides, et al) ran low temperature tests on the experiment. After freezing the equipment at -13^0 C $\pm$ 1^0 C for five hours, it was found that ignition time had increased significantly from 13 $\pm$ .2 seconds to as much as 19.6 seconds. It was also decided that new microcontroller should allow for low temperature data acquisition i.e. it should be able to sample in the negative temperature range.

The 1992 MGI team (Garrant, Lusk, pp. 35-36) came up with a low temperature testing procedure. (See also Parker, 1993 p. 15, for low temperature testing procedure.)

Pressure Transducer

The Entran EPX pressure transducer chosen by the 1994 MGI team does not work below 0^0 C. The 1994-95 Payload Integration Team investigated alternate pressure transducers. It was determined that Barocel Capacitance Manometers would provide pressure measurement that was relatively independent of temperature (as the dielectric constant of the transducer material would have to be changed for erroneous readings.) The MGI design section contains more information on this subject.

Vibration Testing

The 1992 MGI team (Garrant, Lusk, p. 37) developed a procedure for vibration testing of the MGI experiment. (See also Parker, 1993, pp. 15 - 16, for vibration testing procedure.) Areas of concern during the vibration testing will be the thermocouple tree and ion sensor fastenings.

Worst Case Scenario Testing and Power requirements

Calculation of power requirements was done in the Belliveau and Chase's 1994 MQP. In particular, a worst case scenario, in which all the battery power is dumped into one canister and not shut off, is analyzed. According to this analysis, a final temperature of 600 K and pressure of 4.75 atm can be expected. Actual testing of pressure requirements must be completed. The chamber will be able to withstand this temperature as the melting point of Aluminum is between 749-933 K. A hand analysis of the canister under the worst case scenario is included in the MGI design section.

Preflight Testing

The 1992 MGI team (Garrant, Lusk, pp. 33-34) developed a pre-flight procedure for the MGI experiment. Work needs to be done in refining this procedure and a new method of cleaning the lamp reflector should be developed because the current method causes excessive wear of the reflective material.

2.3 RFF

Previous Work

Barry et al(1992) performed experiments to determine the optimum viscosity of the working fluid. The group chose a viscosity of 1.1 centistokes, or in english units, 1.2 ft^2/s because it would provide the greatest range of vortex behavior over the proposed operating range. They also established a preliminary test protocol for the experimental hardware, and selected and purchased two small pumps to circulate the working fluid.

Lelani et al(1992). formulated a mathematical model of a Rankine combined vortex. First, they mathematically modeled a free vortex. After that they modeled a forced vortex. They then combined the two models to simulate the Rankine combined vortex. To apply this model to the RFF experiment, they created a computer program to calculate the tilt that would be caused by Coriolis effects.

Cyr et al(1993) determined the vibrational modes of the RFF experiment to ensure that they were not low enough to pose a threat to the space shuttle. They developed the final test protocol for the experimental hardware. Silicon oil was chosen as the working fluid due to its physical properties, however, a Mitre design review raised the concern that the flashpoint was too low. They tried to develop the experiment operating range however they chose the wrong characteristic length for use in the Reynolds and Froude numbers. They also decided to pass over the still camera in favor of mounting a video camera on the rotational platform.

Belog (1994) revised the experiment timeline to reflect changes in equipment, flowrates and theory. He reviewed the pump selection and chose the smaller pump over

the larger because it was sufficient for the experimental envelope, and did not weigh as much. He also developed a pump performance envelope which was based on theory and not experimental data. Finally he calculated the slip ring transfer power.

Smith (1994) completed a thesis on the direct measurement of circulation in free surface vorticies. He used an experimental setup that was dynamically similar to that used by the Rotational Fluid Flow experiment. The only difference between Smith's experiment and the rotational fluid flow experiment was the larger geometry of Smith's vortex chamber, and the fact that gravity was limited to 32.17 ft/s^2. By collecting ground based data on vortex formation at one gravity, he established a database of information that could be used to estimate the behavior of the experiment in space.

Rotational Fluid Flow Experimental Concept

For many fluid mechanic phenomena, there is a dependence on multiple scaling parameters. For a vortex there are three governing parameters. These three parameters have customarily been arranged as the Reynolds number representing the dependence on viscous forces, the Froude Number representing the dependence on gravitational forces, and the Weber number representing the dependence on surface tension forces.

When attempts are made to scale up vortex flow in laboratory models to prototype dimensions, problems are encountered. When models are used to study a certain configuration, the results are valid only if there is geometric, kinematic, and dynamic similitude. Geometric similarity implies that the model and the prototype have the same shape, so that the linear relationship between the model and the prototype are

17

related by a constant scale factor. Kinematic similarity requires the velocities between the prototype and the scale model be related by a constant scale factor. Dynamic similarity requires that the forces be related in the same way

Because the Reynolds number has a nonlinear relationship to the Froude number, the only way to maintain the dynamic similitude between the model and the prototype is to vary the gravity inversely with the diameter of the vortex chamber. While this is impossible on earth, it can be achieved in the micro-gravity conditions of space.

EXPERIMENTAL APPARATUS

The objective of this experiment was to create vorticies under varying gravity levels for different flowrates. Data would be gathered on how these vorticies formed under the varying conditions, and from the analysis of this data, the effect of the Froude number vs. the Reynolds number and the Weber number could determined.

The experimental hardware consists of a vortex chamber, a video camera, a pump, a motor, a mirror assembly, various controllers, an ultrasonic flowmeter and a master central processing unit. All of these components are mounted on a rotating platform which will be rotated to induce different gravity levels. The mechanical hardware can be divided into three major groups, the vortex generation system, the data collection system, and the rotating platform system.

Vortex Generation System

The vortex generation system consists of the vortex chamber, the pump system, and the aluminum tubing. The vortex chamber consists of two pieces of cylindrical Lucite, a cap, a base, and a transducer mount located about one third of the way from the

bottom of the cylinder. The base has two holes, both for filling the experiment with the working fluid before launch. The vortex chamber will be mounted on the rotating platform horizontally with the cap at the center of the platform and the base at the edge. The pump circulates fluid from the bottom of the chamber and injects it tangentially to the flow at the top of the chamber. Tangential injection creates a circular flow field in the chamber. At a certain circulation that flow creates a vortex.

Rotating platform system

The rotating platform consists of a hollow cylinder with two plates mounted on either end. within the hollow cylinder is an axle, about which, the platform spins. on the axle, are also mounted slip rings from which the platform can draw power from the battery boxes mounted upon the integrated support structure. An electric motor is used to rotate the platform by means of a rubber belt, which transfers mechanical power from the motor to the platform. This electric motor is equipped with an optical encoder which determines the rotational speed of the platform.

Data Collection System

The data collection system consists of eight components, the video camera, the camera box, the camera controller, the ultrasonic transducers, the ultrasonic flowmeter, the mirror assembly, the lamp, and the RFF CPU.

The video camera is a Sony handycam, and it will be secured in the camera box. The camera box will be connected to the camera controller by means of a hermetic connector. The camera controller, the RFF CPU and the ultrasonic flowmeter will be mounted on the rotating platform placed out of the view of the camera. The ultrasonic

transducers will be mounted on the vortex chamber. The mirror assembly will be

mounted on the rotating platform at an angle to give the camera a full field of view of the

vortex chamber, and the lamp will be placed behind the vortex chamber to give sufficient

illumination for the camera to record the formation of the vortex.

3.0 Design and Implementation

The design and implementation section focuses on the major accomplishments of this project. This includes analysis, design and manufacturing of major experiment components. It is broken down into sections containing accomplishments in each experiment and the integrated support structure (ISS).

3.1 IONOSPHERIC PROPERTIES AND PROPAGATION

EXPERIMENT

3.1.1 Vibration of Antenna

The critical dimensions from the electrical side of the antenna are the projecting

area of the cap and the distance between the ground plane and the bottom of the antenna

cap (Labonte). For the antenna assembly, the ground plane is the flat antenna base plate,

as can be seen in Figure 1. This has been confirmed by the 1994 IPPE MQP. Using

these specifications, an antenna with a thicker supporting rod was modeled. It was found

that increasing the area of the rod will increase the necessary area of the antenna cap,

since the rod blocks the projection area of the cap. However, through calculations, it was

found that the necessary change in diameter of the cap would be from 4.0 in to 4.0485 in.

The loss of area due to the size of the rod was found to be negligible.

NASA has strict safety standards on any structures placed outside a GAS

Canister. One of the important considerations is the vibration of the structure. NASA

requires that the fundamental frequency of a structure be above 35 Hz. (Peden, 1993).

Doing a modal finite element analysis on Images to find the frequencies, it was found

that the lowest natural frequency of vibration for the antenna increased from about 53 Hz

to 77 Hz when the diameter of the antenna rod was changed from 0.5 inches to 0.625

inches.

As well as modify the thickness of the supporting rod, the thickness of the

antenna cap was also modified on IMAGES 3-D Finite Element software to find the

changes in resonant frequency for different plate thickness'. The resonant frequency for the lowest mode shape is shown in Table 1 below for different antenna dimensions:

Table 1: *Change in frequency for different dimensions*

Cap thick. (in)	Rod Diameter (in)	Antenna Height (in)	Resonance (Hz)
.0625	0.5	12.5	53.51
.0625	0.625	12.5	77.12
.03125	0.5	12.5	60.73
0.1	0.5	12.5	46.84

The final dimensions of the antenna parts can be found in Appendix F. Although the antenna with a plate thickness of 1/32 of an inch will create a relatively high frequency of 60 Hz, this part would be extremely difficult to manufacture and would be more likely to fracture than the thicker plates. The antenna with a base rod of 5/8 (0.625) inches will increase the stiffness of the rod and therefore the resonant frequency. Since the mode shape of the lowest resonance involves vibration of the antenna rod and not the cap, it makes sense that the dimensions of the rod will have a larger effect on the frequency than the thickness of the plate. The adjustment of plate thickness will only affect the resonant frequency through the change in mass at the end of the rod. These effects can be seen through the equation:

$$\omega = \sqrt{\frac{k}{m}} \qquad \text{Eq. (1)}$$

The antenna has been modeled on IMAGES 3-D finite element software. A wireframe plot of the actual antenna is shown in Fig. 1. Three different models were

Figure 1
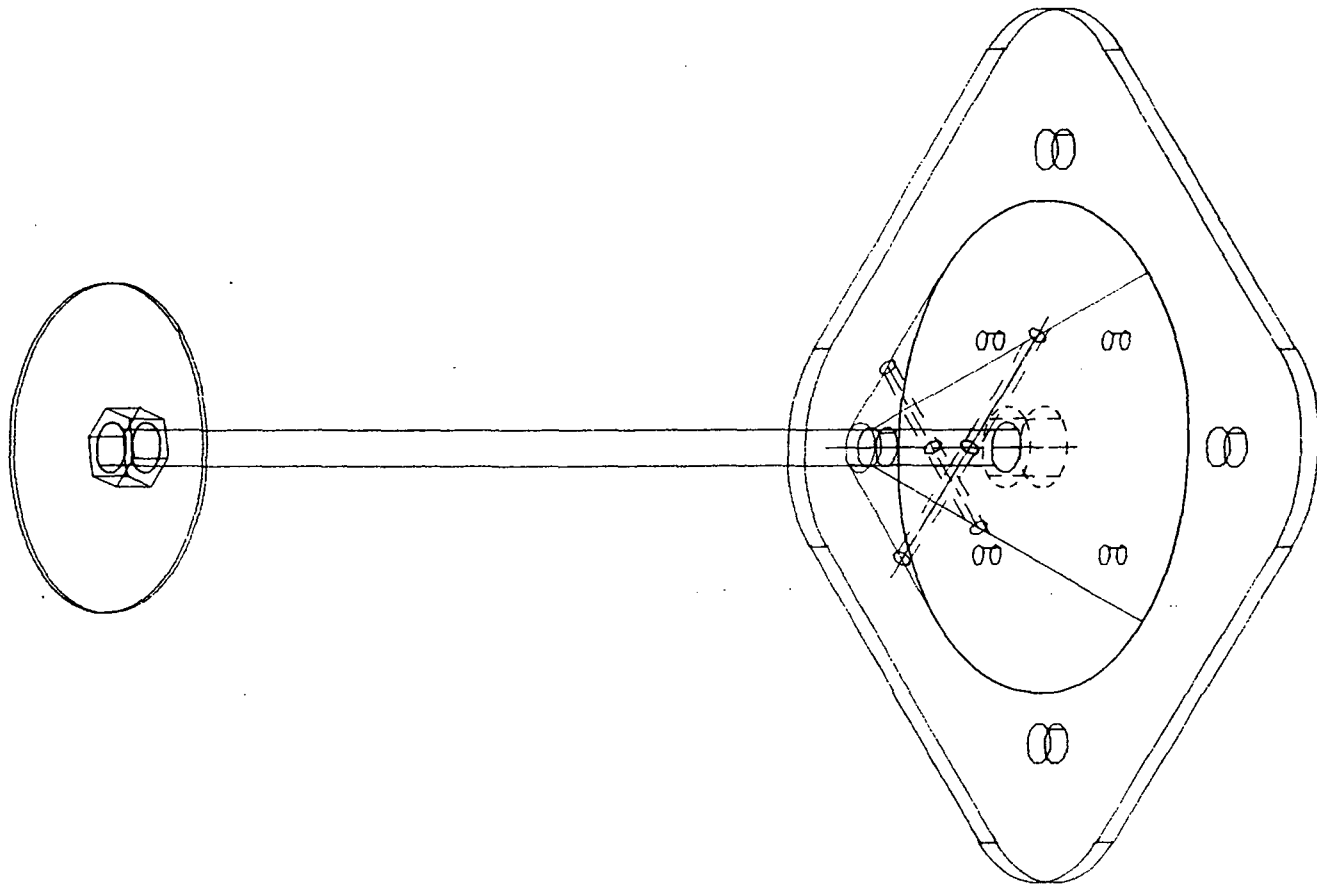
Figure 1: Wireframe plot of antenna (anten.prt)

created to verify the validity of the antenna model. Each version of the antenna includes the Delrin conical base, AMS 5644 stainless steel (17-7ph) rod and antenna cap. Figure 2 shows Version 1, which includes four screws fixed underneath the base that screw into the cone. Version 2, shown in Fig. 3, has included the 0.25 inch thick, 6 inch by 6 inch aluminum base plate underneath the cone to which the screws that go into the cone are fastened. The plate is fixed along the edges, but the rest of the antenna is attached to the cone. Fig. 4 depicts Version 3, which replaces the plate of Version 2 with an 8.5 x 8.5 inch plate that is fastened by four 0.5 inch diameter bolts to the GASCan lid. The GASCan lid is an aluminum plate 20 inches in diameter and 0.625 inches thick. The more conservative approach of adding more detail to the model causes the natural frequency to decrease, but it is still well above the 35 Hz recommended by NASA in the "Gas Experimenter's Guide to the STS Safety Review Process and Data Package Preparation" document (Peden, 1993). The document states "The fundamental frequency of the experiment support structure about any axis must be greater than or equal to 35 Hz. This can be verified by analysis or test."

The IMAGES software has been unable to solve for more than three modal frequencies despite the creation of 604 kilobytes of conventional memory for running the program the program requires 590 kilobytes to insure proper operation. However, the results obtained from IMAGES on the most recent model are consistent with the less complex models made of the antenna. A table of the results for three different models are shown in Table 2. An explanation of how each of the IMAGES 3-D models were created is shown in Appendix A.

```
IMAGES-3D
VER.  2.0
Mode      1
S= 3.000E+00
 6.862E+01 Hz
```

Mode Shape:
Bending of rod
about Y-axis.

Distortion Scale:
3.0

Frequency:
68.62 Hz.

Z

Y

X
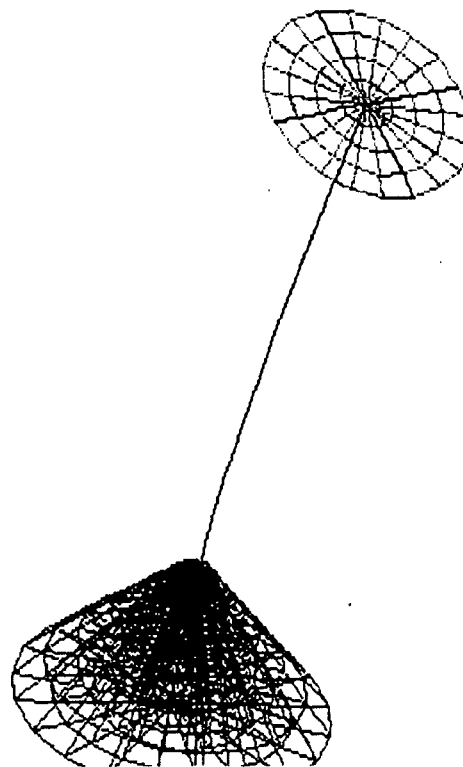
Figure 2: *First mode shape: Antenna with fixed screws.*

(

IMAGES-3D
VER. 2.0
Mode   1
S= 3.000E+00
  6.812E+01 Hz

Mode Shape:
Bending of shaft
about Y-axis.

Distortion Scale:
3.0

Frequency:
68.12 Hz.

Z

Y

X
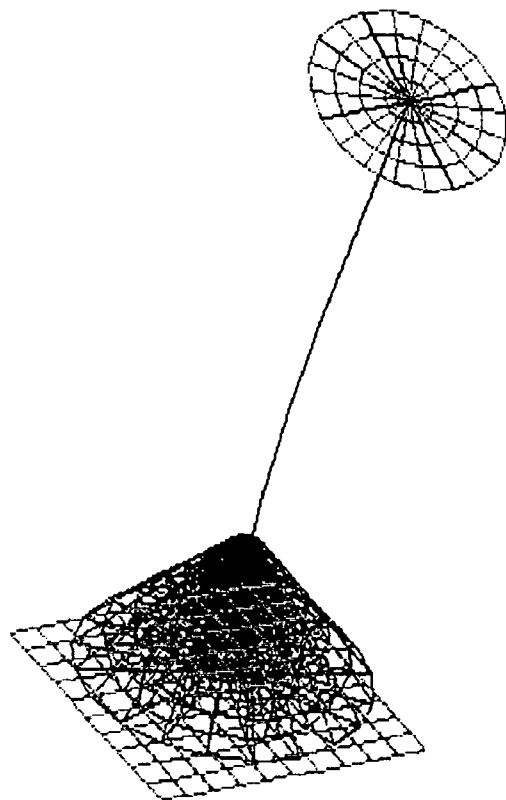
Figure 3:   *First mode shape: Antenna with Aluminum baseplate*

IMAGES-3D
VER. 2.0
Mode   1
S= 3.000E+00
  6.415E+01 Hz

Mode Shape:
 Bending of shaft
 about X-axis.

Distortion Scale:
3.0

Frequency:
64.15 Hz.

Z

Y

X
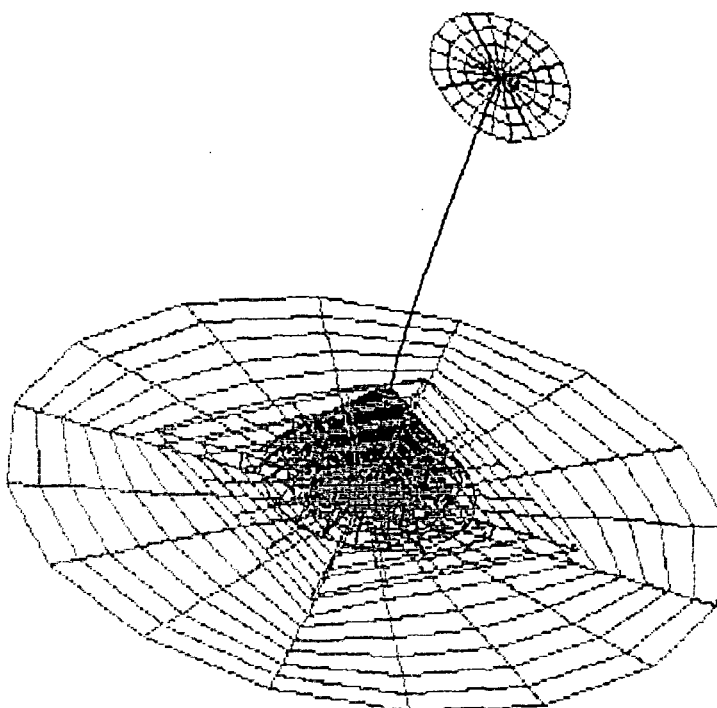
Figure 4: *First mode shape: Antenna with GASCan lid*

Table 2: *Resonant frequency of antenna*

Mode #	Vers 1 (Hz)	Eigenvalue $(rad/s)^2$	Vers 2 (Hz)	Eigenvalue $(rad/s)^2$	Vers 3 (Hz)	Eigenvalue $(rad/s)^2$	Mode shape
1	68.62	185903	68.12	183201	64.15	162466	shaft bending
2	70.63	196917	70.29	195078	65.96	171757	shaft bending
3	186.5	1373280	186.5	1373280	186.5	1373280	cap, longitudinal
4	381.7	5752620	341.9	4613940			cap, rod bending
5	383.1	5792770	342.8	4640230			cap, rod bending

The complete printouts from IMAGES showing the mode shapes and the frequencies for a given setup are shown in Appendix B. Figs. 2-4 show the lowest resonant frequency and mode shape for the three different models of the antenna. The booklet "Simplified Design Options for STS Payloads" (Hamilton, p. 10, 1985) states that the lowest frequency allowed for a secondary structure is 6 Hz. Mark Peden of NASA - Goddard was consulted on the matter of the lowest allowable frequency, and he cited Appendix B of the "Gas Experimenter's Guide to the STS Safety Review Process and Data Package Preparation" document (Peden, 1993) which states that the lowest resonant frequency allowed for a structure is 35 Hz. This requirement is for a "structure", which is not specified as primary or secondary. A secondary structure is a structure that is attached to but separate from the primary structure of the STS (Space Transport System) Payload. The primary structure in this case is the GASCan and the secondary structure is the antenna. Therefore, it is safest to assume that the value of 35

Hz, the higher of the two frequencies, and also the value from the most recently published article, should be used.

3.1.2 Modification of Canister Lid

Modification of a GAS canister lid is highly irregular. This has caused the necessity of a lot of special considerations that are important to this particular canister. There will need to be a hole drilled through the canister to allow the wire to be attached to the antenna from the IPPE CPU. There will also need to be four tapped holes that will go 1/3 of the way through the canister lid. The tapped holes will support the antenna structure, but will not go through the canister lid in order to allow the payload to be sealed. Since the GASCan lid needs to be modified, it will have to be purchased from NASA. The modifications that are done to the lid need to be done either by NASA or a contractor hired by NASA. The cost of the lid and the modification is estimated to be between $3,000 and $5,000. If there will be an IPPE experiment on GASCan II, this is an unavoidable expense. The only other possibility was to use one of the three previous modified GASCan lids held by NASA. However, two of the lids are going to be used again, and the other one is in the possession of the experimenter. It would be more expensive for NASA to inspect that lid again than to allow WPI to purchase and modify a new lid.

3.1.3 Placement of Antenna

It is impossible to place the antenna at a random spot on the mounting plate because consideration has to be made for the purge ports and the battery box vent plumbing circle. The holes drilled for the mounting of the base-plate to the GASCan

mounting plate should not line up with the holes drilled underneath the GASCan for the purpose of attaching the support structure to the lid. A diagram of the placement of holes on the GASCan lid and the placement of the antenna base is shown in Fig. 5. The antenna is offset from the center of the lid at a distance of 4.5 inches and an angle of - 45°. This way, the antenna base does not cover up either of the two purge ports or the battery box plumbing circle. Although not all of the plumbing circle needs to be uncovered, this placement insures the absence of problems. The holes that are going to be drilled into the GASCan lid to attach the antenna base also had to make sure that they didn't line up with any of the holes drilled underneath the canister that go half-way through the bottom of the lid. An outline of the standard GASCan lid and specifications is given in the "Get-Away Special Experimenter Handbook" (p. 15). This diagram assumes the use of a standard mounting plate that will be modified by the WPI GASCan II integration team. If use of a previously modified cap is allowed, then the placement of the antenna will have to be modified, as well ass the antenna base-plate, which has already had holes drilled for the existing design. However, this does not seem likely, as Charlie Knapp from NASA-Goddard has researched the other modified lids with no success.
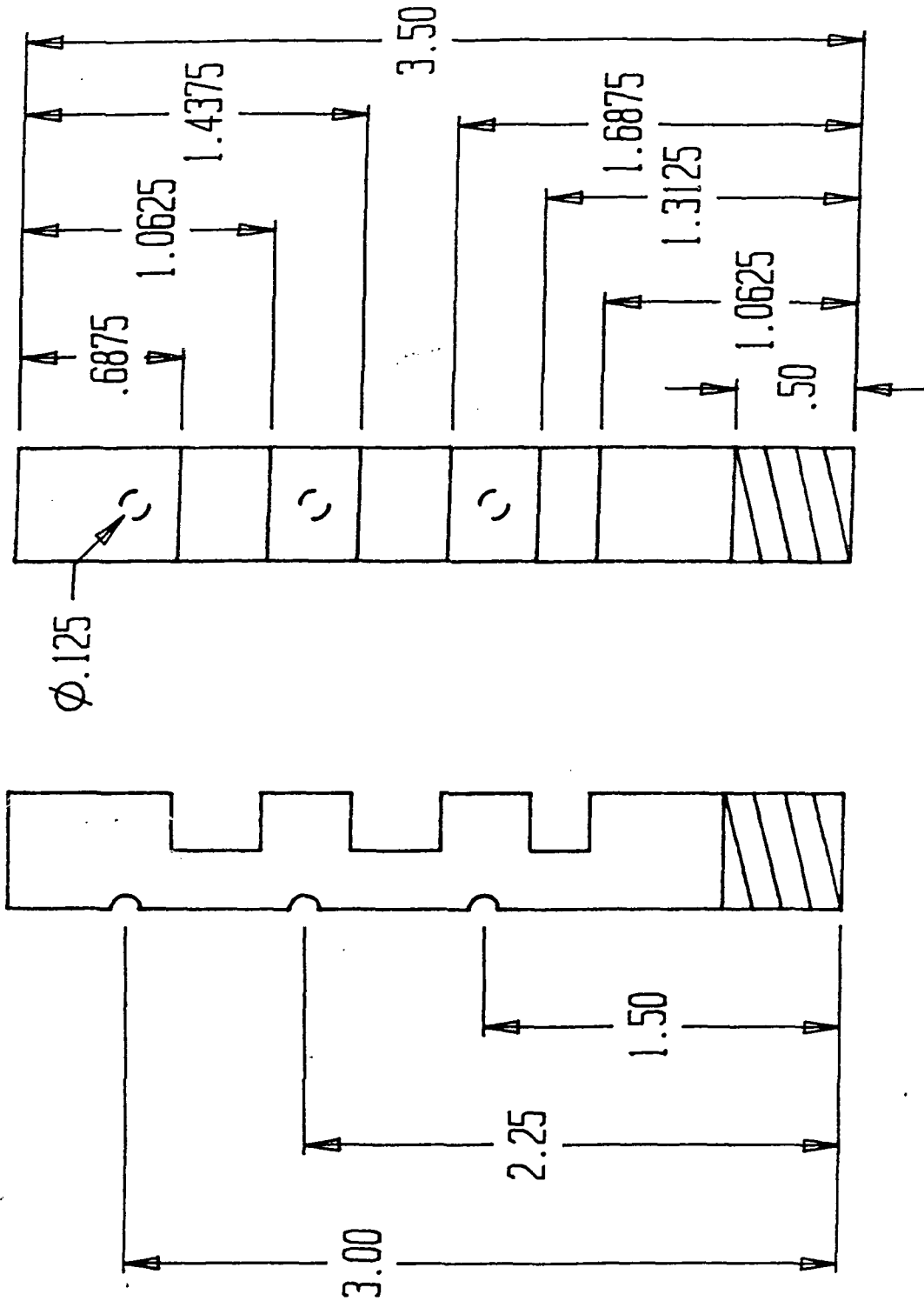
Figure 12 - Thermocouple Tree

32
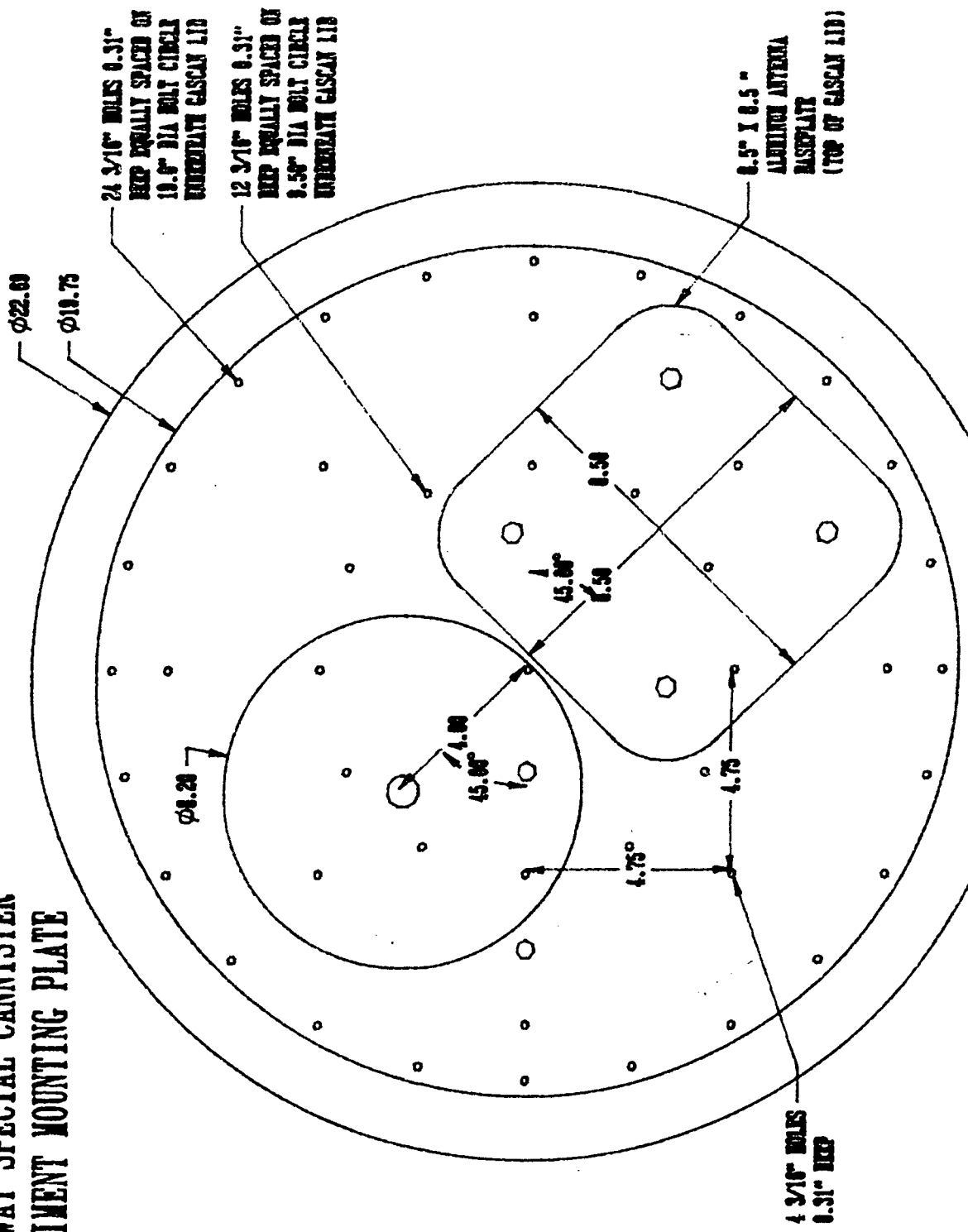
Figure 5: GAScan mounting plate with placement of antenna (gasmount.prt)

3.1.4 Structural Considerations

Any structure outside of the GASCan must be classified as a structure (Gallaway, 1994). Using a weld to restrain the antenna cap will be acceptable as long as the restrained mass, the antenna cap, weighs less than 0.25 lb., the maximum weight for a material specified as a low-released mass (Cooper, 1988). Also, the ratio of plane strain fracture toughness (K_{IC}) to the ultimate tensile strength ($F_{tu} = 170 \times 10^3$ psi) must be less than 0.33/in if the part is pre-loaded in tension (Cooper, 1988, p. 13). Since the antenna cap will not be pre-loaded, the cap can be defined as a low-released mass. This low released mass must also show that "the release of this component will not cause any catastrophic hazard to the STS [Space Transportation System] as a result of subsequent damage to the payload." (p. 13). Since the antenna cap does not have any sharp edges and is not pre-loaded, it meets the requirement of not posing a threat to the Space Transportation System or its crew. The other test that the antenna must be able to withstand is resistance to stress corrosion cracking (p. 30). The material chosen is 17-7ph stainless steel, which is listed in the "Design Criteria for Controlling Stress Corrosion Cracking" handbook as having a high resistance to stress corrosion cracking (Franklin, 1987). Since the part meets all of the requirements of a low-released mass, the part can be classified as non-fracture critical when a Hazard Report is approved by the STS Safety Review Panel.

The antenna assembly itself will need to pass the requirements of a fail safe connection. A fail-safe part is one that meets the following requirements: "(a) it can be

shown by analysis or test that, due to structural redundancy, the structure remaining after failure can withstand the redistributed limit loads; and (b) the failure of the component will not result in the escape from the payload any fragment that violates the requirements of [Low-Released Mass]." (Cooper, 1988). Part (b) of the consideration is satisfied due to the fact that the antenna will be classified as a secondary structure. The analysis to satisfy requirement (a) is provided in the next section.

3.1.5 Stress Analysis

In order to verify the soundness of the antenna structure, a static analysis was done on critical areas of the antenna structure. The analysis completed on the antenna was a margin of safety analysis. In order to determine how the antenna is to be analyzed, the antenna must first be classified as a primary or secondary structure. Since the antenna is on the outside of the canister, it is classified as a secondary structure. This has been verified by Mark Peden at NASA (2/22/95). The design limit load factors for secondary components are given in "Simplified Design options for STS Payloads" as a 40 g load in the most critical direction and 10 g load in each of the remaining orthogonal axes (May, 1985, p. 6).

To understand and verify the results of finite element software, it is necessary to make hand calculations. Procedures for analysis of bolted joints are outlined in the "Systems Engineering Division Bolted Joint Handbook", and "Structural and Vibrational Analyses of the Wake Side Plasma Sensor for the Wake Shield Facility" (Rencis et al., 1991).

The first step in hand analysis is to find the center of gravity of the objects acting on the bolts as well as the mass of the objects. The resultant force is defined as the mass of the antenna multiplied by the gravity factor. A gravity factor of 10.0 is assumed in the x, y, and z directions. Although this is not the actual load case, the results of this simplified load case can be checked to compare to the results gotten through Finite element analysis to verify the results gotten from the IMAGES-3D software. After drawing a free-body diagram, the resultant forces can be found at each bolt. Due to the

35

symmetry of the bolt placement as well as the gravity forces for each direction, the forces on each bolt are the same. A TK Solver for Windows program has been written to find the CG and the mass of each of the links. TK Solver will also be used to find the resultant forces on the bolts as well as the margins of safety in shear and tension. The TK Solver program *BOLTFAIL.TK* for this has been written and is shown in Appendix C. The TK Solver program also includes the calculation of minimum and maximum pre-loads and Margins of Safety for the FEM results to find the more accurate results. The TK Solver program also calculates the mass and the Center of Gravity of all the individual antenna parts, and a tabulation is shown in Appendix D. The weight of the antenna assembly not including the aluminum base-plate is 2.81 lb. and its center of gravity is 6.32 inches from the lid of the GASCan. The weight of the antenna assembly including the weight of the aluminum base-plate is 4.58 lb. and the center of gravity is 3.83 inches from the GASCan lid. In both cases , the center of gravity on the plane of the GASCan lid is at the center of the antenna assembly, 4.5 inches from the center of the lid at an angle of -45°. A list of all of the material properties used in IMAGES 3-D and TK Solver are shown in Appendix E. Dimensioned drawings of the individual parts of the antenna are shown in Appendix F.

3.1.6 Analysis Methodology

The forces that act on the joints must first be determined. For a secondary structure that weighs under 20 lb..(the entire assembly weighs 4.58 lb.), NASA suggests a load factor of 40 g's in the most critical direction and 10 g's along the remaining two orthogonal axes (Hamilton, 1985). For the hand analysis, the loads were modeled as a

36

point force acting at the center of gravity of the antenna assembly. For the finite element model, the loads were modeled as gravity forces acing on the antenna. The tensile and shear loads that act on the beams finite element model are equal to the forces that act on the bolts.

In order to determine the minimum required pre-load for each of the joints, it was assumed that there will be no slip between the parts, or that the shear forces will be resisted friction between the fastened parts. It was also assumed that there will be no gap; any tensile forces acting on the joint will be resisted by the fastener pre-load of the joint. The friction force at the fastened parts can be written as:

$$F_{se} = \mu \left[F_p - \frac{K_j}{K_j + K_b} F_{te} \right]$$ **Eq. 2**

where: F_{te} = external shear load, (lb.)

μ = coefficient of friction at joint, (dimensionless)

F_p = pre-load developed in bolt, (lb.)

F_{te} = external tensile load, (lb.)

K_j = stiffness of the joint, (lb./in)

K_b = stiffness of the bolt, (lb./in)

The stiffness of the bolt and the joint can be calculated through the following equations:

$$K_b = \frac{E_b A_b}{L}$$ **Eq. 3**

$$K_j = \frac{E_j A_c}{T}$$ **Eq. 4**

where: E_b = modulus of elasticity of bolt material, (psi)

E_j = modulus of elasticity of joint material, (psi)

A_b = cross-sectional area of the bolt, (in^2)

A_c = cross-sectional area of equivalent cylinder in joint, (in^2)

L = grip length of bolt, (in)

T = grip thickness of part, (in)

The effective tensile Area of a bolt can be found using Table 14-1 of *Machine Design* (Norton, 1994). The cross sectional area, A_c, is calculated from Eq. 2.6 of the Bolted Joint Handbook where:

$$A_c = \frac{\pi}{4}\left[\left(D_w + 0.1T\right)^2 - D_h^2\right]$$ **Eq. 5**

$$\text{if } D_j > 3\, D_w$$

where: D_j = diameter of joint or length of shortest side, (in)

D_w = diameter of bolt head or washer, (in)

D_h = diameter of hole, (in)

The minimum required pre-load can be solved for from Eq. 2 as:

$$F_{P_{min}} = \frac{F_{se}}{\mu} + \frac{K_j}{K_j + K_b}\, F_{te}$$ **Eq. 6**

The largest bolt loading for F_{se} and F_{te} are used to calculate values for F_{Pmin}. If all bolts are loaded to the specifications for the most critical bolt, the value for F_{Pmin} will be a conservative value. The maximum allowable pre-load allowed in a bolt is dependent on the force at which the bolt will yield:

$$F_{P_{max}} = .65 F_{ty}$$ **Eq. 7**

where: F_{Pmax} = maximum allowable pre-load in joint, (lb.)

F_{ty} = Load at which bolt will yield, (lb.)

The margin of safety for the joint fasteners, or bolts, can be determined using Eq. 3.2 in the "Bolted Joint Handbook" (1990):

$$MS_y = \frac{1}{\sqrt{\left(\dfrac{f_t}{F_{ty}}\right)^2 + \left(\dfrac{f_s}{.55 F_{ty}}\right)^2}} - 1 \qquad \textbf{Eq. 8}$$

$$MS_u = \frac{1}{\sqrt{\left(\dfrac{f_t}{F_{tu}}\right)^2 + \left(\dfrac{f_s}{F_{su}}\right)^2}} - 1 \qquad \textbf{Eq. 9}$$

where:
$$f_t = \left(FS_p\right)\left(F_{p_{min}}\right) + \left(F_{se}\right)\left(\frac{K_b}{K_j + K_b}\right)\left(F_{te}\right)$$

$$f_s = \left(FS_e\right)\left(F_{se}\right)$$

MS_y = Margin of Safety against yield, (dimensionless)

MS_u = Margin of Safety against ultimate failure, (dimensionless)

F_{ty} = tensile yield load for bolt, (lb.)

F_{tu} = tensile ultimate load for bolt, (lb.)

F_{su} = shear ultimate load for bolt, (lb.)

FS_p = pre-load factor of safety, (1.3, dimensionless)

The bolted joint handbook describes the method by which the pre-load force and torque recommended for the bolt may be found. Initial hand calculations estimate a torque of 277 lb.-in. The maximum suggested pre-load force determined through hand for the 0.5 inch diameter bolt used is 2770 lb. and the minimum suggested pre-load force is 126 lb. The equation used to find the required pre-load torque is given below:

$$T = F_p KD \qquad \textbf{Eq. 10}$$

where: T = applied toque, (in-lb.)

F_p = pre-load in bolt, (lb.)

K = torque coefficient, (= 0.2, dimensionless)

D = nominal bolt diameter, (in)

Using IMAGES 3-D to calculate the forces on the bolts and screws in the antenna model, the maximum and minimum pre-load as well as the Margin of Safety for the yielding and ultimate failure of the bolts and screws can be determined using equations stated in a TK Solver program. The four tables below show the axial and shear forces, the maximum and minimum pre-load allowed on the bolt, and the Margins of Safety against yielding and failure applied to the bolts and screws. Table 3 shows this data for the bolts attached to the GASCan lid, Table 4 shows the data for a fail-safe (the most critical bolt is removed) analysis of the bolts on the GASCan lid. Table 5 gives the data for the setscrews that attach to the Delrin cone, and Table 6 is the data for a fail-safe analysis of the setscrews.

The fail-safe analysis for the antenna bolts was done by removing the most critical bolt from the antenna assembly and completing a stress analysis. If all antenna bolts still have a positive margin of safety, then the assembly can be considered fail-safe. NASA also suggests using A-286 Alloy bolts, which have a yield stress three times higher than that of normal government issued 18-8 stainless steel bolts. (p. 23, Bolted Joint Handbook).

Table 3: *Bolts between base and GASCan lid*

	F Axial (lb.)	F Shear (lb.)	Max Pre-load	Min Pre-load	MS yield	MS ult
	Load Case:	10 g in all dir				
1	15.91E0	6.646E0	8.762E3	26.063E0	218.518E0	341.531E0
2	11.95E0	39.865E0	8.762E3	132.071E0	55.662E0	96.001E0
3	**39.64E0**	**83.198E0**	**8.762E3**	**279.902E0**	**25.039E0**	**42.964E0**
4	11.95E0	39.865E0	8.762E3	132.071E0	55.662E0	96.001E0
	Load Case:	40 g in Z dir, 10 g in X and Y				
1	20.12E0	107.784E0	8.762E3	353.539E0	20.534E0	36.228E0
2	47.8E0	153.295E0	8.762E3	508.391E0	13.693E0	24.128E0
3	**75.49E0**	**197.99E0**	**8.762E3**	**660.617E0**	**10.19E0**	**18.03E0**
4	47.8E0	153.295E0	8.762E3	508.391E0	13.693E0	24.128E0
	Load Case:	40 G in Y dir, 10 g in X and Z				
1	57.44E0	75.955E0	8.762E3	261.709E0	25.741E0	43.32E0
2	29.75E0	40.99E0	8.762E3	140.873E0	48.895E0	81.847E0
3	**81.6E0**	**151.976E0**	**8.762E3**	**513.96E0**	**13.055E0**	**22.628E0**
4	53.48E0	109.609E0	8.762E3	369.119E0	18.712E0	32.254E0
	Load Case:	40 g in X dir, 10 g in Y and Z				
1	57.44E0	75.951E0	8.762E3	261.698E0	25.742E0	43.321E0
2	53.48E0	109.412E0	8.762E3	368.486E0	18.743E0	32.305E0
3	**81.17E0**	**151.976E0**	**8.762E3**	**513.835E0**	**13.064E0**	**22.648E0**
4	29.75E0	40.828E0	8.762E3	140.35E0	49.06E0	82.107E0

Table 4: *Bolts between base and GASCan lid (Fail-Safe)*

	F Axial (lb.)	F Shear (lb.)	Max Pre-load	Min Pre-load	MS yield	MS ult
	Load Case:	10 g in all dir				
1	31.97E0	70.838E0	8.762E3	237.801E0	29.763E0	51.038E0
2	39.72E0	94.629E0	8.762E3	316.8E0	22.2E0	38.339E0
4	39.71E0	94.629E0	8.762E3	316.796E0	22.201E0	38.34E0
	Load Case:	40 g in Z dir, 10 g in X and Y				
1	11.7E0	26.722E0	8.762E3	89.599E0	80.81E0	137.528E0
2	100.8E0	259.796E0	8.762E3	867.347E0	7.514E0	13.472E0
4	100.8E0	259.731E0	8.762E3	867.137E0	7.516E0	13.475E0
	Load Case:	40 g in Y dir, 10 g in X and Z				
1	152.5E0	158.051E0	8.762E3	554.164E0	11.266E0	19.094E0
2	24.88E0	98.754E0	8.762E3	325.793E0	22.137E0	38.769E0
4	112.6E0	212.903E0	8.762E3	719.508E0	9.052E0	15.908E0
	Load Case:	40 g in X dir, 10 g in Y and Z				
1	90.06E0	199.861E0	8.762E3	670.885E0	9.905E0	17.448E0
2	112.6E0	212.976E0	8.762E3	719.744E0	9.049E0	15.903E0
4	24.88E0	98.739E0	8.762E3	325.743E0	22.14E0	38.775E0

Table 5: *Screws between base and Delrin cone*

	F Axial (lb.)	F Shear (lb.)	Max Pre-load (lb.)	Min Pre-load (lb.)	MS yield	MS ult
	Load Case:	**10 g in all dir**				
1	23.72E0	9.377E0	1.964E3	30.906E0	31.556E0	49.41E0
2	23.73E0	9.386E0	1.964E3	30.935E0	31.534E0	49.376E0
3	**38.37E0**	**11.419E0**	**1.964E3**	**37.901E0**	**22.122E0**	**34.342E0**
4	38.37E0	11.437E0	1.964E3	37.957E0	22.106E0	34.32E0
	Load Case:	**40 g in Z dir, 10 g in X and Y**				
1	1.815E0	7.454E0	1.964E3	24.096E0	67.421E0	116.442E0
2	1.852E0	7.444E0	1.964E3	24.064E0	67.418E0	116.377E0
3	**60.45E0**	**14.834E0**	**1.964E3**	**49.53E0**	**14.92E0**	**23.152E0**
4	60.41E0	14.873E0	1.964E3	49.655E0	14.91E0	23.139E0
	Load Case:	**40 g in Y dir, 10 g in X and Z**				
1	23.72E0	29.401E0	1.964E3	95.502E0	14.025E0	23.714E0
2	116.8E0	29.115E0	1.964E3	97.162E0	7.188E0	11.429E0
3	38.37E0	30.321E0	1.964E3	98.875E0	12.07E0	19.999E0
4	**131.4E0**	**32.034E0**	**1.964E3**	**106.983E0**	**6.343E0**	**10.137E0**
	Load Case:	**40 g in X dir, 10 g in Y and Z**				
1	116.8E0	29.084E0	1.964E3	97.061E0	7.192E0	11.434E0
2	23.73E0	29.431E0	1.964E3	95.599E0	14.012E0	23.692E0
3	**131.4E0**	**31.993E0**	**1.964E3**	**106.85E0**	**6.347E0**	**10.142E0**
4	38.37E0	30.364E0	1.964E3	99.013E0	12.057E0	19.98E0

Table 6: *Screws between base and Delrin cone (Fail-Safe)*

	F Axial (lb.)	F Shear (lb.)	Max Pre-load	Min Pre-load	MS yield	MS ult
Load Case:		10 g in all dir				
1	62.03E0	11.012E0	1.964E3	37.243E0	16.391E0	25.117E0
2	14.65E0	17.15E0	1.964E3	55.728E0	24.462E0	40.763E0
4	76.68E0	13.438E0	1.964E3	45.475E0	13.125E0	20.205E0
Load Case:		40 g in Z dir, 10 g in X and Y				
1	62.03E0	8.963E0	1.964E3	30.634E0	17.452E0	26.577E0
2	58.6E0	16.877E0	1.964E3	56.07E0	14.362E0	22.449E0
4	120.6E0	17.096E0	1.964E3	58.496E0	8.539E0	13.25E0
Load Case:		40 g in Y dir, 10 g in X and Z				
1	62.03E0	32.709E0	1.964E3	107.235E0	9.565E0	15.604E0
2	78.46E0	47.424E0	1.964E3	155.158E0	6.667E0	11.139E0
4	169.7E0	42.586E0	1.964E3	142.085E0	4.621E0	7.534E0
Load Case:		40 g in X dir, 10 g in Y and Z				
1	248.1E0	34.869E0	1.964E3	119.367E0	3.647E0	5.941E0
2	107.7E0	46.405E0	1.964E3	152.683E0	5.844E0	9.642E0
4	169.7E0	39.714E0	1.964E3	132.819E0	4.777E0	7.749E0

A hand analysis of the bolts was done in order to verify the validity of the analysis on IMAGES. The reaction forces on the bolt were done using the equations in the Analysis Methodology section. Equilibrium equations and symmetry of the bolts are used to develop equations to solve for the resultant forces on the bolts. The weight of the antenna is multiplied by the gravity load specified by NASA in the Bolted Joint Handbook (a limit load of 10 gravity's in the two axes, X and Y, defining the plane of the GASCan lid, and 40 g's in the axis, Z, perpendicular to the lid) and placed as a concentrated load at the center of gravity. The antenna orientation and placement of center of gravity, is shown in Fig. 6. There are two possibilities for analysis. The first is

Figure 6

CENTER OF GRAVITY
INCLUDING AL BASEPLATE
(0,0,2.96)

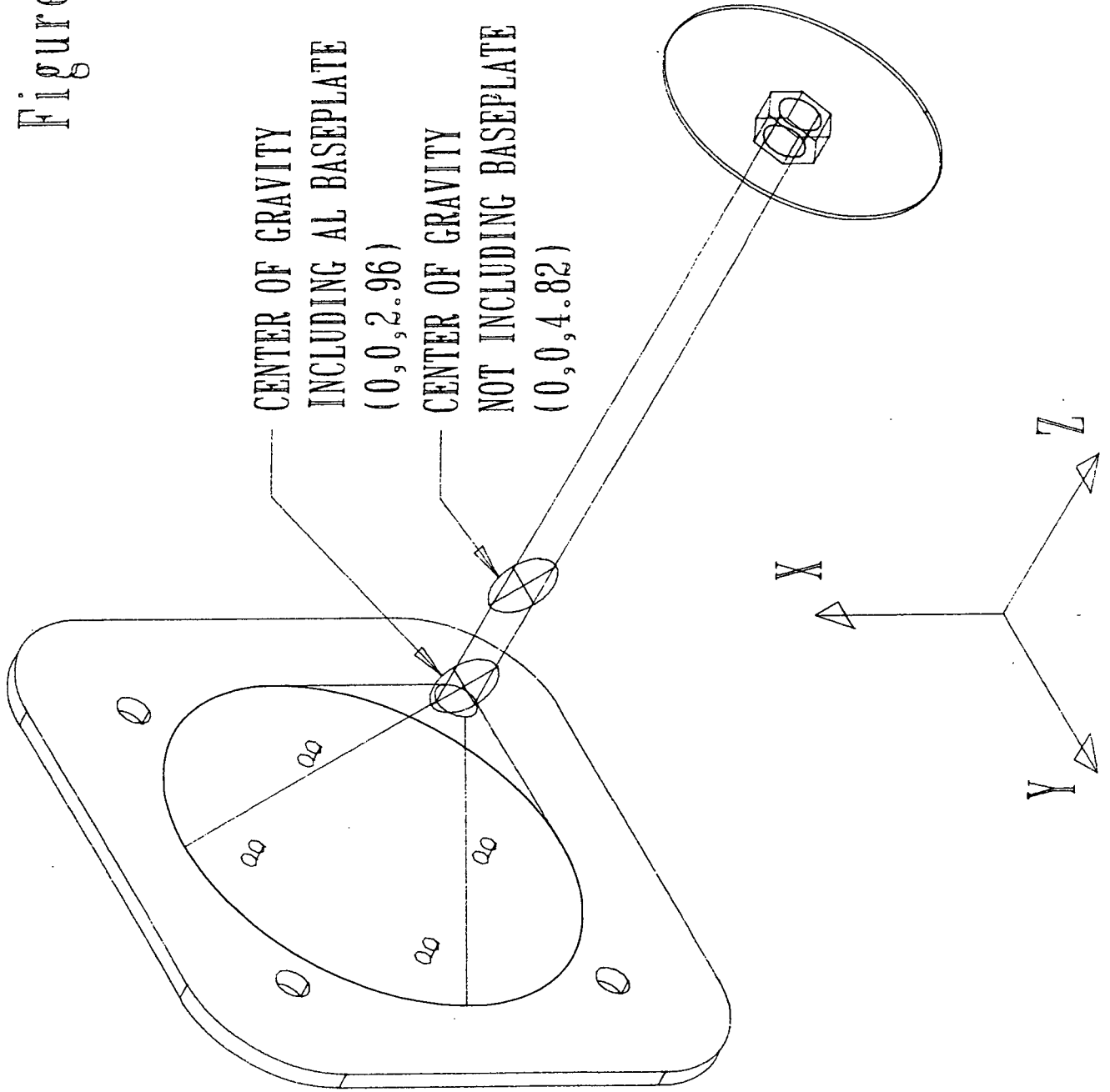CENTER OF GRAVITY
NOT INCLUDING BASEPLATE
(0,0,4.82)

X

Y

Z

Figure 6: Loading diagram including center's of gravity (antload.prt)

to neglect the weight of the base since it will move the center of gravity further away from the lid but it will decrease the shear force on the individual bolts. The second choice is to include the weight of the aluminum base plate. Although this will decrease the resultant moment, it will increase the shear forces. The same TK Solver program *BOLTFAIL.TK*, shown in Appendix C, that was used for the calculation of center of gravity and IMAGES 3-D based Margins of Safety was used to calculate the forces and Margins of Safety through the hand analysis. The hand results are generally more conservative and less accurate due to the modeling of the problem, but the results shown in Tables 7-10 are comparable to the results received through the IMAGES based analysis. All hand calculations were done assuming a 10 g load in all directions in order to keep the analysis simple. The results are then compared to the IMAGES results for a 10 g load.

Table 7: *Hand analysis of bolts between base-plate and GASCan lid*

Bolt #	F Axial (lb.)	F Shear (lb.)	Max Pre-load	Min Pre-load	MS yield	MS ult
	Load Case:	10 g in all dir				
1	51.6	32.4	119.4	8762	51.5	82.7
2	51.6	32.4	119.4	8762	51.5	82.7
3	51.6	32.4	119.4	8762	51.5	82.7
4	51.6	32.4	119.4	8762	51.5	82.7

Table 8: *Hand analysis of bolts between base-plate and GASCan lid (Fail-Safe)*

Bolt #	F Axial (lb.)	F Shear (lb.)	Max Pre-load	Min Pre-load	MS yield	MS ult
	Load Case:	10 g in all dir				
1	103.1	43.2	8762	169.2	34.3	54.4
2	80.2	43.2	8762	162.5	37.2	59.7
4	103.1	43.2	8762	169.2	34.3	54.4

Table 9: *Hand analysis of screws between Delrin cone and base-plate*

Bolt #	F Axial (lb.)	F Shear (lb.)	Max Pre-load	Min Pre-load	MS yield	MS ult
	Load Case:	10 g in all dir				
1	66.824	33.367	1964	106.3	9.318	15.143
2	66.824	33.367	1964	106.3	9.318	15.143
3	66.824	33.367	1964	106.3	9.318	15.143
4	66.824	33.367	1964	106.3	9.318	15.143

Table 10: *Hand analysis of screws between Delrin cone and base-plate (Fail-Safe)*

Bolt #	F Axial (lb.)	F Shear (lb.)	Max Pre-load	Min Pre-load	MS yield	MS ult
	Load Case:	10 g in all dir				
1	133.6	43.157	1964	142.9	5.39	8.81
2	110.8	43.157	1964	142.3	6.02	9.87
4	133.6	43.157	1964	142.9	5.39	8.81

There are four different load cases for each IMAGES table. The 10 g load case assumes that the antenna is a primary structure; NASA states that the structure must withstand limit loads of 10.0 g's in all directions with a factor of safety of 2.0 (Peden, 1993). However, the three other load cases are done for a secondary structure; NASA also states in "Simplified Design Options for STS Payloads" that a secondary structure

that weighs less than 20 lb. must have a limit load of 40 g's in the most critical load direction and 10 g's in each of the two remaining directions (Hamilton, 1985). It has been verified by NASA and Mark Peden that the antenna structure is to be classified as a secondary structure (1995). The margins of safety calculated are positive and therefore acceptable for the case of a secondary structure.

The placement of the bolts on the GASCan lid are allowed to be anywhere as long as the antenna does not cover any of the purge ports already existing on the GASCan lid. The size of the bolts are allowed to be determined by us and can therefore stay at the existing sizes shown in the TK Solver program *BOLTFAIL.TK* shown in Appendix C. If the bolts were going to go through the GASCan lid a sealing material would have to be used to completely seal the inside of the canister from the outside. According to NASA, the use of RTV-142 should not be used as a sealant because it has not been able to meet product specifications in recent years (Peden, 1994). For safety considerations, it has been chosen to place the bolts so that they go 0.31" into the GASCan lid, but not through the lid. A fine thread bolt has been chosen to reduce the effects of vibration on loosening the bolts. A course thread bolt will reduce the possibility of the bolt threads stripping, but the chances of the bolt loosening are more likely than the chances of the threads shearing.

The final consideration is for the steel pins that secure the antenna rod to the Delrin cone. The yield stress for AMS 5644 stainless steel is 140×10^3 psi, and the largest stress possibly encountered is 7074 psi, giving a margin of safety of 18.8.

3.2 MICRO-GRAVITY IGNITION EXPERIMENT (MGI)

Analysis, design and manufacturing of parts pertaining to the MGI experiment follow. This section is subdivided into areas concerning parts manufactured, redesign of the MGI chamber plate, a discussion of a pressure transducer as an alternate means of ignition detection, and a pressure vessel, sealant and bolt analysis of the canister under the 'worst-case scenario.' The canister mounting brackets are then discussed.

3.2.1 MGI components manufactured by the 1994-95 Payload Integration team

The 1994-95 Payload Integration team completed manufacture of the following MGI components: (the person responsible for manufacturing of the part is credited for reference purposes)

- MGI Mounting brackets [Andy Beaupre]

- Welding of MGI Canisters [Paul Curci, City Welding]

- Machining of Teflon backplates [Steve Derosier and 1994-1995 Payload Integration Team, WPI]

- Machining of redesigned chamber plates [1994-1995 Payload Integration Team]

- Machining of thermocouple trees [Steve Derosier]

With the above completed, the MGI canisters are as completed as possible. What remains is purchase of the aluminum oxide ceramic backplates, infrared heat lamps, heat flux gauge and pressure transducers, and manufacturing of the heat flux back block.

3.2.2 Redesign of MGI chamber plate

The endplate for the MGI canisters was redesigned to correctly fit the purge and check valves after much difficulty. The correct thread size for the check valve is 9/16-18NF and 1/4-18 NPTF for the purge valve. An ARIES drawing of the plate is shown in Fig. 7.

Holes for the hermetic seals were machined into the endplates for three of the four MGI canisters (the control chamber has no electrical passthrough). It was decided that the current 12 pin thermocouple passthroughs, which are manufactured by Omega, should be retained for the final design, despite some previous reports of leakage problems. The leakage problem is located between the plate and connector and not through the pin holes. This situation will occur with any pass through. In addition, the current passthroughs meet the MIL-C-26500E standard. An alternate source of hermetic seals, manufactured by Newark, was located. These connectors vary from $30 to $100 each depending on the number of contacts. These connectors were identical to the current connectors and the extra cost was not justified. Use of a silicone sealant to supplement the passthroughs will be adequate.
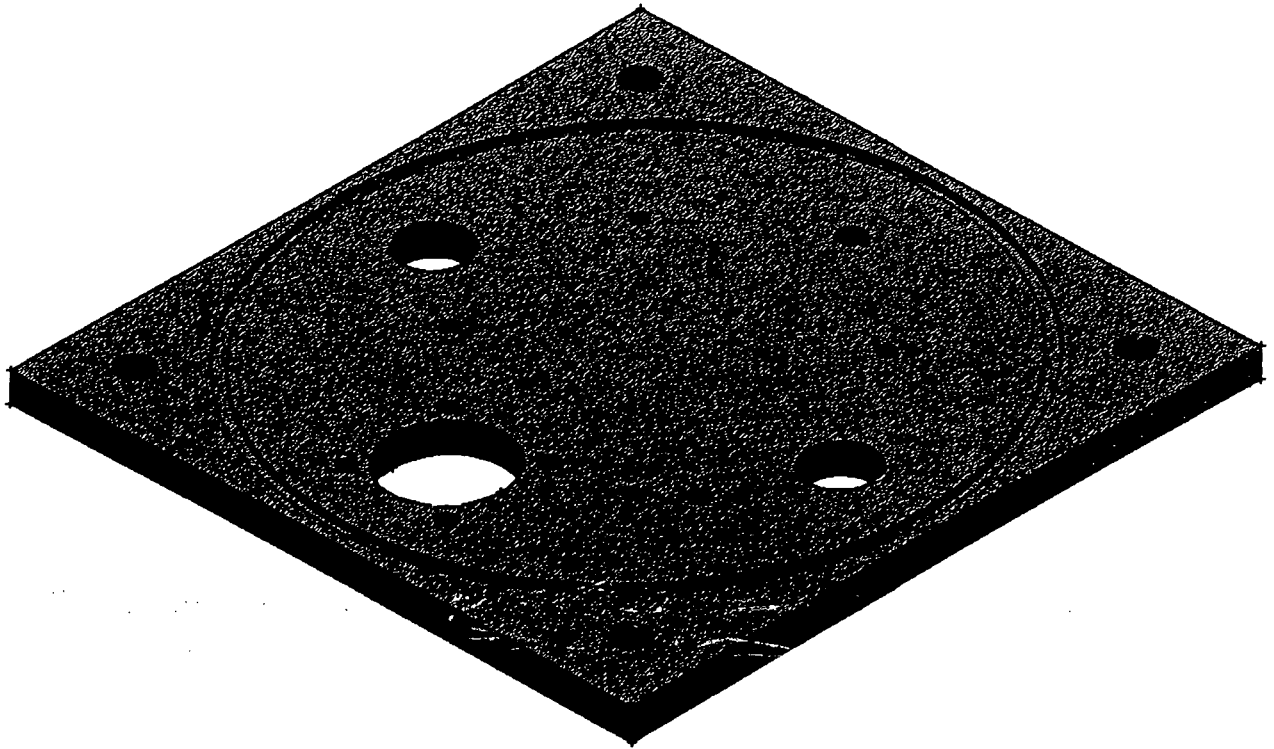
Figure 7 –
MGI Canister End Plate

The heat flux gauge holding block for the control chamber of the MGI experiment was redrawn in ARIES because no current drawings exist on disk. (See Fig. 8) This still needs to be machined of Al 2024-T4 which the 1994-95 Payload Integration Team has in its possession.

Finally, the endplate hole for the Entran EPX pressure transducer was eliminated as a different pressure transducer must be decided upon. This is discussed next.

3.2.3 Discussion of a pressure transducer as an alternate means of ignition detection

There is a problem with the current pressure transducer. A previous micro-gravity ignition MQP suggested problems with the accuracy below 0^0 C. The 1994 MGI MQP suggested the only reason to include a pressure transducer was to monitor any significant pressure changes during the ignition process. However, a Mitre review showed concern that pyrolysis products may become an important factor in low-g conditions and prematurely shut off the lamp. A second concern is that the lamp will remain on longer than necessary if combustion products do not trigger the ion sensor. Although the most recent MQP has obtained repeatable results using the ion sensor, the pressure transducer should be included as a backup source of ignition detection. Pressure waves produces at the onset of ignition will be registered on the transducer, marking ignition time. For this reason, a more reliable pressure transducer has been found.

A Barocel capacitance manometer will produce results that will not vary significantly over large temperature gradients. Edwards High Vacuum International produces temperature controlled manometers. The Model 655 capacitance manometer incorporates a hermetically sealed and heated enclosure containing the pressure sensing
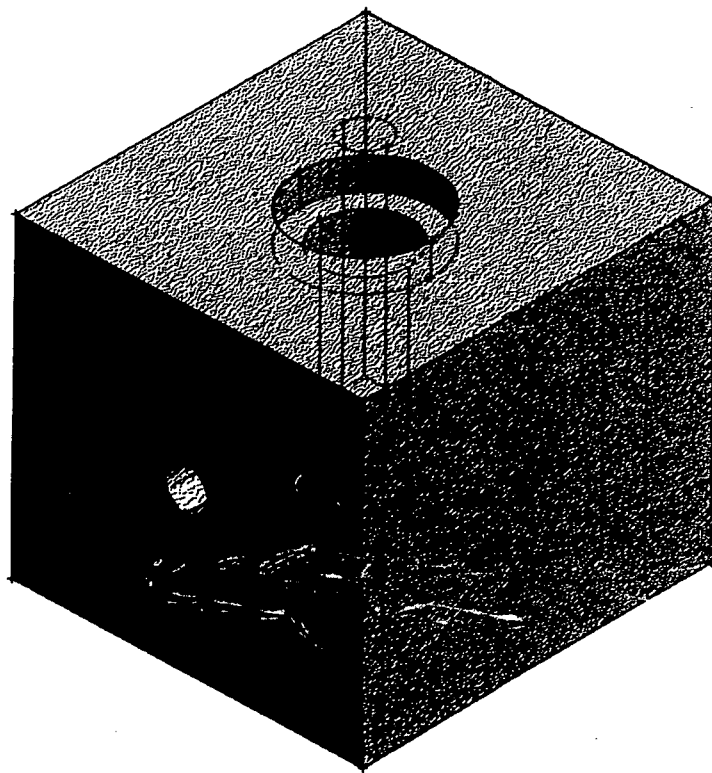
Figure 8 -
MGI Control Chamber Back Block

element and critical electronic circuitry. This means that changes in ambient temperature, humidity and atmospheric pressure have minimal effect on the reading. Barocel Type 655 is controlled to a temperature of 113^0 F. Its average price is $1,500. As three transducers would be needed the total cost would be $4,500.

3.2.4 Pressure Vessel Analysis

As defined by the 1994 MGI MQP by Belliveau and Chase, a worst case scenario could arise in which all the power from the battery box was to drain into one of the ignition chambers and not be shut off. According to their calculations, a final temperature and pressure of 600K and 4.75atm, respectively, can be expected if this situation were to occur. Since the melting point of aluminum alloys is between 749K and 933K, the worst case temperature will compromise the canister's integrity. However, with regard to the worst case pressure, no analysis has yet been completed. A analysis of a 5 atm internal pressure in the canister follows.

According to Norton (1995), when the wall thickness of a cylindrical pressure vessel is less than 1/10 of the radius, the cylinder can be considered thin-walled. The MGI canister has a radius of 2.41 in and a wall thickness of 0.095 in. This results in a wall thickness / radius ratio of 1/25, so the canister may be considered thin walled. The stress distribution across the thin wall can be approximated as uniform and the following expression results (for a close-ended cylinder):

$$\sigma_a = pr / 2t \qquad\qquad\qquad \textbf{Eq. 11}$$

where σ_a = axial stress
  p = pressure
  r = radius

t = wall thickness.

For the given situation this yields:

$\sigma_a = 69.85psi\ (2.41\ in.)\ /\ 2\ (0.095in.) = 886\ psi$

The canister is made of aluminum 6061-T6 which has a tensile yield strength of 36,000

psi. If we calculate the factor of safety we find:

$F.S. = 36,000\ psi\ /\ 886\ psi = 40$

The canister will easily withstand the 4.75 atm (69.85 psi) pressure that can be

expected under the worst case scenario.

3.2.5 Bolt Analysis

The bolt loadings for an MGI Canister were calculated following NASA's

Systems Engineering Bolted Joint Handbook (1990), SED Engineering Handbook EHB-

2. The bolts in question fasten the endplates to the cylinder portion of the canister. The

only significant loading that the endplates may receive will be due to the 'worst case'

scenario in which the internal pressure of the cylinder will reach 4.75 atm (69.85 psi).

This load may be calculated from the internal pressure multiplied by the surface area of

the endplate which is inside the cylinder. This was calculated to be:

$(16.8\ in^2)\ (69.85psi) = 1.18\ kip$

The only other loading will be the weight of the endplate which is insignificant

compared with the possible worst case load. Under a 20g load the weight of an endplate

is at most 10 lb. This corresponds to 0.4 *psi* distributed load.

The SED handbook gives the following for the above factors of safety:

Table 11 - *SED handbook information*

type of loading	condition	FS
external load	yield	FS_{ey}=2.00
	ultimate	FS_{eu}=2.60
preload	calibrated torque wrench, K Estimated (0.2)	Fs_p=1.30 F_{pmax}=0.65 F_{ty}

Following the bolt analysis methodology, the following was calculated assuming a 1/4"-20 UNC A-286 series stainless steel bolts of 3/4 inches in length:

Table 12 - *Margin of Safety for Bolt Loaded in Tension Only*

Margin of Safety (yield case)	7.708
Margin of Safety (ultimate case)	4.282
Torque to preload (in-lb.)	13

The SED Bolted Joint Handbook, specifies that as long as the above values are positive, the design is considered safe. The bolts were analyzed under a 395 lb. tensile load which represents the fail-safe case where only 3 bolts support the structure.

3.2.6 Sealant Analysis

The joint will leak unless the clamping forces are sufficient to create more pressure at the gasket than exists in the cylinder. The minimum clamping pressure can be found from the total area of the gasketed joint and the minimum clamping force F_m. (Norton, 1995) Therefore,

57

$$p_{avg} = F_m / A_j = 4F_m / \pi (D_o - D_i)^2 \qquad\qquad \text{Eq. 12}$$

where p_{avg} = average pressure
A_j = area of the joint
D_o = outer diameter of the gasket
D_i = inner diameter of the gasket.

The minimum clamping force, F_m, is calculated from <u>Machine Design</u> by Norton (p. 767) as 720 lb. Substituting the appropriate values in the above equation yields:

$$p_{avg} = F_m / A_j = 4 \,(720lb) / \pi \,(4.815in. - 4.625in.)^2 = 25,400\, psi$$

The preload force calculated in the above bolt analysis was 247 lb. It can be seen that because the preload force is smaller than the minimum clamping force, a clamping pressure of greater than 25,400 psi will not be achieved and the cylinder will leak in the worst case scenario. Therefore we set the minimum preload equal to a value greater than the minimum clamping force of 720 lb. and conduct another bolt analysis. A minimum force of 800 lb. was chosen. The analysis the yields:

Table 13 - *MGI Canister Bolt analysis*

Margin of Safety (yield case)	2.249
Margin of Safety (ultimate case)	1.095
Torque to preload (in-lb.)	40

The margins of safety are still positive and the bolt choice is still acceptable.

3.2.7 MGI Mounting Brackets

A complete structural analysis of the MGI mounting brackets was conducted by the 1993-1994 Payload Integration Team. For convenience, some of the key results are mentioned here.

The brackets were machined from 6061-T6 aluminum. The brackets will be mounted to the ISS using 1/4" UNC 300 series stainless steel bolts. For a safety analysis of the mounting brackets see Appendix O of the GASCan II Payload Integration by Brown et al (1994).

3.3 ROTATIONAL FLUID FLOW

3.3.1 FLUID SELECTION

Although Cyr et al(1993) had already chosen silicon oil as a working fluid, concerns were raised at a Mitre Design Review over the low flashpoint of silicon oil and the possibility that it could pose a safety threat.

With that in mind the search for an alternative operating fluid was begun. The first step was to find fluids that had suitable physical properties. First, they had to have low viscosity, with a relatively flat temperature - viscosity curve. Second they had to have a low freezing point. Third they had to have a high flashpoint, and finally they needed to have low weight.

Table 14 - Fluid viscosities at 25 Degrees Celsius

Fluids	Kinematic Viscosity in Centistokes (pure fluids)
	25 degrees centigrade
water	0.89
ethanol	1.3606994
ethylene glycol	14.520202
methanol	0.6873894
acetone	0.3873908
glycerol	740.50583
Methylene Chloride	2.219275
R-11	1.9307692
silicon oil	0.65-2500000
R12	0.4983819
R21	vapor at 25 degrees c
R22	vapor at 25 degrees c
R113	vapor at 25 degrees c
R114	vapor at 25 degrees c
ammonia	0.3966418
R123	0.0384798

The first step towards the selection of a working fluid was determining the viscosity of the various fluids. The kinematic viscosity was determined by using the equation:

$$\upsilon = \frac{\mu}{\rho}$$
                                                                 Eq. 13

where:
        ν stands for the kinematic viscosity of the fluid
        μ stands for the dynamic viscosity of the fluid
        ρ stands for the density of the fluid

Of the 16 fluids mentioned in table 1, ethanol, ethylene glycol, glycerol, methylene chloride, and R-11 had viscosities above the 1.1 centistokes specified by Cyr et al. These fluids would not create vorticies within the operating envelope of the experiment and so were dropped from consideration.

Table 15 - Physical properties for various fluids

Fluids	freezing point	density	solubility	flash point
	degrees centigrade	g/cm^3		degrees centigrade
water	0	1	miscible	nonflammable
methanol	-97.6	0.7914	miscible	19
acetone	-94.8	0.7899	miscible	-19
silicon oil	-85	0.818	insoluble	37
R12	-252	0.618	insoluble	nonflammable
R21	-211	0.624	insoluble	nonflammable
R22	-256	0.598	insoluble	nonflammable
R113	-31		insoluble	nonflammable
R114	-137		insoluble	nonflammable
ammonia	-107.9	0.60508	insoluble	nonflammable
R123		15.33272	insoluble	nonflammable

The next property that was examined was the freezing point. To be able to resist the cold temperatures that would be encountered in the space shuttle payload bay, the

freezing point of the fluid should be lower than -35 degrees Celsius. The physical properties of the remaining fluids were collected in table 2. Water and R-113 were the only fluids in table 2 that did not have a low enough freezing point. These fluids were also dropped from consideration.

The flashpoint was the next property considered. Three fluids, acetone, methanol, and silicon oil were flammable. Acetone and Methanol had very low flashpoints. They also had high vapor pressures, and therefore had a very high chance of bursting into flame if there was an accidental spark. They also happen to be toxic. The third fluid silicon oil had a flashpoint of 37 degrees Celsius, or 99 degrees Fahrenheit. Under normal conditions, this would not pose a problem, however, while the shuttle is on the launchpad awaiting launch, the payload bay can easily surpass 100 degrees Fahrenheit.

The last property that was examined was the density. The only fluid that failed was R-123. This fluid had a very high density, over 15 times that of water, which would make it too heavy to use in the experiment. Of the remaining fluids, ammonia could not be used because its viscosity was too low, and the other refrigerants could not be used because they turn to vapor in the temperature range in which the experiment will be operated.

It should be noted that other properties were also taken into account, but were not critical. They were the surface tension, which would affect the Weber number of the experiment, the refractive index, which would affect the ultrasonic flow measurement system, and the toxicity, which could pose a safety concern.

Silicon oil was the only fluid which was not ruled out because of its properties. There is a concern about the flashpoint of the fluid, however this problem can be rectified by filling the vortex chamber with an inert gas such as nitrogen, the silicon oil would not have any oxygen with which to combust.

Otherwise silicon oil is the perfect fluid for the experiment. It can be purchased with a viscosity of 1 centistoke. It has a relatively flat temperature-viscosity curve. It has a low freezing point, it has a low density, it is non-toxic, has a low refractive index, and a surface tension comparable to that of water. It was re-selected as the working fluid for the experiment.

3.3.2 PERFORMANCE ENVELOPE

The purpose of the Rotational Fluid Flow experiment was to study the effect of gravity on the formation of vorticies. In order to do this, the Rotational Fluid Flow, from here on referred to as the RFF, experiment, needed to be related to similar ground based data at one gravity.
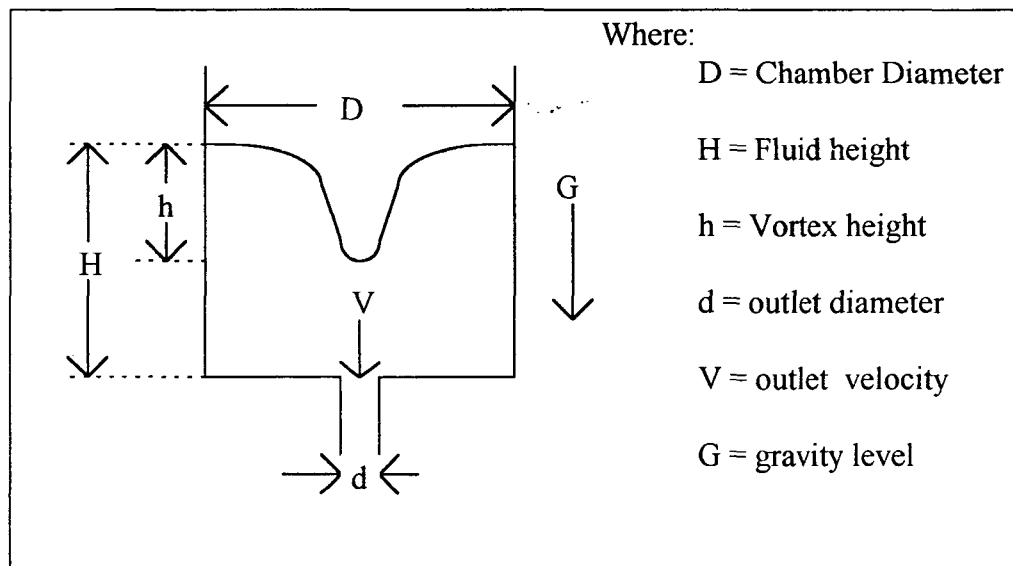

Figure 9: Important Parameters for Dimensional Analysis

This was accomplished by ensuring that the nondimensional geometric parameters H/D and d/D were similar, where H stands for the fluid height, d stands for the outlet drain diameter, and D stands for the container diameter. These nondimensional geometric parameters relate the geometry of Smith(1994)'s experimental setup to that of the RFF experimental setup. Smith(1994) had a H/D ratio of 1.394, which was similar to the 1.227 ratio for the RFF experiment. Smith also had a range of outlet diameters from 0.675 to 0.125 inches. The 0.25 inch outlet diameter yielded a ratio of 0.0416 which was very close to the 0.039 ratio for the RFF experiment. Because the d/D ratios of the .25 inch outlet diameter of the thesis and the RFF experiment are so similar they should demonstrate similar behavior at one g. Therefore the .2 to .4 range of Froude numbers for the 0.25 inch outlet in Smith's thesis should be valid for the RFF experiment, and the 0.18 to 0.38 ft^2/s range for the circulation should also be valid.

By using the range of Froude numbers it was possible to determine the range of flow rates for the experiment. Using the equation:

$$Fr_H = \frac{V_{out}}{\sqrt{gH}} = \frac{4Q}{\pi d^2 \sqrt{gH}}$$ **Eq. (14)**

where

V_{out} stands for the velocity of the fluid at the outlet

d stands for the drain diameter

Q stands for the flowrate

g stands for the gravity level

H stands for the fluid height

and substituting in the values for the Froude number, the outlet diameter, earth standard gravity, and the fluid height, the flow rates could be solved. The maximum flowrate was determined to be 0.086 gallons per minute. The minimum flowrate was determined to be 0.043 gallons per minute. These flowrates are similar to the 0.1 gallon per minute flowrate that Smith used in his 0.25 inch diameter outlet experimental run. These flowrates should ensure that the size of the vortex varies from a mere dimple on the water surface to a fully formed vortex on the verge of drawing air into the drain.

From the new calculations of the Froude and Reynolds numbers, the performance of the experiment was determined:

Table 16 - Froude numbers at various flowrates

Froude number @ minimum flowrate

.2G	.4G	.6G	.8G	1G	1.2G	1.4G	1.6G	1.8G	2G
0.44	0.31	0.25	0.22	0.2	0.18	0.16	0.15	0.14	0.14

Froude number @ medium flowrate

.2G	.4G	.6G	.8G	1G	1.2G	1.4G	1.6G	1.8G	2G
0.67	0.47	0.38	0.33	0.3	0.27	0.25	0.23	0.22	0.21

Froude number @ maximum

.2G	.4G	.6G	.8G	1G	1.2G	1.4G	1.6G	1.8G	2G
0.89	0.63	0.51	0.44	.4	0.37	0.33	0.31	0.29	0.28

At the minimum flow rate there was air entrainment at .2 G's. Between .4 G's and 1G the vortex shrinks from a full vortex on the verge of air entrainment to just a dimple in the water. From 1.2 G's to 2 G's there was no vortex formation

At the medium flow rate air entrainment occurs between .2 and .4 G's. Beginning at .6 G's the vortex ceases to pull in air. Between .8 G's and 2 G's the vortex shrinks down to a dimple.

For the maximum flow rate air entrainment occurs between .2 G's and .8 G's. Between 1 G and 2 G's the vortex goes from being on the verge of pulling in air, to having a height of about half that of the fluid.

3.3.3 DETERMINATION OF CRITICAL RADIUS

The angular velocity of the fluid in the forced vortex was found by using the relation of the tangential velocity to the angular velocity:

$$V_\theta = \Omega r \qquad \qquad \textbf{Eq. (15)}$$

To find the relationship between the critical radius, the circulation, and the angular velocity, relationships between the tangential velocity and the circulation (Smith, p. 10) were used:

$$V_\theta = \frac{\Gamma r}{2\pi a^2} \text{ for r}\leq\text{a} \qquad \qquad \textbf{Eq. (16)}$$

$$V_\theta = \frac{\Gamma}{2\pi r} \text{ for r}\geq\text{a} \qquad \qquad \textbf{Eq. (17)}$$

Where:
    Γ = Circulation
    π = Pi
    a = Critical radius
    r = radius at which angular velocity is taken
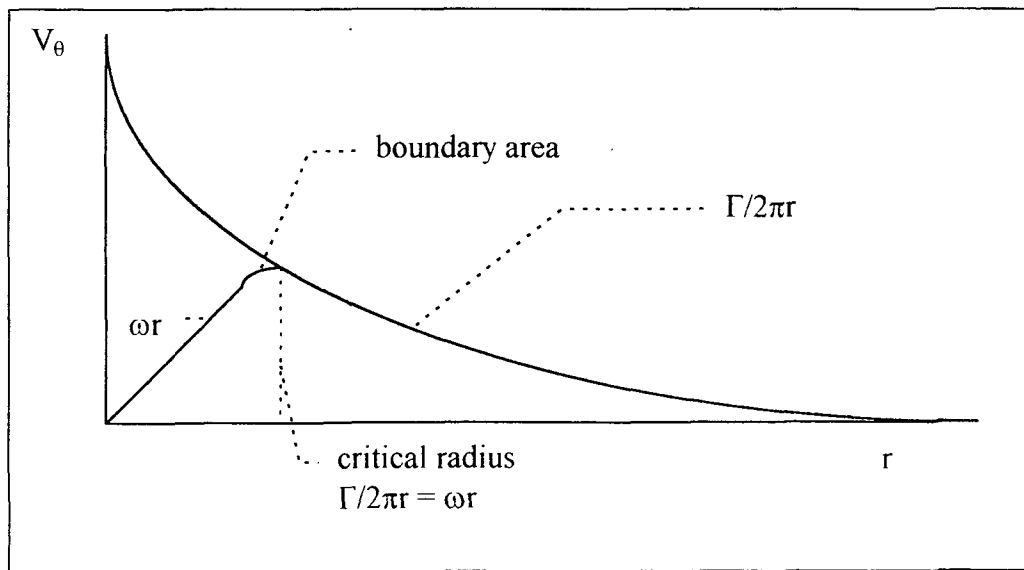
Figure 10 - Diagram of angular velocity in a Rankine combined vortex

The critical radius was found where the angular velocity of the free vortex (Eq. 15) equaled the angular velocity of the forced vortex (Eq. 16). This is where the edge of the forced vortex meets the edge of the free vortex, creating the Rankine combined vortex. To do this analytically Eq. 16 was simplified into Eq. 17 when r was equal to a. Therefore:

$$V_\theta = \frac{\Gamma}{2\pi r} \qquad \text{Eq. (18)}$$

Eq. 18 could be rewritten as:

$$V_\theta = \frac{\Gamma}{2\pi r_c} \qquad \text{Eq. (19)}$$

This equation was then substituted into Eq. 15 and the critical radius was solved for.

$$r_c = \sqrt{\frac{\Gamma}{2\pi\Omega}} \qquad \text{Eq. (20)}$$

Where:

Γ denotes the circulation

Ω denotes the angular velocity of the fluid.

The values of .18 to .38 ft^2/s at 1 G Smith(1994)for the range of circulation were substituted into the above equation. Because the experiment was being conducted within a 4 inch diameter chamber, the critical radius could range from a minimum of 0 inches to a maximum possible critical radius of 2 inches. By picking an arbitrary value within this range, a critical radius could be found. The problem with this was that there were an infinite number of critical radii that could be found. Therefore a minimum critical radius of 0.2 inches or 0.0166 feet, and a maximum critical radius of 2 inches were substituted

into Eq. 17. This yielded a minimum and maximum angular velocity which were used in a program to figure out what the Coriolis effects might be on the experiment. The actual critical radii can not be estimated until the experiment is run in space and the video footage has been analyzed.

3.3.4 DETERMINATION OF CORIOLIS EFFECTS

Because the vortex chamber would be located on a rotating platform in order to create the artificial gravity levels required by the experiment, there was some concern as to whether Coriolis acceleration would cause a problem for the experiment. In Cyr et al(1993), the number of .544 gallons per minute was given as the minimum flowrate needed to overcome the effects of Coriolis acceleration. Lelani and Muth(1992) developed a mathematical model of a combined Rankine vortex was developed. From this model they were able to determine the amount of tilt that would be caused due to Coriolis effects. However, in order to accurately model a vortex, the critical radius at which the free and forced components of the Rankine combined vortex join must be known.

The equations for free and forced vorticies (Eq. 15 and 16) were used in a computer program to solve for the critical radius. These equations related the circulation to the tangential velocity, and were equal when the radius r was equal to the radius a. That radius was known as the critical radius. It could be seen that when r was equal to a, Eq. 16 simplified into Eq. 17. Rewriting Eq. 21 at the critical radius yielded:

$$V_\theta = \frac{\Gamma}{2\pi r_c} \qquad\qquad \textbf{Eq. (21)}$$

Equation 21 also had another form, that of the forced rotation:

$$V_\theta = \Omega r \quad \text{for } r \leq r_c \qquad \text{Eq. (22)}$$

By varying the parameters independently and solving for the angular velocity where Eqs. 21 and 22 were equal, it was thought that a single correct value could be found for the critical radius, but unfortunately it was found that there were an infinite number of different critical radii that could be found. For any angular velocity, a critical radius could be found, and vice versa..

Another approach was taken. Because the range of critical radii was known, since it must be within the range from the center to the container walls, it was decided to vary the critical radius and find the range of angular velocities that could be used. By using Eq. 21, the range of tangential velocities was found by substituting in the range of circulation's, from .18 to .38, and varying the critical radius from 1% to 100% of the overall container radius. The tangential velocity ranged from 0.1718 to 36.287 ft/s. This range was then substituted into Eq. 22, and for various radii from 1% to 100% of the container radius the angular velocity was found. The resulting range of angular velocities was from 1.0 rad/s to 2.2 x 10^4 rad/s.

The range of angular velocities of the platform was found by using the equation

$$g = \omega^2 r_p \qquad \text{Eq. (23)}$$

where:

g stands for the gravity level (ft/s^2)

ω stands for the angular velocity of the platform (rad/s)

r_p stands for the radius of the platform (ft)

Since the gravity levels at which the experiment would operate were known, and the radius of the platform is constant, the angular velocities were easily obtained. The angular velocities ranged from 2.8 rad/s to 8.9 rad/s.

Once the range of fluid angular velocities, critical radii, and platform radii had been found, the pressure difference could be found by using the equation:

$$\Delta p = 2\rho\omega\Omega r_c^2 \ln\left(\frac{r}{r_c}\right)$$

Eq. (24)

where

p stands for the pressure (lb./ft^2)

ρ stands for the density (lb./ft^3)

ω stands for the platform angular velocity (rad/s)

Ω stands for the fluid angular velocity (rad/s)

r_c stands for the critical radius (ft)

r stands for the container radius (ft)

By substituting in the definition for the circulation:

$$\Gamma = 2\pi\Omega r_c^2 \qquad \text{when } r < r_c$$

Eq. (25)

into Eq. 24, it can be rewritten as

$$\Delta p = \frac{\rho\omega\Gamma \ln\left(\frac{r}{r_c}\right)}{\pi}$$

Eq. (26)

This was translated into inches of tilt by dividing by the density and artificial gravity and multiplying by 12 inches per foot which yielded:

$$\Delta height = \left| \frac{\omega \Gamma \ln\left(\dfrac{r}{r_c}\right)}{\pi G} \right| \qquad\qquad \textbf{Eq. (27)}$$

This equation was used to find out how much tilt there would be at a certain radius,

gravity level, and circulation. Because there were no specific values for the different

parameters of the equation, a range of tilts were found for the radii from the center to the

container wall for a specified gravity level and circulation.

From the tilt data it was found that at less than a certain critical radius the tilt

would be greater than .29 inches. This level was important because it was the clearance

between the top of the cylinder and the height of the fluid filled to a tenth of an inch

above the height of the inlet. If the tilt was greater than this amount then there would be

no vortex formation because the free surface would be lost. The minimum percentage of

the critical radii with respect to the container radius for each circulation and gravity level

are tabulated below.

Table 17 - Table of minimum critical radii at a circulation of .18 ft²/s and various gravity levels for which the tilt will not affect the performance of the experiment

.2 G's	.4 G's	.6 G's	.8 G's	1 G	1.2 G's	1.4 G's	1.6 G's	1.8 G's	2 G's
39%	26%	21%	15%	11%	10%	8%	7%	6%	5%

Table 18 - Table of minimum critical radii at a circulation of .38 ft²/s and various gravity levels for which the tilt will not affect the performance of the experiment

.2 G's	.4 G's	.6 G's	.8 G's	1 G	1.2 G's	1.4 G's	1.6 G's	1.8 G's	2 G's
62%	55%	44%	40%	36%	32%	28%	27%	26%	23%

what these tables signify are that if experiment was run for a circulation of .18 ft^2/s and 0.2 gravities, then if the critical radius was less then 39% of the container radius, the tilt would be large enough to contact the top of the container. In direct observation of the experiment during operation it was noticed that the critical radius typically varied between 2 and 20 percent of the container radius. If this range holds true in space, then for a circulation of .18 ft^2/s the surface of the fluid would probably tilt enough to contact the top of the container and interrupt the formation of a vortex. For a circulation of .38 ft^2/s there would always be too much tilt to form a vortex. That is speculation, however, since the range of critical radii are unknown, and will not be known until the RFF experiment is performed in space.

3.3.5 PLACEMENT OF COMPONENTS

This is the layout of the components. It shows relative placements, but it is not to scale

RFF CPU
6 in x 6 in
x 2.5 in
height

Motor

Motor and
Pump
Controllers.
5 in (width) x
6 in (length)x
5 in (height)
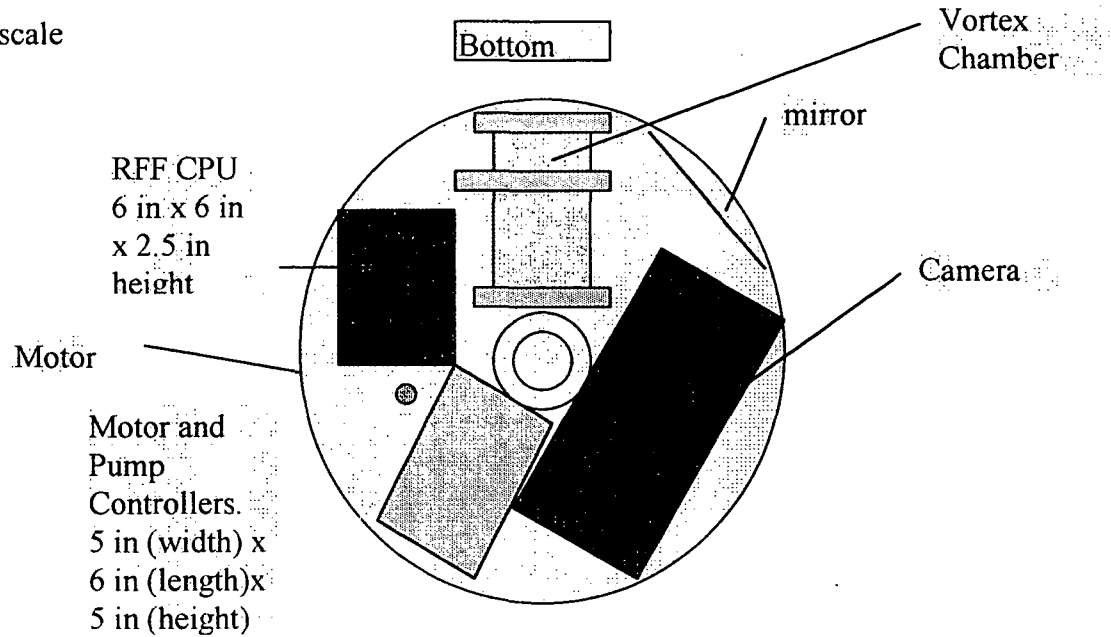
figure 11 - Component layout on the RFF lower plate

Lamp

Pump

Motor

Motor and
Pump
Controllers
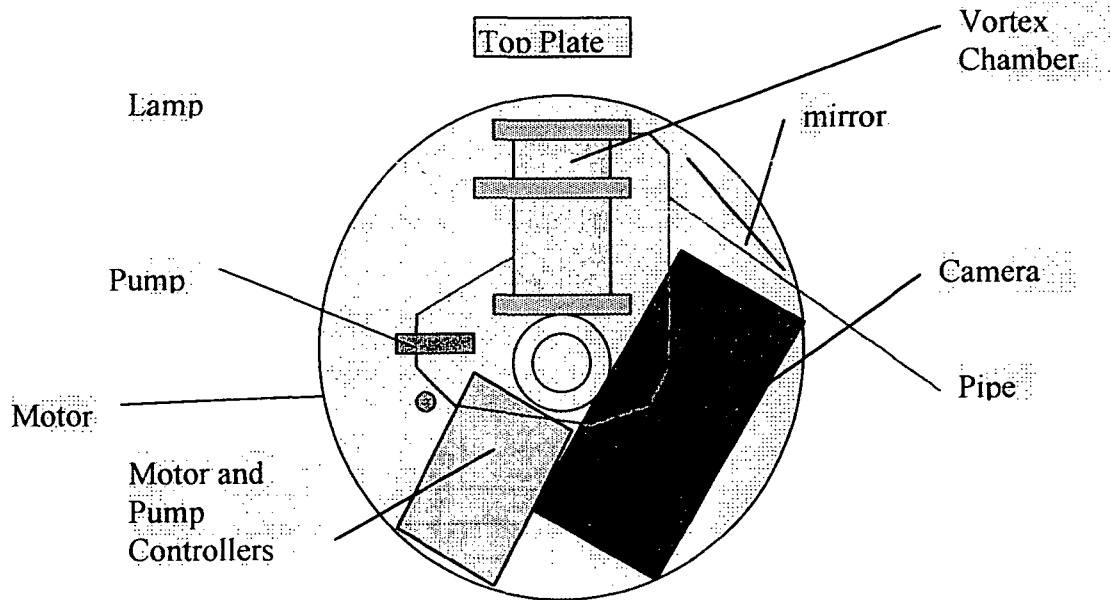
figure 12 - Component layout on the RFF upper plate

This is the most logical layout, considering the number of components that must be mounted on the rotating platform. It will be subject to change once the sizes of the motor controller and pump controller boards, the RFF CPU, and ultrasonic flowmeter have been determined, however, unless there are drastic changes in the size of the unknown components, all changes should be relatively minor. Currently, there is a space 6 inches long, 5 inches wide, and 5 inches high that is allocated for the motor and pump controllers, which would be stacked on top of each other as specified by the electrical engineering payload integration team. There is a 6 inch wide by 6 inch long by 2.5 inch high space allocated for the RFF CPU. The 2.5 inch ceiling is given to enable the pump to be mounted on the top plate, right above the CPU.

3.3.6 MIRROR ASSEMBLY

The dimensions for the mirror assembly were determined using Cadkey 5. First lines were extended from the desired viewing area of the vortex chamber, see figure 9. Then lines were extended from the lens of the camera box. These lines converged on a point that would have been the apparent position of the virtual image. The angle formed by the outside two lines was bisected with a line. This line would be perpendicular to the mirror on the platform. As long as the mirror was perpendicular to this bisector, and it had a large enough reflecting surface to reflect the image, then the mirror would always reflect an image into the camera, however this freedom is constrained by the need to keep the mirror on the platform.

As can be seen in figure 10 the angle between the lines of reflection from the far side of the chamber to the far side of the camera lens is 154.2 degrees, and the angle for

the near side of the chamber and lens is 82.8 degrees. The width of reflection is 1.84

inches. This is the worst case scenario for the mirror. It represents the closest that the

mirror can be to both components and still reflect the full image.
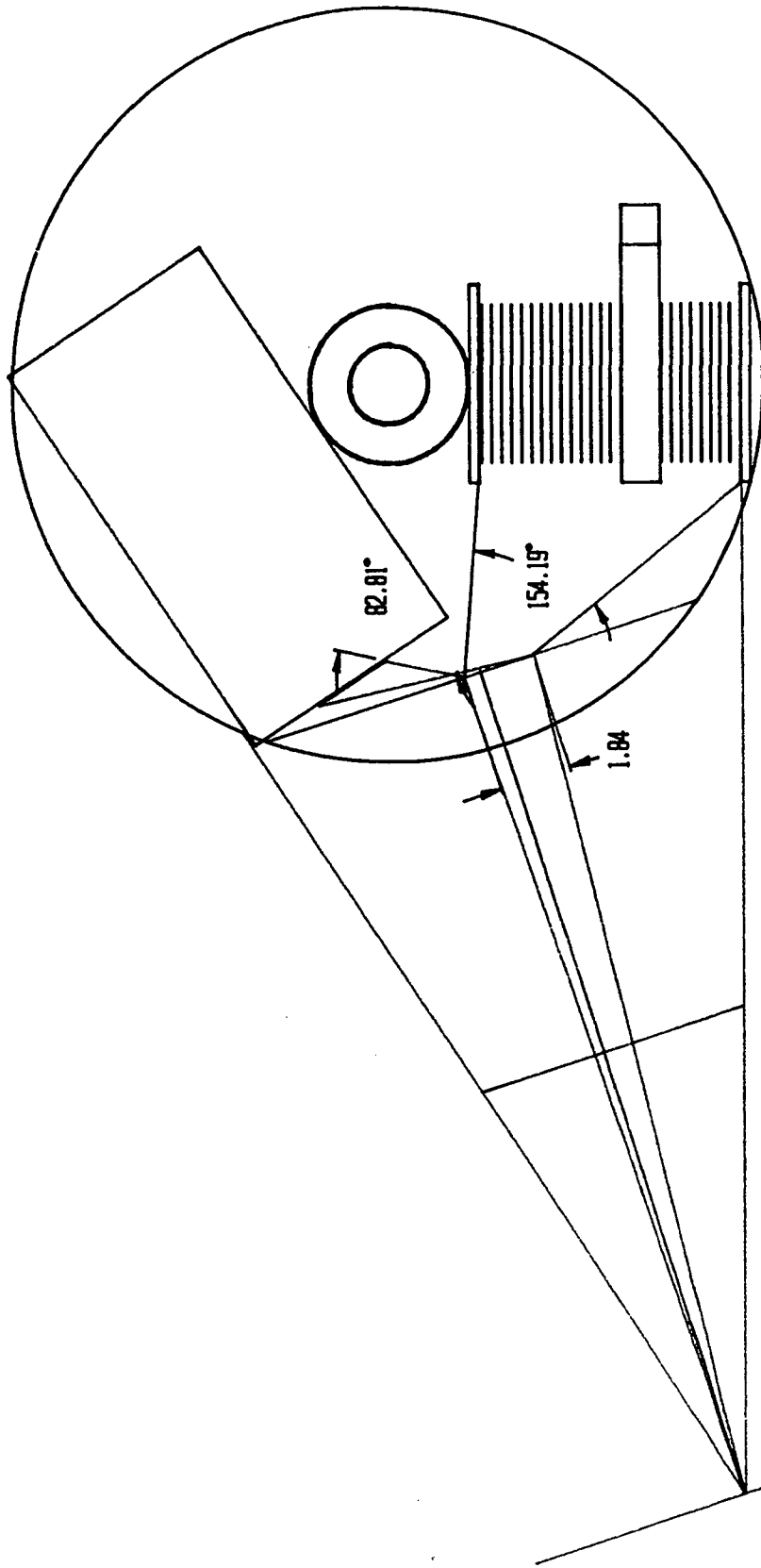
82.81°

154.19°

1.84

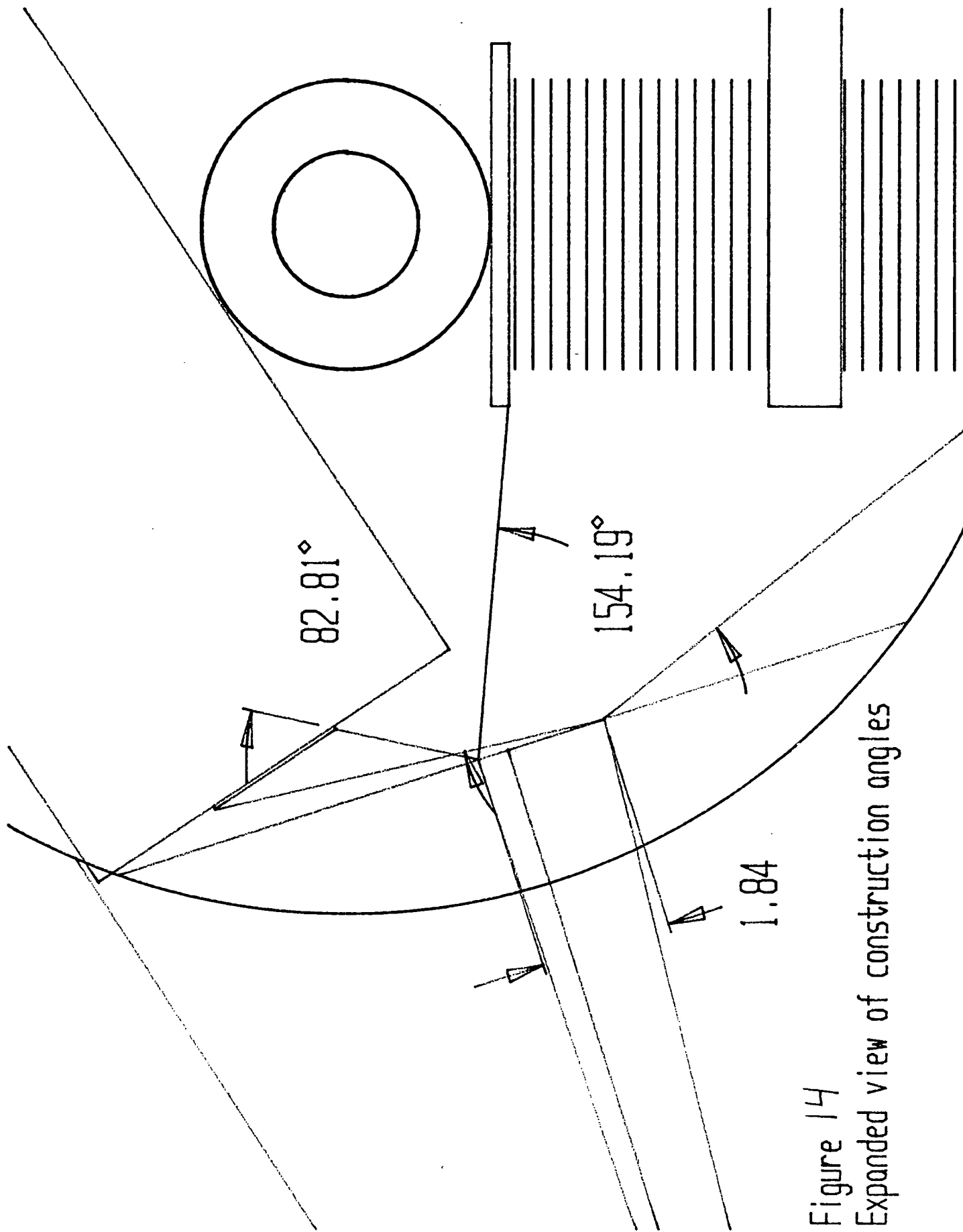Figure 13 Plot of Construction angles for mirror

82.81°

154.19°

1.84

Figure 14
Expanded view of construction angles
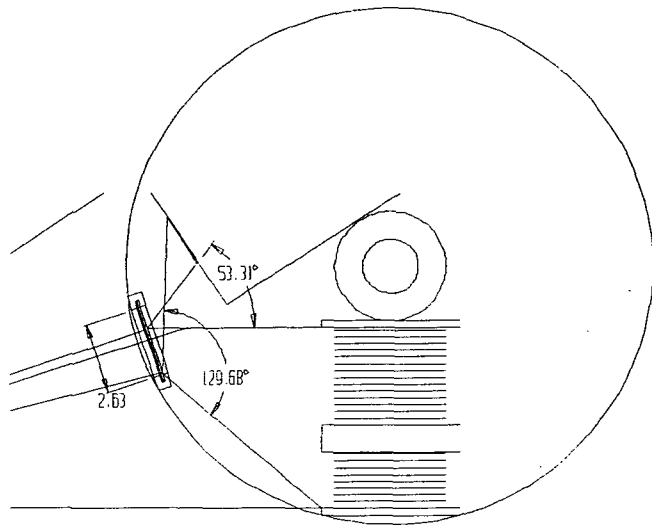
Figure 15 - Expanded view of mirror assembly placement

A mirror assembly was then designed using this data. Using Cadkey 5, a sample mirror was placed as far out toward the edge of the platform as possible while still reflecting the full image of the vortex chamber into the camera box. It was determined that the maximum width of the mirror assembly was 3.63 inches, while the angle of reflection between the near side of the chamber and lens was 53.31 degrees and the angle between the far side of the chamber and lens was 129.68 degrees. This arrangement will provide a complete view of the vortex chamber, however, the view will be distorted. Due to the limited space available for the mirror, it is impossible to get a better viewing angle.

The mirror assembly would be made out of .5 wide x .5 inch high 6061-T6 aluminum bar stock.
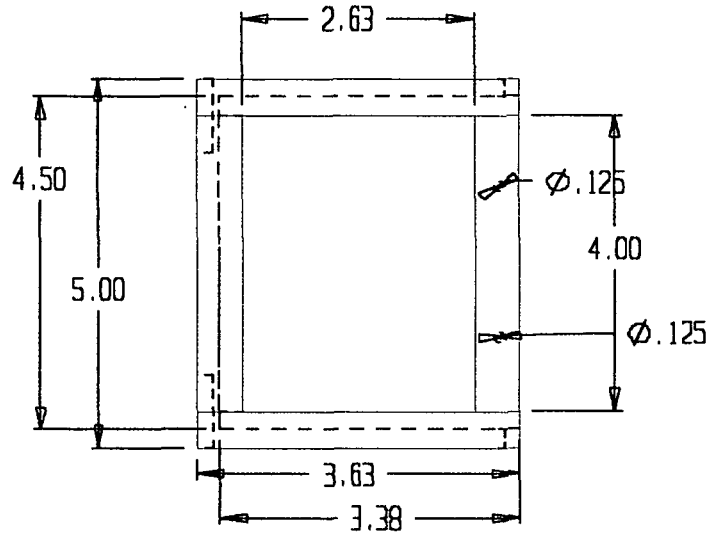
Figure 16 - Front view of mirror assembly

The top and bottom pieces of stock would have grooves .25 inches in depth and .125 inches in width cut along 3.38 of the 3.63 inches of the length of the bar stock. The side pieces would be different. The left bar would be .5 inches wide x .5 inches high x 4 inches long. A groove of .25 inches in depth, and .125 inches in width would be milled out of the right face of the bar. The right bar would be .5 inches wide x .1875 inches high x 4 inches in length. This would allow the mirror to slide over the right bar into the groove possessed by the other three bars. This groove would be padded with a thin strip of rubber to cushion the mirror. The four bars should be joined by brazing, so that there is very little warping. This in turn would allow the mirror to slide easily into the groove. A mirror that was 4.5 inches high and 3 inches wide was required for the assembly. This would allow just enough space on the right bar to screw two padded mirror holders, of

81

the type that can be found in most hardware stores, in to the assigned holes to secure the mirror into place.
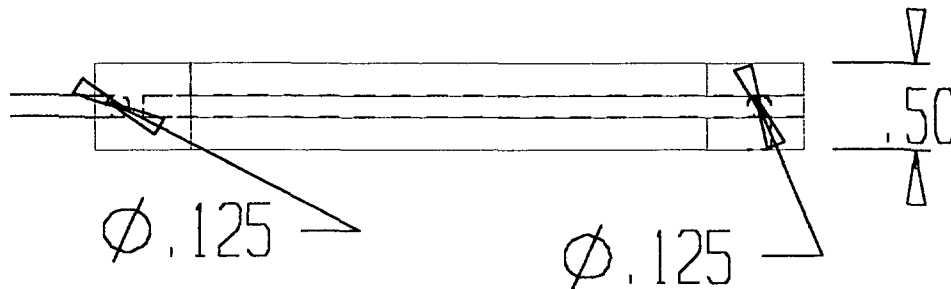

Figure 17 - Top view of mirror assembly

The left hand side of the mirror assembly would be bolted to the RFF platform using eighth inch diameter one inch long screws. The right hand side of the mirror assembly would be secured by eighth inch diameter quarter inch long screws. These screws could not be made any longer because they would interfere with the passage of the mirror into the groove. These screws should be more than adequate to hold the mirror assembly in place. The volume of the bar stock minus the volume of the grooves and the volume of the screw holes is 2.93 in^3. Since aluminum 6061-T6 has a density of .098 lb./in^3 the weight of the mirror assembly minus the mirror is .287 lb.. If the mirror weight is estimated to be .5 lb., then the total weight of the assembly would be .787 lb.. Under a 20 G load, this would equal a weight of 15.75 lb.. Insignificant compared to the strength of the screws.
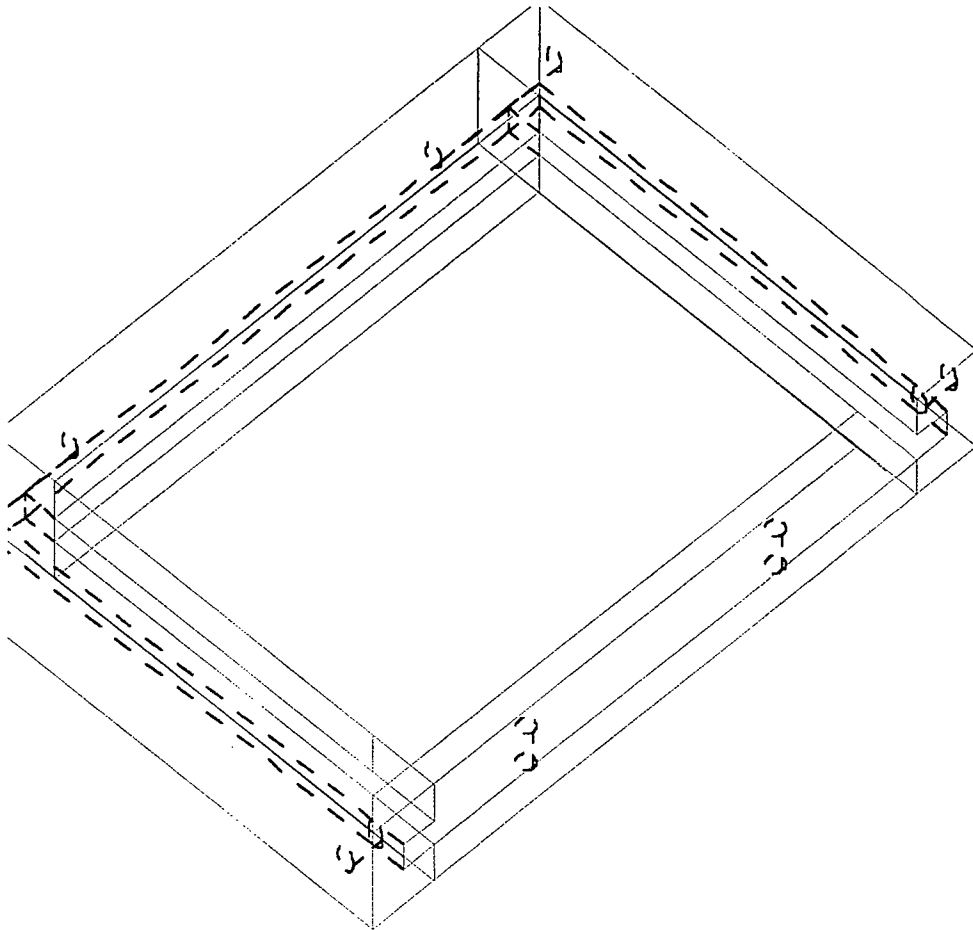
Figure 18 - Isometric view of mirror assembly

Figure shows an isometric view of the mirror assembly. An Aries version will be

provided in the final draft.

3.3.7 MOUNTING OF COMPONENTS

Currently the plan is to bolt everything into place. The Vortex chamber would be

bolted to the platform through the top and bottom plates. The same would be true of the

camera box. The mirror will be held in place by two brackets which would be bolted to

both plates. The mirror brackets are essentially pieces of bar stock which have grooves

machined in them to slide the mirror into. Each end of the bracket is then bolted into the platform. The motor has already been bolted into place. The pump will be attached to a special, vibration damping base which will be bolted to the top plate. How the motor controller, pump controller, and RFF CPU boards will be bolted into place will depend on how they are packaged. The lamp will be bolted to the top plate in line with the aluminum block through the middle of the vortex in order to reduce the glare in the camera.

3.3.8 FLUID FILLING METHOD

Because of the choice of silicon oil as the working fluid for the experiment, the vortex chamber must be filled in such a way as to ensure that no air is left in the chamber for the liquid to react with. The process should also be relatively easy to ensure that the technicians who prepare the GASCan for launch experience no problems with filling the chamber. Becz et al(1993) developed a fluid filling procedure that was expanded upon this year:

Fluid filling procedure:

1. Open the filling hole and the purge hole on the Vortex Chamber.

2. Fill the chamber with the silicon oil.

3. Close both holes.

4. Run the pump for one minute to insure that the air in the pipes is purged.

5. Open both holes again.

6. Using a noncombustive gas, the a hose from the tank containing the gas will be inserted into the fluid filling hole, while the purge hole is left open. The noncombustive gas will be used to purge the system for a minimum of two minutes which will ensure that all combustive gasses have been evacuated.

7. Both holes will be shut, and any spillage will be wiped up.

The interface between the hose and the hole in the vortex chamber needs to be investigated. It is possible that a special connector will be needed.

3.4 Integrated Support Structure (ISS)

Analysis, design and manufacturing of parts pertaining to the ISS follows. This section is subdivided into areas concerning parts manufactured, redesign of the lateral bumpers, battery box redesign, and a FEA of the ISS support legs.

3.4.1 ISS Components Manufactured by 1994-1995 Payload Integration Team

The 1994-95 Payload Integration team completed manufacture of the following ISS components: (the person responsible for manufacturing of the part is credited for reference purposes)

- X-cell (quantity 2) and J-cell (quantity 3) battery boxes. [1994-1995 Payload Integration Team, Welding - Paul Curci]

- Welding of the Tri-wall Structure

Materials for the ISS lateral bumpers, ISS support legs and battery enclosure are in the possession of the Payload Integration team.

3.4.2 Lateral Bumper Redesign

The lateral support bumpers were redesigned from the 1993-1994 design. The redesigned bumper is shown in Fig. 19. An exploded view of the bumper assembly is shown in Fig. 20. Figures 21 and 22 show the bumpers in their correct mounting position on the battery enclosure. A dimensioned drawing is shown in Appendix F. The redesign was necessary as there were no complete dimensioned drawings left from last year's team to work from. Also, in order for their design to work, it would not be accessible from the lower portion of the GASCan, as NASA requires.

Using the guidelines set out by NASA's GAS Experimenter's Handbook, the bumper design must meet the following guidelines:

- A minimum surface area of 4 square inches should be used for each bumper pad. The bumper face should have a 9.875 in. radius where it contacts the container.

- Bumpers should be equally spaced around the circumference of the payload.

- Where the bumper contacts the container wall, it should be faced with a resilient material at least 1/8 inch thick to protect the container. If the container is evacuated, a non-outgassing material such as Viton should be selected. If the bumper face is not round, it should have a minimum radius of 0.4 inches.

- It is very important to provide a positive locking device for the bumpers. You should not depend on friction or a set screw alone to hold them in place.

- After installing your payload in the container, bumper adjustment should be accessible from the open lower end of the container.
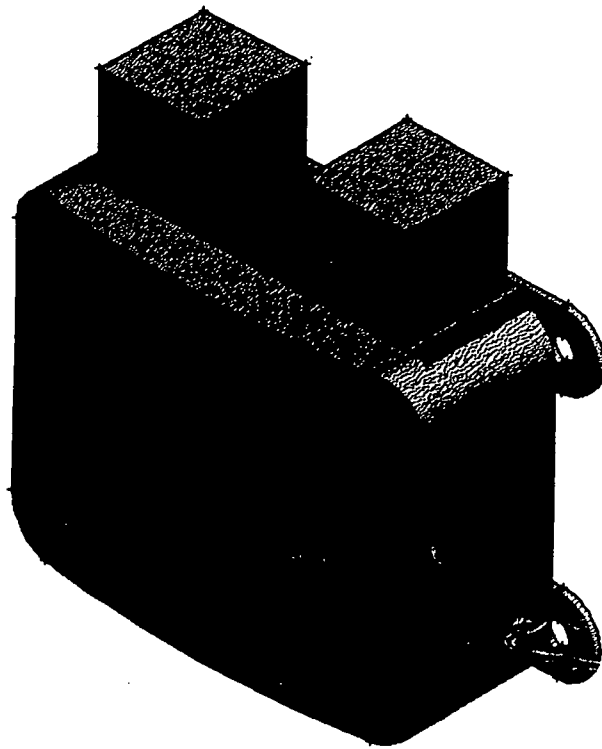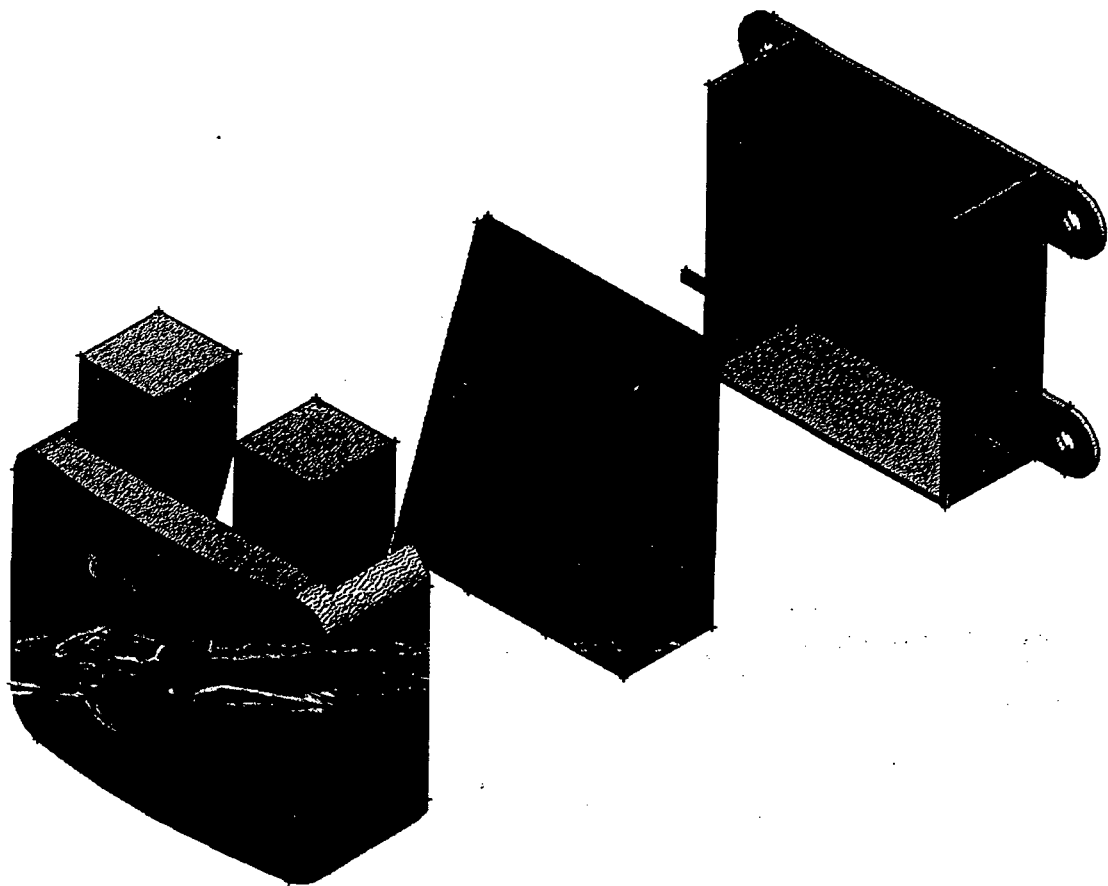
Figure 19 -
Lateral Bumper Assembly

Figure 20 -
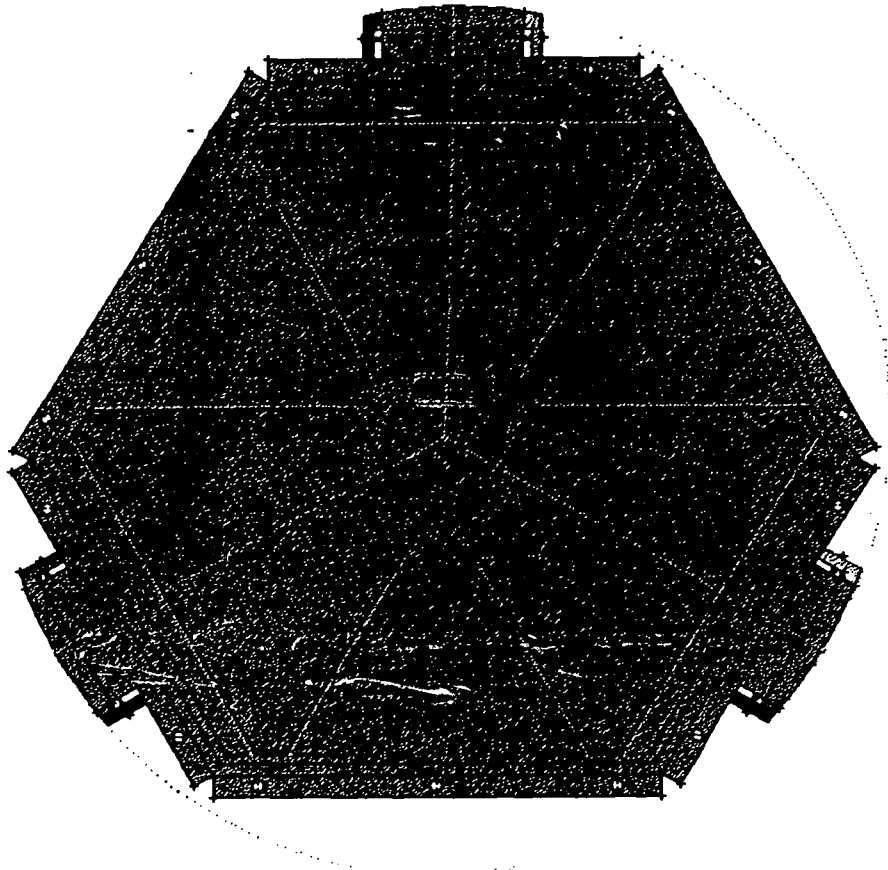Exploded View of Lateral Bumper Assembly

C-2

Figure 21 -
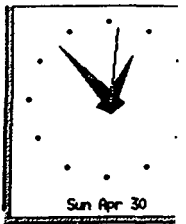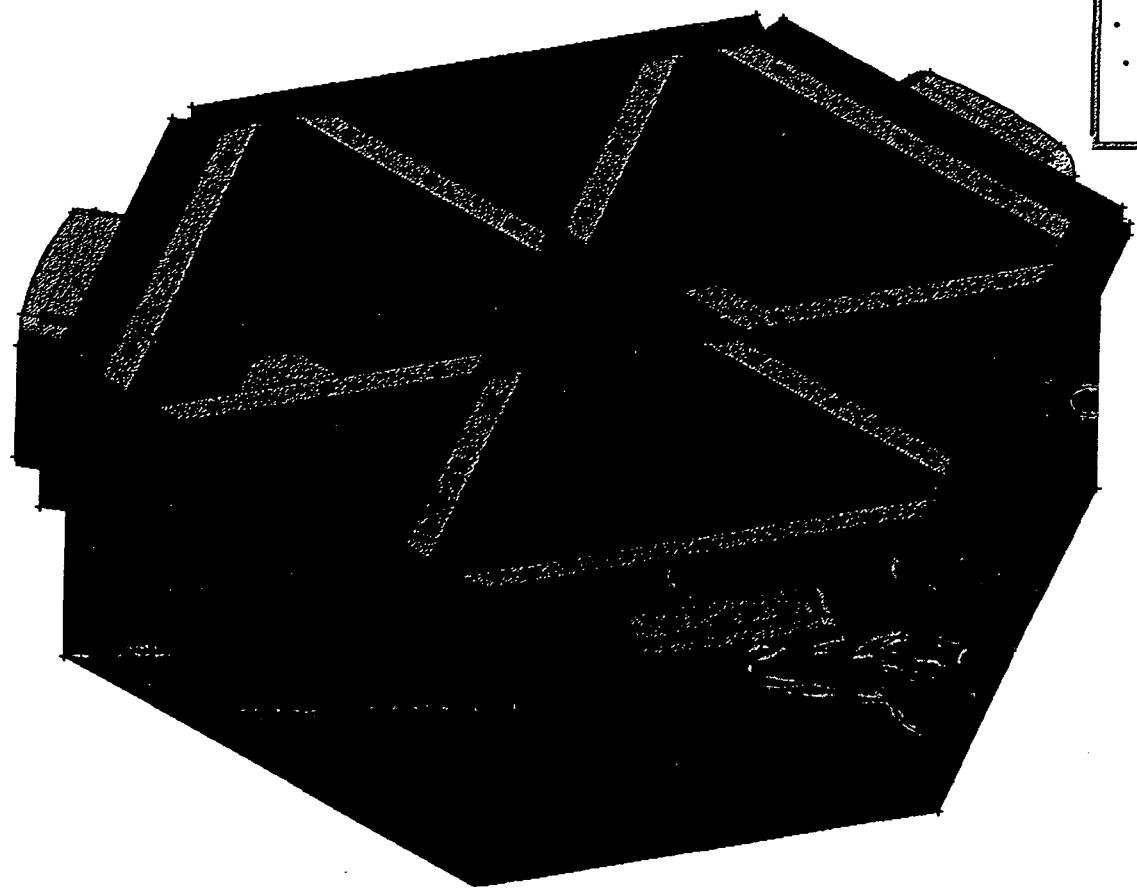Battery Enclosure showing bumper attachment

Figure 22 -
Battery Box Battery Enclosure Showing Bumper Attachment

This design was modeled qualitatively from the previous design including many of the same features. The design consists of the main bumper body (Al 2024-T4), an internal wedge (Al 2024-T4), a bumper bracket (AISI 1010 steel), two 1/8 steel pins, a 3/8" 24 UNF 300 series stainless steel bolt, two nylon locking nuts a 300 series stainless steel flat washer and lock washer.

Changes from the previous model include the elimination of stainless steel as the material for the internal wedge. This has been replaced with Al 2024-T4. This substitution translate to a weight savings. The assembly weighs 2.3 lb. There will be 3 bumper assemblies on the ISS, translating to 6.9 pounds. The current design is about 1.5 times larger than the previous design. The area of contact is 12.8 square inches, with radii of 0.4 in at the corners. This larger bumper size will reduce the stresses on the GASCan wall and conversely, the battery enclosure wall to which it is fastened.

The amount of bumper adjustment has been increased in this design through the addition of two one inch protrusions. A screw and washer push against these protrusions as the screw is tightened, sliding the bumper against its internal wedge. This design fastens the internal wedge against the mounting bracket with four 1/8"-40 UNC 300 series stainless steel bolts. The bumper plate is fastened to the rest of the assembly by two 1/8 inch steel pins that fit to a guide track. This keeps the bumper assembly intact while it is not wedged against the GASCan's inner diameter. The bumpers allow for 0.312 inches of adjustment. The distance that the bumpers must span is 1.825 inches. The distance they are capable of spanning is 2.000 inches. This extra adjustability will provide a margin of safety for dimensional errors inherent in manufacturing.

In order to prevent loosening of the bumper assembly during the mission, two nylon locking nuts are countersunk into the bottom of the internal wedge. This will also allow tightening of the 3/8 bolt to be the only adjustment necessary to change bumper position. The bumper assemblies will be mounted to the battery enclosure with the bolt head facing down, so bumper adjustment will be possible from the lower end of the container.

A 1/8 inch Viton strip will be fixed to the surface of the bumper pad as described in the 1993-1994 Payload Integration MQP by Brown et al.

Most of the force on the bumper will be against the bumper plate. The size of the internal wedge parts preclude any problems concerning stress. The most likely situation for failure is at the mounting bracket. The wedge design will deflect some of the lateral force in a direction that will cause a shear force at the four attachment bolts. Assuming that the bumpers support half of the weight of the ISS at any time, a force of 2, 000 lb. can be expected under a 20g load. This force can be applied in two different ways. Two of the bumpers may support the load. In this case, the load applied to each bolt is 167 lb. in shear and 289 lb. in tension, for the fail-safe case. The second way the force may be applied is that all the force will be directed at a single bumper. The angle of the internal wedge deflects some of this load into shear; this value was calculated to be 596 lb.. In this case, the load applied to each bolt is then 199 lb. shear for the fail-safe case. There is no substantial tensile load in this case.

The bumper will fail in one of two ways: either the bolts will break or the bumper bracket will fail in tearout. The bearing stress can be calculated as:

$$\sigma_b = F / A_{bearing} \qquad \qquad \text{Eq. 28}$$

where F is the applied force and $A_{bearing} = ld$ where l is the length of bearing contact and d is the diameter of the pin or hole

Using the bearing stress equation yields a stress of 13 ksi. AISI 1010 steel has a tensile strength of 50 ksi, which is a factor of safety of 3.8.

Assuming 1/4"-28 UNF A-286 series stainless steel bolts, a bolt analysis yields and using a tensile load of 289 lb. and a shear load of 199 lb. simultaneously yields:

Table 19 - *Margin of Safety for Bolt Loaded in Tension and Shear*

Margin of Safety (yield case)	2.191
Margin of Safety (ultimate case)	1.048
Torque to preload (in-lb.)	41

The above bolt analysis superimposed the two worst case (20g) loads of tension and shear, with positive margins of safety resulting.

3.4.3 Battery Box Redesign

Before beginning the redesign, the concerns and guidelines of the previous MQP were addressed. These concerns were determined by NASA, the battery manufacturer, and by the 1993-94 Payload Integration Team:

- The batteries to be used are Gates Sealed-Lead J and X cell batteries.

- Since the J cell batteries produce significant amounts of hydrogen and oxygen, they must be housed in a container which is: a) sealed, b) corrosion-proof, and c) vented.

- The battery box must be vented through a) the upper end plate, and b) two 15 psi differential pressure relief valves.

93

- The J-cell batteries should be stored in a metal container because hydrogen can permeate a plastic container at a rapid rate.

- The batteries must supply adequate power to the experiments ; 27 J-cells and 12 X-cells are needed to fulfill the power requirement.

- The allotted space for the battery box is :
    R_{max} = 9.875 in (Radius of the middle plate)
    $Height_{max}$ = 6.0 in (Space between middle plate and RFF experiment)

- Weight must be a factor due to the overall GASCan weight constraint of 200 lb.

- The battery box and its interior must be easily accessible. Once the box is removed from the ISS, the batteries must be accessed within 5 minutes.

- The battery box design must facilitate electrical hook-up. After mechanically fastening the battery box to the ISS, the two vent lines and all electrical lines must be connected to the outside of the box within 5 minutes.

- The X-cells, in small quantities, do not need to be vented or pressurized, while the J-Cells need to be pressurized and vented in any quantity.

- Batteries of a certain string must be placed in close proximity to each other to facilitate ease of wiring, and they should be packed tightly to prevent them from falling out.

- Faulty batteries must be easily accessible for testing and replacement.

Again, the motivation for the battery box redesign was the lack of documentation present from previous MQPs. This battery redesign took into account factors that previous groups seemed to overlook including weight, size and manufacturability.

X-cell Design

94

The previous battery box had the x-cells distributed in four boxes, three batteries in each. The redesigned x-cell box places six batteries in each container, saving weight and producing a smaller foot print than four separate boxes, saving space.

The two x-cell battery boxes are constructed of 0.0625 inch AISI 1010 sheet steel. Initially, the chosen material was 6061-T6 aluminum. Due to the small thickness of the battery box walls, (0.125 inches using aluminum), welding of the structure would cause significant deformation due to thermal stresses. The only option for manufacturing the battery boxes was folding. After consultation with the WPI machine shop, it was discovered that, although pure aluminum (which is too weak) may be folded, other stronger grades of aluminum will tend to crack when folded. It was also found that aluminum will corrode more readily than steel. Therefore, the low carbon steel was chosen for strength. formability and corrosion resistance.

The redesigned x-cell battery box is shown in Figs. 23 and 24. Dimensioned drawing are in Appendix F. The open slot located at the bottom of the battery box allow the battery terminals to protrude. These slots also serve the purpose of reducing the weight of the battery box. A Viton rubber insert will be placed at the bottom of the battery box in order to provide a firm seat for the batteries and damp vibrations.
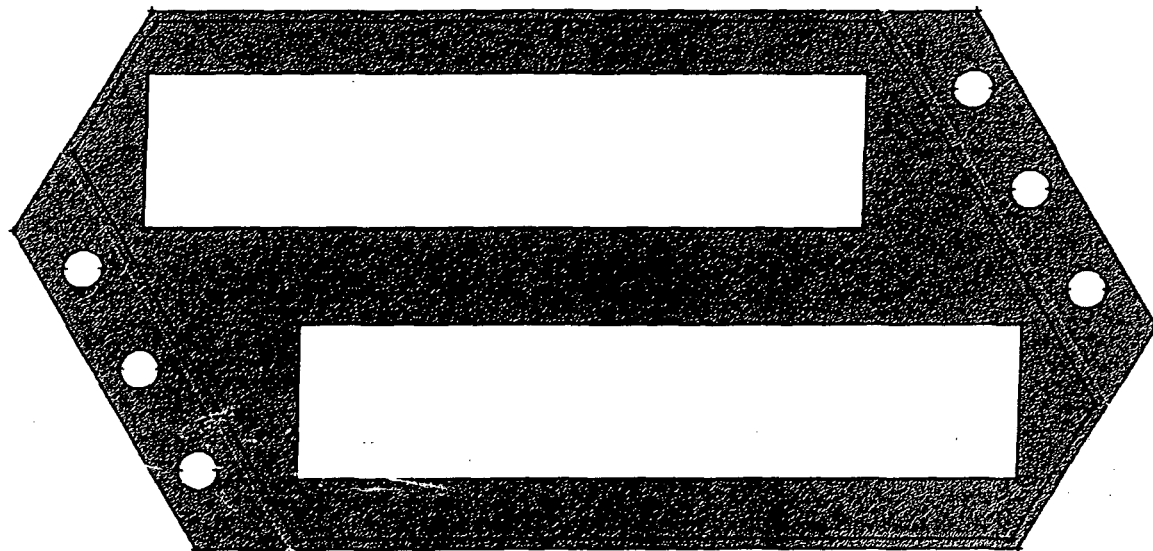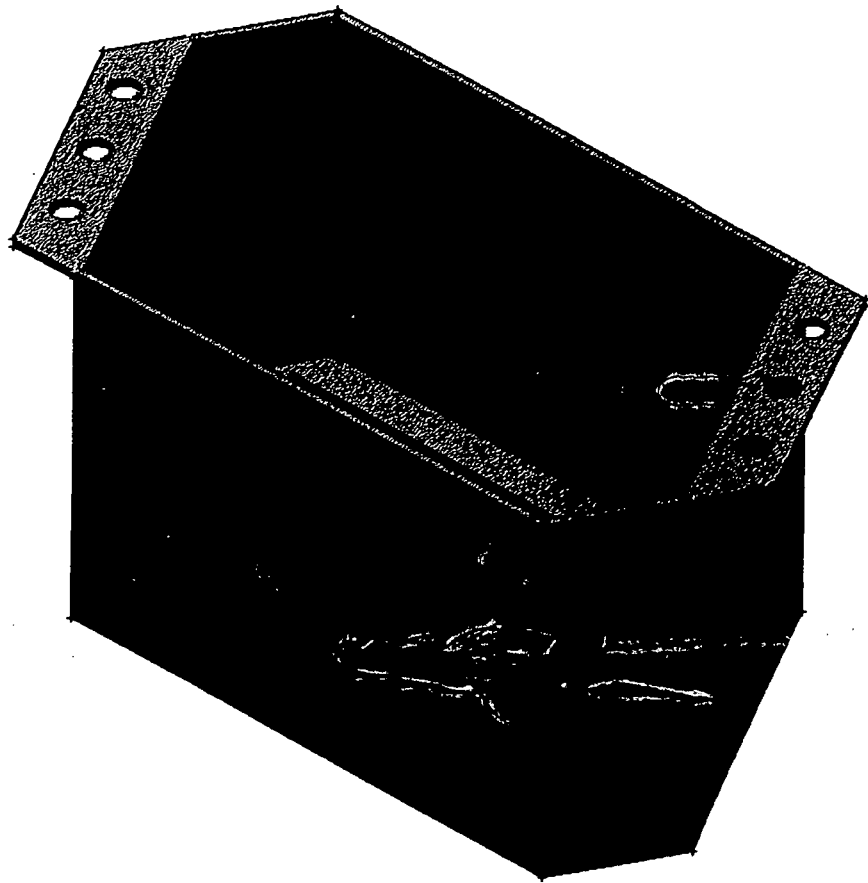
Figure 23 -
x-cell battery box

Figure 24 -
x-cell battery box

opposite sides of the flange opposite the flanges with the MGI canisters. The weight of the batteries will help offset the moment caused by the weight of the MGI canisters.

J-cell Design

The J-Cells are placed in three containers, 9 batteries per container. Here also, the footprint is smaller than the previous design. The weight of the three boxes can be distributed evenly across the ISS plate by mounting them 120^0 apart from each other.

The j-cell boxes are manufactured of AISI 1010 0.0625 inch sheet steel, for reasons cited above. Figures 25 and 26 show the final design. A dimensioned drawing is shown in Appendix F. The slots at the bottom of the j-cell box serve the same purpose as in the x-cell box and a Viton insert will also be utilized here. The j-cell batteries give off significant amounts of hydrogen and oxygen. Therefore, they must be situated in a sealed enclosure and vented to the NASA battery vent turret interface via stainless steel plumbing. This sealed enclosure is the subject of the next section.

Sealed Enclosure

Figure 27 shows the sealed j-cell battery enclosure in comparison to the ISS plate to which it is bolted. Figure 28 shows a top down view of the battery enclosure. Dimensioned drawings are presented in Appendix F.
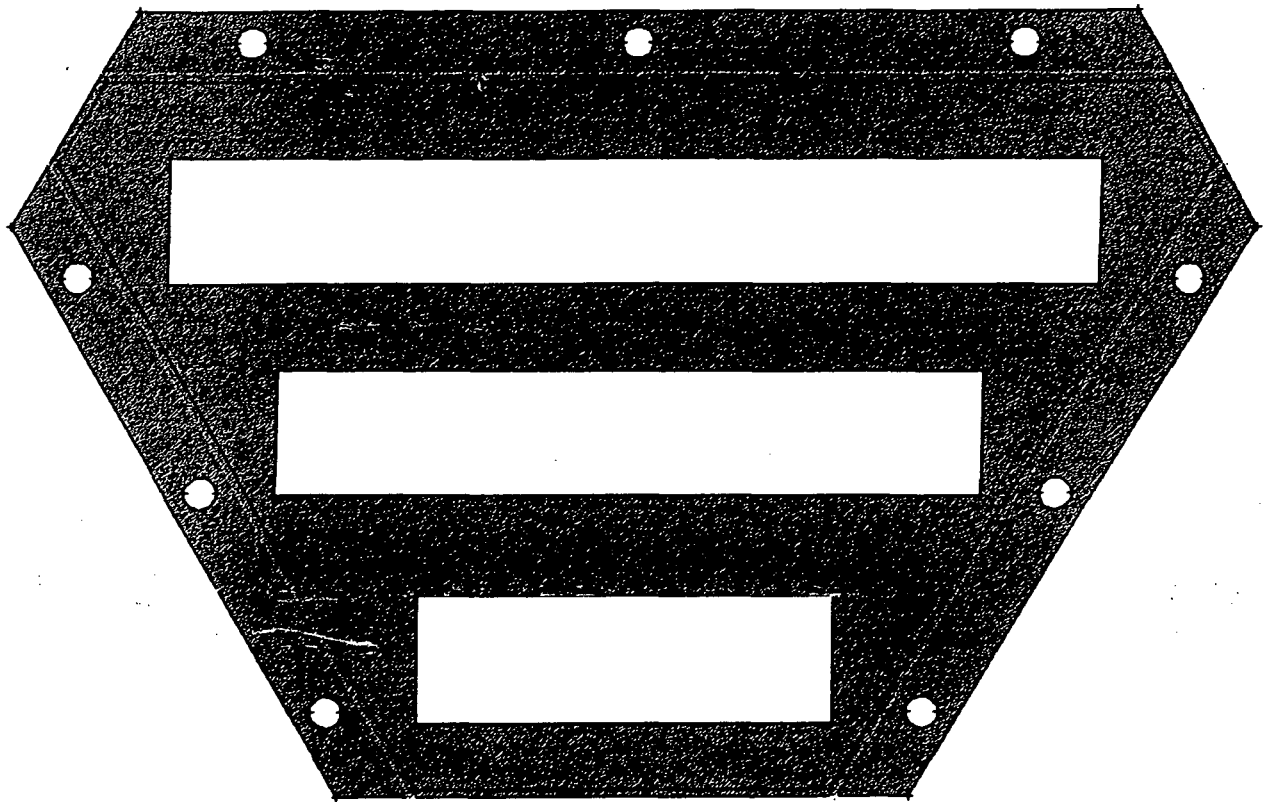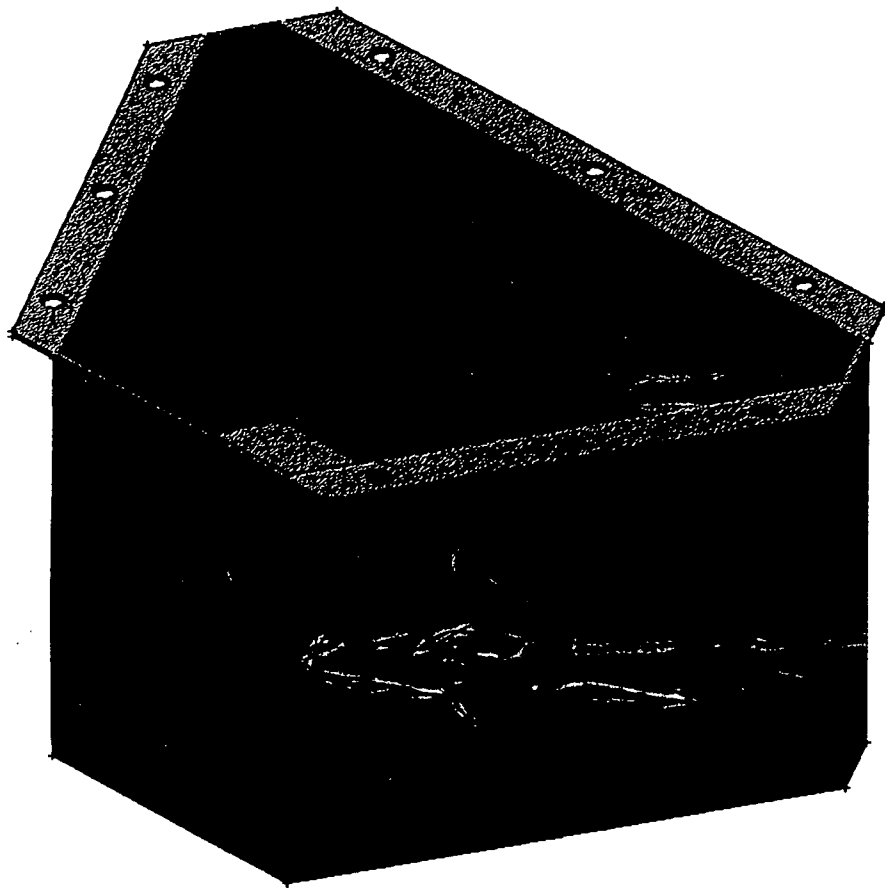
Figure 25 -
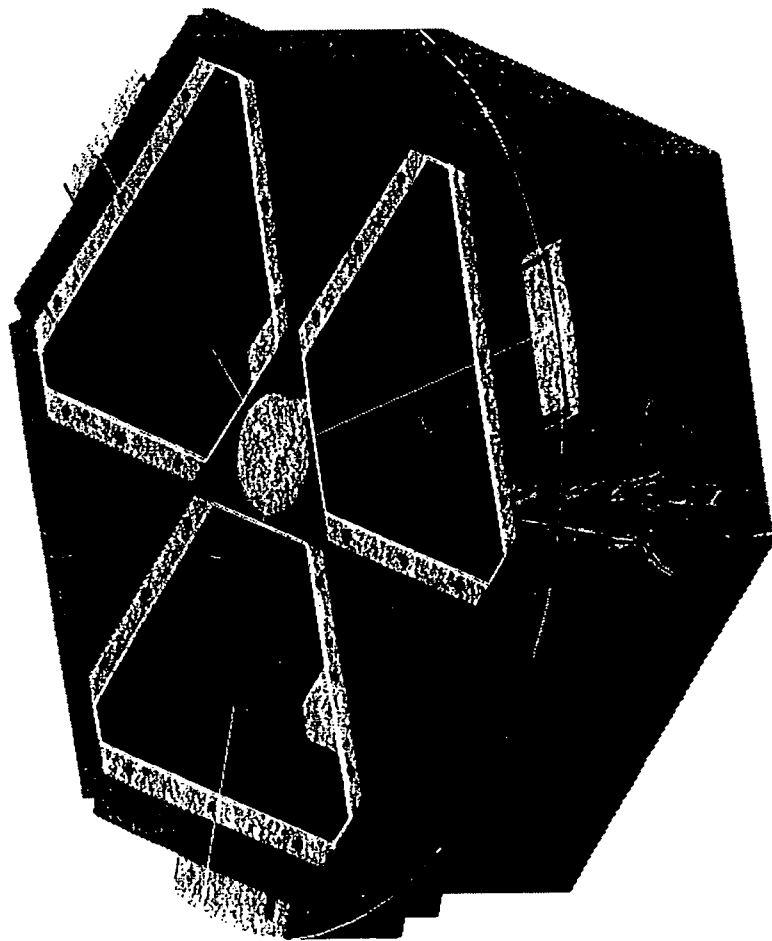J-Cell Battery Box

Figure 26 -
J-cell battery box

Figure 27 -
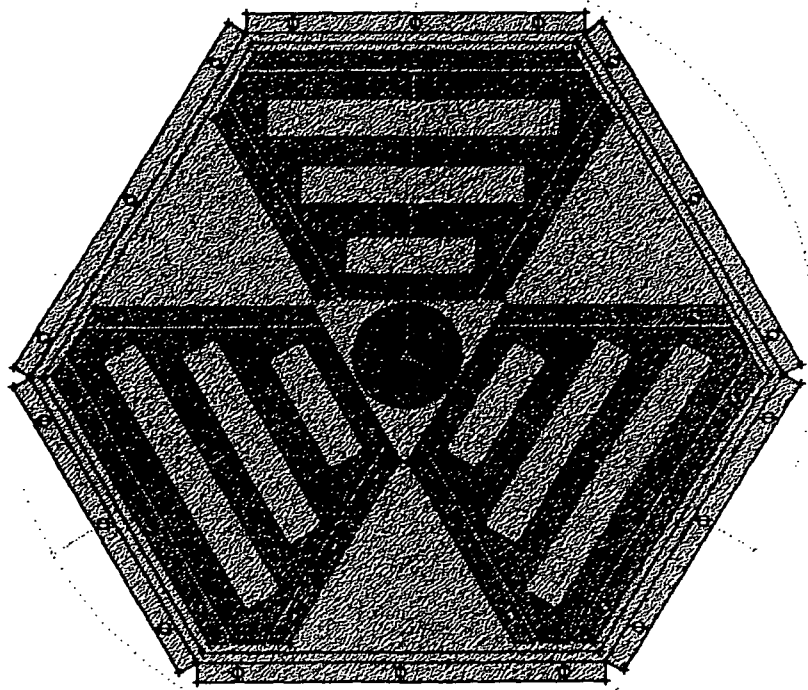Translucent View of Battery Box Assembly

Figure 28 -
Battery Box Assembly

The guidelines set out by the previous Integration team specified a maximum radius of 9.875 in. and the maximum height 6 inches for placing the battery enclosure. The height of the redesigned j-cell sealed enclosure is 5.875 inches. The battery enclosure fits entirely within the required radius. The current design offers over and 1/8 inch clearance between the battery enclosure and rotating RFF platform, while offering a 5/8 inch of clearance between the battery terminals and the battery enclosure.

Last year's Payload Integration MQP decided it was necessary for the enclosure to be 1/4 inch thick as it is a load bearing structure. The battery enclosure will be made of Al 6061-T6. The entire structure will be welded, as folding is not possible. When it becomes necessary to weld the structure, care should be taken in cutting the material to the correct dimensions to allow for proper welding of the structure. Paul Curci (see Appendix I) should be consulted before machining of the battery enclosure takes place.

The issue of battery removal/maintenance was investigated. To remove the battery box enclosure, the RFF platform is removed (via pin connection) and the enclosure is then slid down the shaft. The wiring between the RFF and ISS is connected/disconnected via a multi-pin connector. This should allow access to the batteries within 5 minutes.

An important issue in the design of the j-cell enclosure is the choice of materials for sealing the enclosure. A material recommended from previous MQPs and investigated by this year's group is Viton. Viton is a thermosetting elastomer that is resistant to hot oils, synthetic lubricants, gasoline, jet fuels, dilute mineral acids, aqueous salt solutions, alkali, and chlorinated solvents. Additionally, it was found that Viton A

will resist hydrogen corrosion up to 190^0 F. (Kroschwitz, 1987) Since NASA recommends Viton, Viton seals will be employed throughout the structure for consistency.

Corrosion Protection

The battery boxes will be painted to prevent corrosion from the lead acid batteries and general humidity. Corrosion and Corrosion Protection Handbook, by Philip A. Schweitzre, P.E., was consulted for a coating that would have a high chemical resistance. Polyamine Epoxy resin was chosen. Polyamine epoxy is chemically resistant to acids, acid salts, alkalies and organic solvents. Its limitations include the fact that it is harder and less flexible than other epoxies. In addition, it is less tolerant of moisture during application, however, it offers the greatest chemical and solvent resistance of the epoxies. When dry, it is resistant to temperatures of 225^0 F.

Bolt Analysis

The following table gives a breakdown of the weight of the x- and j-cell battery boxes.

	material	weight (lbf)	% of total battery weight
x-cell cages (2)	AISI 1010	2.2	2.6
j-cell cages (3)	AISI 1010	6.9	8.5
j-cell enclosure	Al 6061-T6	13.24	16.5
x-cell batteries	--------------	9.75	12.1
j-cell batteries	--------------	49.95	62.3
Total Weight		80.16	

Table 20 - Breakdown of Battery weight

From the above table, battery box weights under 20g loads may be determined.

For the x-cell battery box, under a 20g load (the ultimate case), the maximum possible load case will be 120 lb. in both tension and shear. Assuming 6 bolts, a fail-safe analysis would require that each bolt be able to withstand 24 lb. in tension and shear. Assuming a 1/8"-44 UNF A-286 stainless steel bolt, the bolt analysis under the above conditions yields:

Table 21 - _Margin of Safety for Bolt Loaded in Tension and Shear_

Margin of Safety (yield case)	6.233
Margin of Safety (ultimate case)	3.624
Torque to preload (in-lb.)	3

As the above margins of safety indicate, the bolt choice is acceptable.

For the j-cell battery box, under a 20g load (the ultimate case), the maximum possible load case will be 380 lb. in both tension and shear. Assuming 12 bolts, a fail-safe analysis would require that each bolt be able to withstand 35 lb. in tension and shear. Assuming a 1/8"-44 UNF A-286 stainless steel bolt, the bolt analysis under the above conditions yields:

Table 22 - _Margin of Safety for Bolt Loaded in Tension and Shear_

Margin of Safety (yield case)	3.960
Margin of Safety (ultimate case)	2.171
Torque to preload (in-lb.)	4

As the above margins of safety indicate, the bolt choice is acceptable.

For the battery enclosure, under a 20g load (the ultimate case), the maximum possible load case will be 265 lb. in both tension and shear. Assuming 18 bolts, a fail-safe analysis would require that each bolt be able to withstand 15 lb. in tension and shear.

However, the battery enclosure can also expect a maximum shear force of 2000 lb. from the lateral bumpers. The fail-safe load case is then 15 lb. in tension and 127 lb. in shear. Assuming a 1/4"-28 UNF A-286 stainless steel bolt, the bolt analysis under the above conditions yields:

Table 23 - *Margin of Safety for Bolt Loaded in Tension and Shear*

Margin of Safety (yield case)	5.655
Margin of Safety (ultimate case)	3.211
Torque to preload (in-lb.)	22

As the above margins of safety indicate, the bolt choice is acceptable.

3.4.4 FEM of ISS Support Legs

A finite element model of the ISS legs on ARIES. The ISS legs mount to the tri-wall and support the weight of the entire experiment structure. The ISS and RFF are suspended from these three legs which are in turn bolted to the top of the GAS canister's cover. The part is shown in Fig. 29. There is a particular bolting arrangement which is supplied in NASA's GAS Experimenter's Handbook. This bolting arrangement defines the geometry of the leg, which has already been determined by the 1993-94 Payload Integration MQP by Brown et al. The dimensions were double checked for accuracy by this integration team.

Figure 29 -
ISS Support Leg

ultimate case is then defined as a 20g load. In order to determine the loading, the maximum structure weight of 200 lbf was multiplied by the acceleration of gravity. This produces a yield load of 2000 lbf and an ultimate load of 4000 lbf. If two legs must support these loads for the design to be considered fail-safe, then the two legs must each support 1000 lbf and 2000 lbf for the yield and ultimate case, respectively. These loads were applied in the positive x and z directions and the negative y direction.

A restraint case was developed to approximate the effect of the leg being bolted in place. All six degrees of freedom (DOF) were restrained at the bolt holes. The restraint case and load case are shown graphically against the support legs in Fig. 30.

To begin, a trial material of AISI 4130 tempered steel was assumed. This material has a yield strength of 132 ksi and an ultimate strength of 150 ksi. Elongation of this tempered alloy is 17%, which shows that it has remained ductile after tempering. Ductility is a desired quality as the material will be better able to 'absorb' high local stresses (i.e. stress concentrations).

It was decided to model half of the leg, bisected along is axis of symmetry in order to save computer time. The ANSYS FEM package was used to perform a linear, static 3D stress analysis. ARIES automesh feature was employed which automatically determines a mesh pattern using tetrahedral and triangular patterns as appropriate. A mesh of 2,297 elements and 670 nodes was generated.

The result of the FEM analysis with the 10g load is shown in Figs. 31 and 32. The result with the 20g load is shown in Figs. 33 and 34.
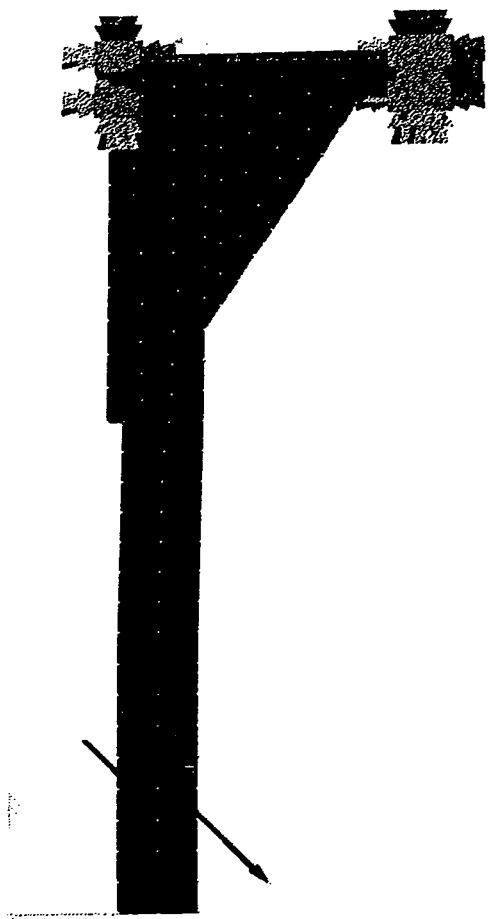
108

Figure 30 –
FEM Showing Loading and Constraints of ISS Support Leg

CONTOUR

VON_MISES
STRESS
lbf/(in*in)

1.24962E+05
1.21064E+05
1.17165E+05
1.13267E+05
1.09368E+05
1.05470E+05
1.01571E+05
9.76730E+04
9.37746E+04
8.98762E+04
8.59777E+04
8.20793E+04
7.81808E+04
7.42824E+04
7.03840E+04
6.64855E+04
6.25871E+04
5.86886E+04
5.47902E+04
5.08918E+04
4.69933E+04
4.30949E+04
3.91964E+04
3.52980E+04
3.13996E+04
2.75011E+04
2.36027E+04
1.97043E+04
1.58058E+04
1.19074E+04
8.00894E+03
4.11050E+03
2.12064E+02

Figure 31 -
FEM of ISS Support Leg (10g)

Figure 32 –
FEM of ISS Support Leg (10g)

CONTOURS
VON_MISES
STRESS
lbf/(in*in)

1.24962E+05
1.21064E+05
1.17165E+05
1.13267E+05
1.09368E+05
1.05470E+05
1.01571E+05
9.76730E+04
9.37746E+04
8.98762E+04
8.59777E+04
8.20793E+04
7.81808E+04
7.42824E+04
7.03840E+04
6.64855E+04
6.25871E+04
5.86886E+04
5.47902E+04
5.08918E+04
4.69933E+04
4.30949E+04
3.91964E+04
3.52980E+04
3.13996E+04
2.75011E+04
2.36027E+04
1.97043E+04
1.58058E+04
1.19074E+04
8.00894E+03
4.11050E+03
2.12064E+02

Figure 33 -
FEM of ISS Support Leg (20g)

CONTOURS

VON_MISES
STRESS
lbf/(in*in)

2.49924E+05
2.42127E+05
2.34330E+05
2.26533E+05
2.18736E+05
2.10939E+05
2.03143E+05
1.95346E+05
1.87549E+05
1.79752E+05
1.71955E+05
1.64158E+05
1.56361E+05
1.48565E+05
1.40768E+05
1.32971E+05
1.25174E+05
1.17377E+05
1.09580E+05
1.01783E+05
9.39865E+04
8.61896E+04
7.83928E+04
7.05959E+04
6.27990E+04
5.50022E+04
4.72053E+04
3.94084E+04
3.16116E+04
2.38147E+04
1.60179E+04
8.22099E+03
4.24128E+02

Figure 34 –
FEM of ISS Support Leg (20g)

The FEM plot of the 10g load case shows the variation of the von Mises effective stresses over the entire support leg. From this, the maximum von Mises stress is seen to be approximately 63 ksi. The material strength of AISI 4130 steel is 132 ksi. The factor of safety is determined as:

$$\sigma_y / \sigma_e = N_s \quad \text{where} \quad \sigma_y = \text{yield strength of the material}$$
$$\sigma_e = \text{von Mises effective stress}$$
$$N_s = \text{factor of safety}$$

Using the above, the yield factor of safety was determined to be 4.2.

The FEM plot of the 20g load shows the maximum von Mises effective stress to be approximately 135 ksi. The factor of safety is determined as:

$$\sigma_u / \sigma_e = N_s \quad \text{where} \quad \sigma_u = \text{ultimate strength of the material}$$
$$\sigma_e = \text{von Mises effective stress}$$
$$N_s = \text{factor of safety}$$

Using the above, the ultimate factor of safety was determined to be 2.1. It should be noted that although higher local stresses are depicted on the effective stress contour plots, these values should not be regarded as the true maximum stresses. Stress concentrations arise due to the fact that the model is an approximation of the actual structure. For example, the bolt holes on the FEM are approximated as polygons with sharp corners. These sharp corners give rise to local stress concentrations that do not exist in the actual structure. Therefore, maximum values of effective stress may be determined by examining areas slightly removed from these localized stress concentrations. In reality, any stress concentrations that exist in the actual structure will be relieved by local yielding.

The above factors of safety are acceptable for the fail-safe case. Due to availability, the material actually purchased for the ISS Support Legs was AISI 4140 which has material properties nearly identical to AISI 4130.

CONCLUSIONS

This year's team accomplished the design of the x- and j- cell battery boxes, the IPPE antenna and baseplate, the mirror assembly, the battery enclosure, and the lateral bumpers. This year's team also fabricated the x and j cell battery boxes, the IPPE antenna and baseplate, the MGI canisters, the MGI mounting brackets, and the tri-wall welding.

The experimental hardware for the IPPE antenna and MGI experiments is complete from the mechanical standpoint. The only thing that is required is integration with the electrical hardware for these experiments. The working fluid for the rotational fluid flow experiment has been chosen, and the performance envelope has been plotted. The tri-wall structure for the integrated support structure has been rewelded and the X and J cell battery boxes have been made.

The remaining work consists of the fabrication of remaining parts, the mounting of the components on the integrated support structure, integrating the experiments with the data collection hardware, and testing to prove that the hardware is flight ready.

RECOMMENDATIONS FOR FUTURE WORK

IPPE:

The antenna rod still needs some machining. The top of the antenna rod needs to be single-point threaded due to the hardness of stainless steel. Also, two AMS 5644 stainless steel pins have to be press fit into the rod. Also, the bottom of the antenna rod has to be drilled and threaded to allow an electrical connection. The drawing for the rod is in **Appendix F**. Also, a hermetic connector has to be purchased for the connection between the outside of the canister and the IPPE circuit board. Also, the final dimensions have to be gotten in order to place it on the Integrated Support Structure.

MGI:

What remains to complete the MGI is purchase of the aluminum oxide ceramic backplates, infrared heat lamps, heat flux gauge and pressure transducers, and manufacturing of the heat flux back block. The background section on the MGI experiment highlights each area of concern and should be referenced for details.

RFF:

A number of concerns still need to be addressed. These include the camera box and controller, the ultrasonic flowmeter, the mirror assembly, the purchase of the silicon oil, the placement of the lamp, the mounting of the components and the balancing of the rotational platform.

CAMERA BOX

The camera box needs to have the camera mounted in it. Foam has been cut to hold the camera, however a mounting the camera by screwing it in from the bottom

would allow easier access. A hole needs to be cut in to the back of the box for a hermetic seal to connect the camera to the camera controller and power supply.

CAMERA CONTROLLER

A electrical engineering student is currently working on the video camera controller. Apparently the control interface that was going to be used with the video camera was incompatible with the camera. The electrical engineering student is in the process of altering the camera for use with the control interface. When the controller is done, a housing will need to be designed so that the board can be mounted on the rotational platform.

ULTRASONIC FLOWMETER

A Panametrics 6860 ultrasonic flowmeter was obtained for the purpose of measuring the flowrate of the working fluid under operating conditions. After talking with a Panametrics representative it was found that the ultrasonic transducers which have already been purchased are unsuitable for use with the flowmeter. However, the 1 MHz ultrasonic transducers which were used by Smith (1994) might be suitable, if the set-up information which he used in his experimental set-up can be obtained.

MIRROR ASSEMBLY

The mirror assembly has been designed, however, because of the limited space available on the rotational platform, a desirable viewing angle cannot be obtained. The present design would present a full view of the vortex chamber, but the view would be distorted. If more space can be made available on the rotational platform, then a good viewing angle can be achieved. If more space cannot be made available then a stress

analysis still needs to be completed, however, hand calculations have shown that there should be no problems as far as failure of the frame. The aluminum must be purchased, the frame must be fabricated, and a padding material to be put into the grooves of the frame must be chosen to isolate the mirror from vibration.

PURCHASE OF THE WORKING FLUID

Silicon oil can be purchased from the William F. Nye company (see Appendix O)

PLACEMENT OF THE LAMP

The lamp has to be mounted upon the top plate of the Rotational platform. It has to be placed in a position to produce the best video camera recording, while avoiding glare which could prevent the camera from seeing the image of the vortex. A suggestion is to mount a piece of translucent plastic between the lamp and the vortex chamber, to diffuse the light from the bulb.

MOUNTING OF THE COMPONENTS

All of the components should be bolted to the rotational platform. A previous MQP team had wanted to fabricate brackets to hold the vortex chamber in place, however these brackets would add unnecessary weight doing the same task that could be accomplished by a few bolts. Therefore it is recommended that the vortex chamber also be bolted in place.

Housings need to be made to mount the motor controller and pump controller boards, the RFF CPU, and the ultrasonic flowmeter onto the rotational platform. While designing these housings, the fact that pipes carrying the working fluid will pass over, under or through these housings should be taken into account.

BALANCING OF THE COMPONENTS.

The rotational platform needs to be balanced to insure a steady artificial gravity level while the experiment is being conducted. Because of the number and size of the components that must be mounted on the rotational platform, the components will probably need to be mounted on the platform with the intent fitting them all in, and not with the intent of placing them in a balanced configuration. If this is the case then when the platform is balanced, extra weight will have to be added in certain places on the platform. One way of doing this would be to use the lead weights which are used when balancing tires. They are compact and relatively cheap.

ISS:

Machining of the lateral bumpers, ISS support legs, and machining and welding of the battery box enclosure must be completed. Dimensioned drawings are placed in Appendix F. Materials for these items have already been ordered and are in the lab. In addition, holes must be drilled in battery box flanges for the specified bolts. The battery box enclosure will have to be coated with the chemical epoxy as described in the design section.

BIBLIOGRAPHY

Baril, D.G., 1993, "Rotational Fluid Flow In Micro Gravity Environment", Major Qualifying Project, Worcester, MA.

Bauccio, M., <u>ASM Metals Reference Book, 3rd Edition</u>. Materials Park, OH: ASM International, 1994.

Becz, S., Norval R., 1993, "Micro Gravity Rotational Fluid Flow Experiment", Major Qualifying Project 94C005M, Worcester Polytechnic Institute, Worcester, MA.

Belliveau, L., Chase, M., 'Micro-gravity Ignition', Major Qualifying Project 94D244M, Worcester, MA, 1994.

Belog, J., 1994, "Rotational Fluid Flow", Major Qualifying Project, Worcester Polytechnic Institute, Worcester, MA.

Brown, H. B., Buzby, J.G., and Doyle, B.J., 1994, "GASCan II Payload Integration", Major Qualifying Project 94D-177M, Worcester Polytechnic Institute, Worcester, MA.

Coolidge, A. P., and Daigle, J.J., 1992, "Ionospheric Properties and Propagation Experiment", Major Qualifying Project EE-VZB-9000, Worcester Polytechnic Institute, Worcester, MA. p. ii, 3.

Cook, R. D., Franz, C.A., and Maloney, R.C., 1994, "Ionospheric Properties and Propagation Experiment", Major Qualifying Project 94D-217M, Worcester Polytechnic Institute, Worcester, MA.

Cooper, S., Nov 1988, "General Fracture Control Plan for Payloads Using the Space Transportation System (STS)", 731-0005-83, Goddard Space Flight Center, MD., p. 13-14, 30.

Cyr, A., Enters, R., Medicus, J., 1993,"GASCAN II Rotational Fluid Flow", Major Qualifying Project 92D052M, Worcester Polytechnic Institute, Worcester, MA.

Federico, M., Marciello, P., Stanley, E., 1992,"Rotational Fluid Flow", Major Qualifying Project, Worcester Polytechnic Institute 92D061M, Worcester, MA.

Franklin, D.B., July 1987, "Design Criteria for Controlling Stress Corrosion Cracking", MSFC-SPEC-522B, Materials & Processes Laboratory, George C. Marshall Space Flight Center, MD, p. 12.

Gallaway, G., National Aeronautics and Space Administration, Goddard Space Flight Center, interviewed Nov. 1994.

Garrant, K., Lusk, A., 'Micro-gravity Ignition', Major Qualifying Project 92D195M, Worcester, MA, 1992.

Hamilton, D.A., July 1985, "Simplified Design Options for STS Payloads", JSC-20545, Lyndon B. Johnson Space Center, Houston TX, p. 6, 10.

Knapp, C., National Aeronautics and Space Administration, Goddard Space Flight Center, interviewed Nov 1994 - April 1995.

Kroschwitz, J. I., An Encyclopedic Sourcebook of Engineering Properties. New York: Wiley, 1987.

Kyaw, N.S., and Wu, M.S., 1993, "Ionospheric Properties and Propagation Experiment", Major Qualifying Project EE-VZB-, Worcester Polytechnic Institute, Worcester, MA. p. i, iii-v.

Maranghides, A., Roy, P., 'Micro-gravity Ignition', Major Qualifying Project ME GYJ9103, Worcester, MA, 1991.

Norton, R.L., *Machine Design*, Prentice Hall, Edgewood Cliffs, NJ., p. 715.

Parker, S., 'Micro-gravity Ignition', Major Qualifying Project 93E013M, Worcester, MA, 1993.

Peden, M.D., Hernandez Engineering, Inc., Goddard Space Flight Center, Greenbelt, MD, interviewed Dec. 1994- April 1995.

Peden, M.D., July 1993, "Structural Verification for GAS Experimenters", *GAS Experimenter's Guide to the STS Safety Review Process and Data Package Preparation*, National Aeronautics and Space Flight Center, Greenbelt, MD., p. B1-3.

Rencis, J.J., Urekew, T. J., and Scarpino, C., August 1991, "Structural and Vibrational Analyses of the Wake Side Plasma Sensor for the Wake Side Facility", Worcester Polytechnic Institute, Worcester, MA.

Schweitzer, P.A., P.E., Corrosion and Corrosion Protection Handbook, 2nd Edition. New York: Marcel Dekker, Inc., 1989.

Smith, R. H. Jr., April 1994,"The Direct Measurement of Circulation in Free Surface Vorticies", Worcester Polytechnic Institute, Worcester, MA.

References Without Stated Author's:

Almac for Plastics, material properties of Delrin, p. 63 received via fax from Charlie Knapp at NASA Dec. 15, 1994.

"CRC handbook of Chemistry and Physics, 75th ed.", Chemical Rubber Company Press, Cleveland, OH., 1994

"Get-Away Special Experimenter Handbook", 1979, Goddard Space Flight Center (GSFC) Special Payloads Division, MD.

"Laminated Thermosetting Materials", Dec 1989, material properties of G-10 Fiberglass Epoxy, p. 240 received via fax from Charlie Knapp at NASA Dec. 15, 1994.

"Military Standardization Handbook - Metallic Materials and Elements for Aerospace Vehicle Structures", 1983, material properties of 17-7ph stainless steel and Al T-6061, Department of Defense, Washington, D.C., v. 1, pp 2-181-2, 3-221-7.

"Perry's Chemical Engineer's Handbook, 6th ed." McGraw-Hill, New York, NY. 1984

"Properties of Polypenco Industrial Plastics", Craftech Industries, Inc., Hudson, NY, material properties of Delrin, p. 52 received via fax from Charlie Knapp at NASA Dec. 15, 1994.

"Systems Engineering Division Bolted Joint Handbook", November 1990, SED Engineering Handbook EHB-2, NASA Langley Research Center, Hampton, VA.

"The Model 6860 Ultrasonic Flowmeter Operator's Manual", Panametrics Corp. 1988.

APPENDICES

Appendix A

Finite Element Methodology

Properties common to all three versions (Version 1, Version 2, Version 3) of the antenna:

All three versions model the antenna from the Delrin Cone up to the top plate exactly the same way. The antenna cap was modeled as a plate element with four elements in the radial direction and revolved around the Z axis (along the rod) for twenty separate pie shapes. The plate elements are given a density of 0.2775 lb./in^3 despite the antenna's actual density of 0.276 lb./in^3. This is because the linear edges of the finite element model will create a lower mass of the cap than actual. The modified mass allows the circular plate modeled to match the exact masses despite the different densities. This will allow the frequency response of the model to be closer to the actual value due to the equation:

$$\omega = \sqrt{\frac{k}{m}}$$

which defines the resonant frequency of the antenna. If any of the smaller areas affect the stiffness, it will only decrease the stiffness and therefore the ω of the model.

The antenna cap must be restrained from rotation about the Z axis. This is because IMAGES is unable to make a connection that includes rotational when a plate element is placed perpendicular to a rod element. Also, IMAGES will not assume that a plate has stiffness in the radial direction if the plate is not connected to two separate

elements or fixed at two separate locations. Therefore, beam elements of minimal diameter were added to the model in order to simulate the stiffness of the antenna cap.

The Delrin cone is modeled in the center as 3-D wedge elements. The remaining elements going radially out to the edges of the cone are modeled as 3-D brick elements. The density of the cone is slightly increased from the actual value of 0.05128 lb./in^3 to 0.0521 lb./in^3. This value is increased for the same reason that the antenna cap is increased. The roll pins that are within the cone are lined up along each of the nodes that are already existing in the cone. The antenna rod is modeled as 10 beam elements. The nodes that are within the Delrin cone are lined up with the nodes of the cone. The nut, which is welded underneath the antenna cap, is modeled as a single beam element with an area and density equal to the actual value.

Version 1 (File conant.xxx):

(For a reference of model, see Appendix A, Figures 1-5)

The setscrews that screw through the mounting plate and into the Delrin cone are modeled as beam elements that are fixed 0.1 inches underneath the cone.

Version 2 (File conantpl.xxx):

(For a reference of model, see Appendix A, Figures 6-10)

The setscrews of Version 1 are elongated to go 0.125 inches below the base of the cone. The node matches and attaches to the middle of the aluminum plate that is placed underneath the Delrin cone to support the antenna and attach the antenna to the GASCan lid. The plate, modeled 6" square, is fixed from rotation and translation at the edges.

The setscrews are no longer fixed but are restrained from rotation around the Z axis at the plate.

Version 3 (File conant1.xxx):

(For a reference of model, see Appendix A, Figures 11-13)

The plate of Version 2 is enlarged to the actual size of 8.5" square but retains the same thickness. The four bolts that are to screw into the GASCan lid are modeled as beam elements that go to the middle of the GASCan lid (0.625" thick). The GASCan lid is actually included as part of the model and fixed from rotation and translation in all axial directions.

APPENDIX B - IMAGES 3-D MODE SHAPES

IMAGES-3D
VER. 2.0
Mode   1
S= 3.000E+00
 6.862E+01 Hz

Mode Shape:
 Bending of rod
 about Y-axis.

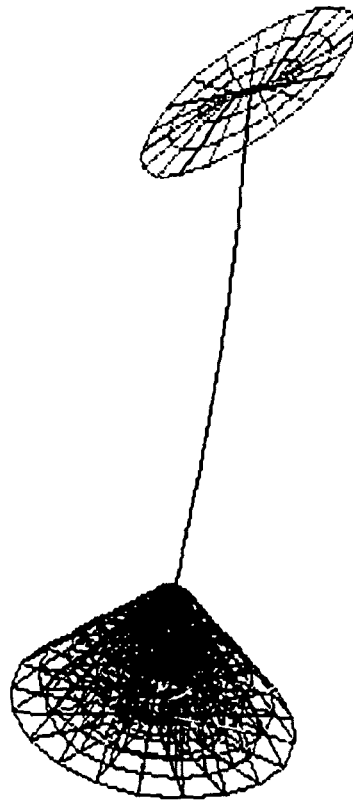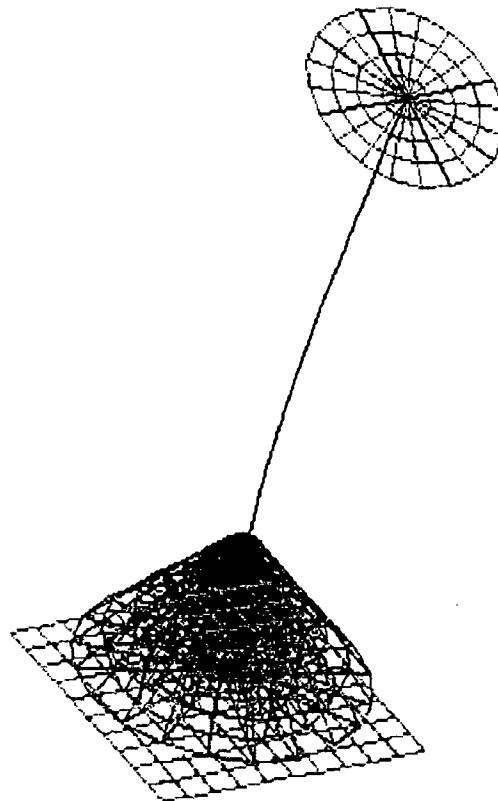**Distortion Scale:**
3.0

Frequency:
68.62 Hz.

Z

Y

X
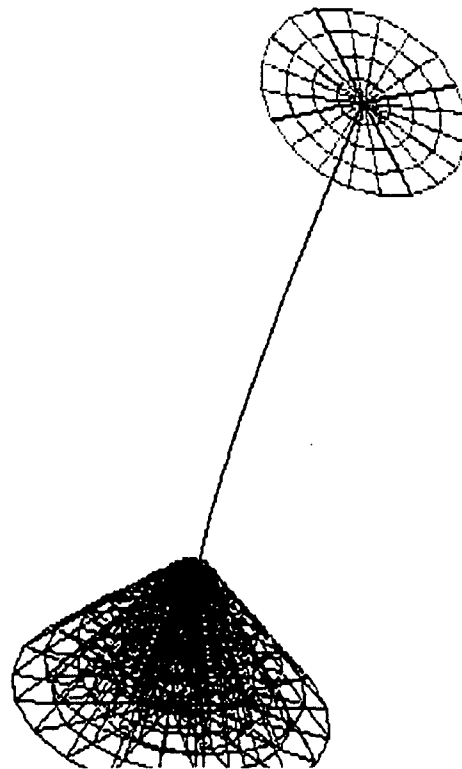
Figure 1: *First mode shape: Antenna with fixed screws.*

IMAGES-3D
VER. 2.0
Mode 2
S= 3.000E+00
7.063E+01 Hz

Mode Shape:
Bending of shaft
about X-axis.

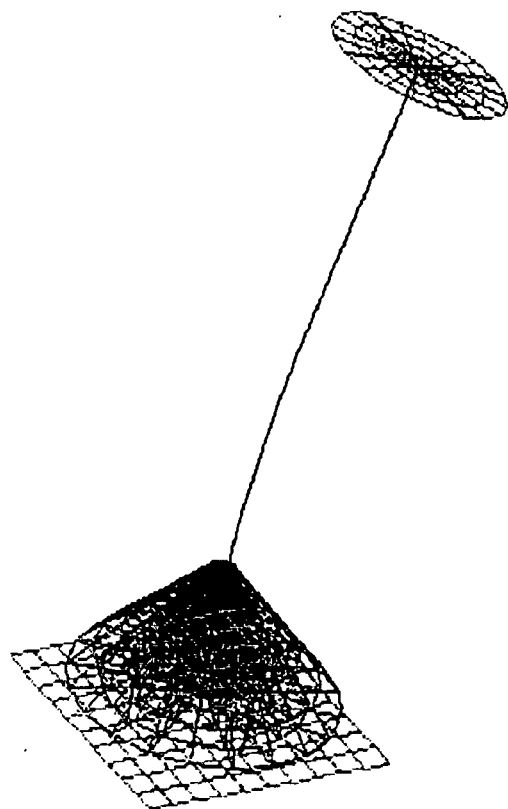**Distortion Scale:**
3.0

Frequency:
70.63 Hz.

Z
Y
X
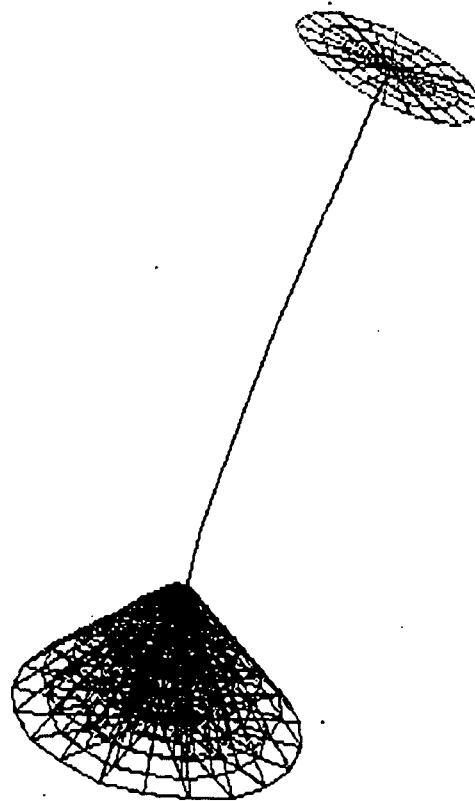
Figure 2: *Second mode shape: Antenna with fixed screws*

IMAGES-3D
VER. 2.0
Mode   3
S= 3.000E+00
   1.865E+02 Hz

Mode Shape:
Longitudinal displace-
ment of cap in radial
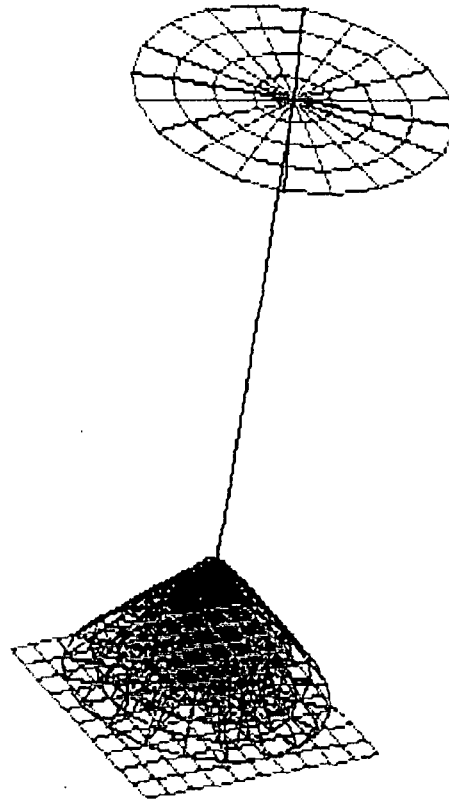direction.

Distortion Scale:
3.0

Frequency:
186.5 Hz

Z
Y
X
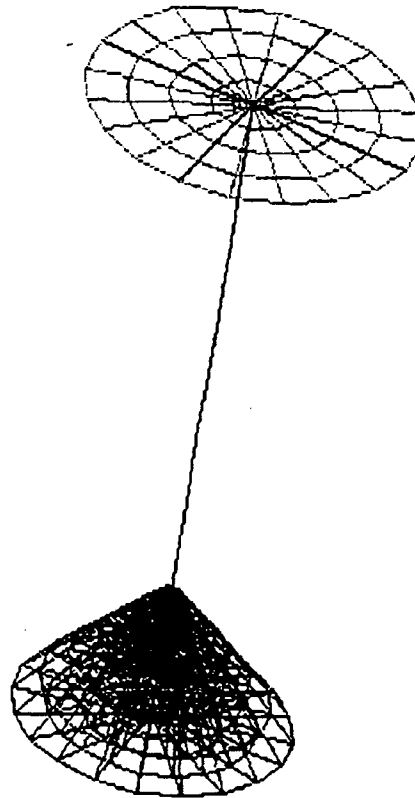
Figure 3: *Third mode shape: Antenna with fixed screws*

IMAGES-3D
VER. 2.0
Mode   4
S= 3.000E+00
  3.817E+02 Hz

Mode Shape:
 Bending of cap
 and shaft about
 Y-axis.

Distortion Scale:
 3.0

Frequency:
 381.7 Hz.

Z

Y

X

Figure 4:   *Fourth mode shape: Antenna with fixed screws*

IMAGES-3D
VER. 2.0
Mode   5
S= 3.000E+00
 3.831E+02 Hz

Mode Shape:
 Bending of cap
 and shaft about
 X-axis.

Distortion Scale:
 3.0

Frequency:
 383.1 Hz.

Z

Y

X

Figure 5: *Fifth mode shape: Antenna with fixed screws*

IMAGES-3D
VER. 2.0
Mode   1
S= 3.000E+00
6.812E+01 Hz

Mode Shape:
Bending of shaft
about Y-axis.

Distortion Scale:
3.0

Frequency:
68.12 Hz.

Z

Y

X

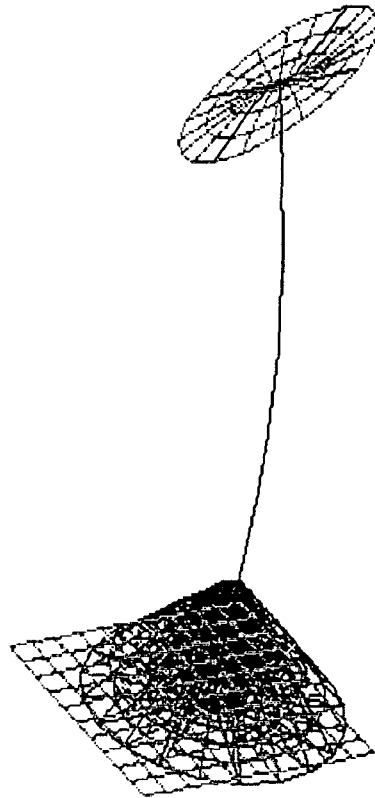**Figure 6:** *First mode shape: Antenna with Aluminum baseplate*

IMAGES-3D
VER. 2.0
Mode   2
S= 3.000E+00
  7.029E+01 Hz

Mode Shape:
Bending of shaft
about X-axis.

Distortion Scale:
3.0

Frequency:
70.29 Hz.

Z
Y
X

Figure 7: *Second mode shape: Antenna with Aluminum baseplate*

IMAGES-3D
VER. 2.0
Mode   3
S= 3.000E+00
   1.865E+02 Hz

Mode Shape:
Longitudinal displace-
ment of cap in
radial direction.

Distortion Ratio:
3.0

Frequency:
186.5 Hz.

Z

Y

X

Figure 8: *Third mode shape: Antenna with Aluminum baseplate*

IMAGES-3D
VER. 2.0
Mode   4
S= 3.000E+00
 3.419E+02 Hz

Mode Shape:
 Bending of cap
 and shaft about
 Y-axis.

Distortion Scale:
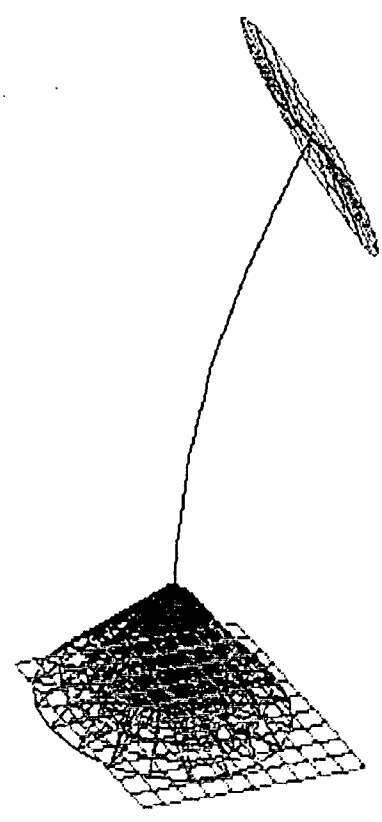3.0

Frequency:
341.9 Hz.

Z

Y

X

Figure 9:   *Fourth mode shape: Antenna with Aluminum baseplate*

IMAGES-3D
VER. 2.0
Mode   5
S= 3.000E+00
  3.428E+02 Hz

Mode Shape:
 Bending of cap
 and shaft about
 X-axis.

Distortion Scale:
3.0

Frequency:
342.8 Hz.

Z
Y
X

Figure 10:   *Fifth mode shape: Antenna with Aluminum baseplate*

IMAGES-3D
VER. 2.0
Mode   1
S= 3.000E+00
  6.415E+01 Hz

Mode Shape:
 Bending of shaft
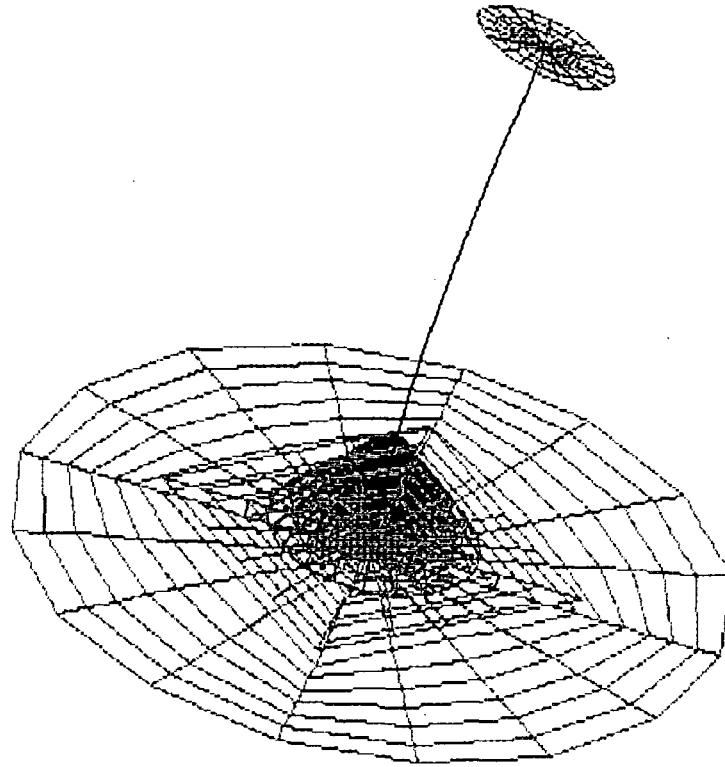 about X-axis.

Distortion Scale:
3.0

Frequency:
64.15 Hz.

Z

Y

X
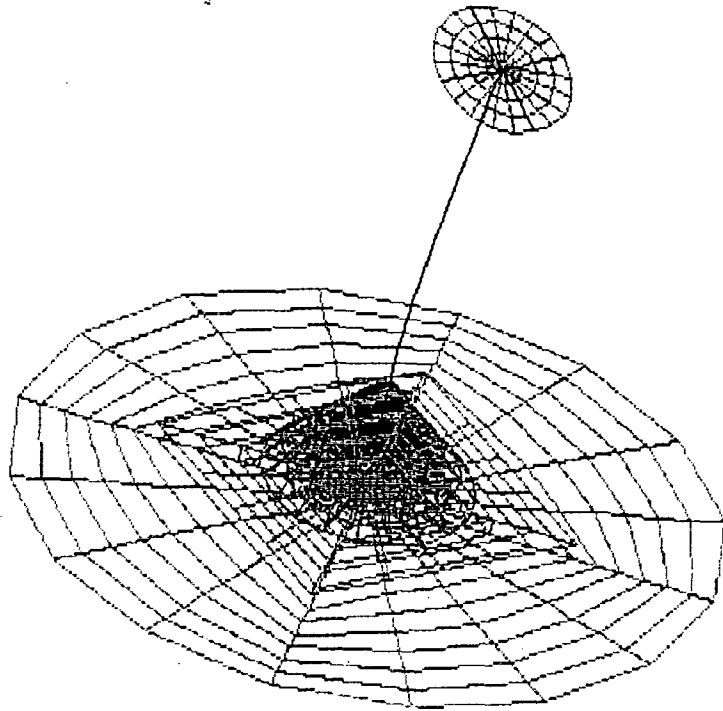
Figure 11: *First mode shape: Antenna with GASCan lid*

IMAGES-3D
VER. 2.0
Mode   2
S= 3.000E+00
 6.596E+01 Hz

Mode Shape:
 Bending of shaft
 about Y-Axis.

Distortion Scale:
3.0

Frequency:
65.96 Hz

Z
Y
X

Figure 12:   *Second mode shape: Antenna with GASCan lid*

IMAGES-3D
VER. 2.0
Mode   3
S= 3.000E+00
  1.865E+02 Hz

Mode Shape:
Longitudinal displace-
ment of cap in radial
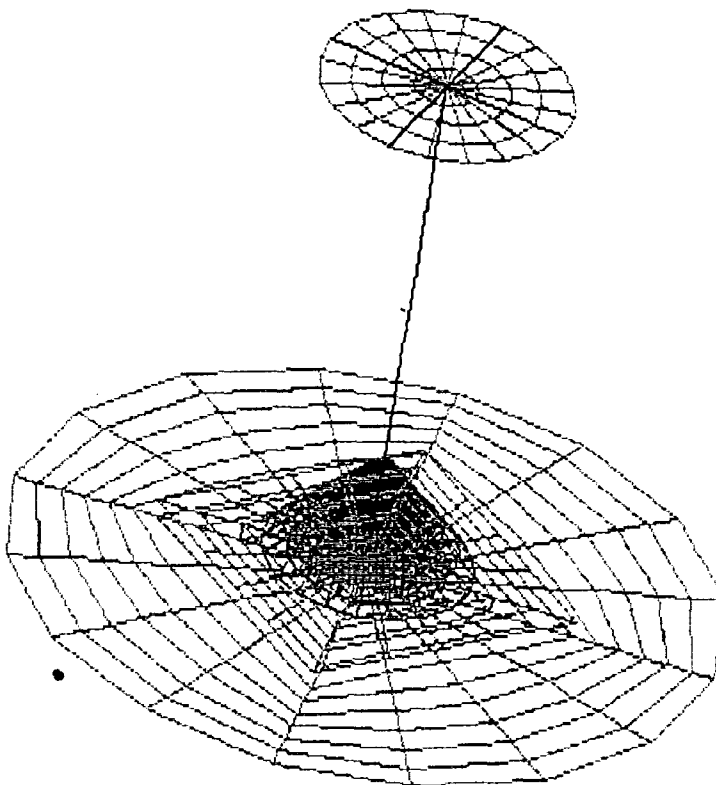direction.

Distortion Scale:
3.0

Frequency:
186.5 Hz.

Z

Y

X

Figure 13: *Third mode shape: Antenna with GASCan lid*

APPENDIX C

TK SOLVER RULE SHEET:

Finding Margins of Safety for bolts on antenna structure

Stiffness of bolts and joint
A_C = PI()/4*(Dw^2-Dh^2)+PI()/8*(Dj/Dw-1)*(Dw*T/5+T^2/100)
K_B = E_B*A_B/L_B
K_J = E_C*A_C/T
A_sh = PI() * Dh * T
T = L_B

Determining the mass of the antenna and structure
M_pla = t_pla*l_pla*w_pla*rho_pla

M_con = 1/3*PI()/4*(D_bas^2*h_bas-D_top^2*h_top)*rho_con
M_rod = PI()/4*D_rod^2*h_rod*rho_rod
M_nut = 6*(D_nut/2)*(D_nut/2*sind(60))*h_nut*rho_rod
M_cap = PI()/4*D_cap^2*t_cap*rho_cap
M_ant = M_con + M_rod + M_nut + M_cap + M_ro1 + M_ro2
M_a_p = M_pla + M_con + M_rod + M_nut + M_ro1 + M_ro2 + M_cap
M_ro1 = PI()/4*D_ro^2*(2*(3-y_ro1))*rho_ro
M_ro2 = PI()/4*D_ro^2*(2*(3-y_ro2))*rho_ro
M_con = 1/3*PI()*((D_bas/2)^2*h_bas-(D_top/2)^2*h_top)*rho_con
y_rod = 1.075 + 1/2*h_rod
y_nut = (13.125+13.625)/2
y_con = (1/3*h_bas*(1/3*PI()/4*D_bas^2*h_bas)*rho_con - (h_con+1/3*h_top)*(1/3*PI()/4*D_top^2*h_top)*rho_con)/M_con
y_BAR = (M_con*y_con+M_rod*y_rod+M_nut*y_nut+M_cap*y_cap+M_ro1*y_ro1+M_ro2*y_ro2)/M_ant
y_bar = (M_pla*y_pla+M_con*y_con+M_rod*y_rod+M_nut*y_nut+M_cap*y_cap+M_ro1*y_ro1+M_ro2*y_ro2)/M_a_p

HAND ANALYSIS
Forces

F_s = SQRT(F_g^2 + F_g^2)
F_g - n_bolt * R1z = 0

***Sum of Moments = 0 ***
F_g * y_BAR - 2 * R1x * (L_tnut) = 0
F_g * y_BAR - 2 * R2x * (L_tnut) = 0
L_tnut = SQRT(2*L_tpr^2)

F_se = F_s / 2 ; (assume shear carried by 2 of four bolts)

F_te = R1x +R1y + R1z

F_g = M_a_p * gfat   ; Force due to gravity loading
F_e = M_a_p * gfat / n_bolt   ; Applied External load
F_e = F_eb + F_ej   ; Applied External load
F_ej = F_eb * (K_J / K_B)
F_p = factor*A_B
F_pmax = 0.65 * F_ty   ; Maximum preload on bolt
sig_ty = F_ty / A_B   ; Conversion of yield stress to force
sig_tu = F_tu / A_B   ; Conversion of ultimate stress to force

f_t = FSp * F_pmin + FSe * (K_B/(K_J + K_B))*F_te ;p. 20 Eq B8
f_s = FSe * F_se

Margin of Safety, Hand Analysis

MS_y = 1/SQRT((f_t/F_ty)^2+(f_s/(0.55*F_ty))^2) - 1 ; Eq. 3.2

MS_u = 1/SQRT((f_t/F_tu)^2+(f_s/F_tu)^2) - 1 ; Eq. 3.2

F_pmin = F_se/u + K_J/(K_J+K_B)*F_te

Tor = F_p * K * D_nom

Finite Element Equations

F_pmini = F_sei/u + K_J/(K_J+K_B)*F_tei

f_ti = FSp * F_pmini + FSe * (K_B/(K_J + K_B))*F_tei ;p. 20 Eq B8

f_si = FSe * F_sei

Margin of Safety, IMAGES Finite Element Results

MS_yi = 1/SQRT((f_ti/F_ty)^2+(f_si/(0.55*F_ty))^2) - 1 ; Eq. 3.2

MS_ui = 1/SQRT((f_ti/F_tu)^2+(f_si/F_tu)^2) - 1 ; Eq. 3.2

F_sei = F_si / 1

F_si = SQRT(Yshear^2 + Zshear^2)

TK SOLVER VARIABLE SHEET

Finding Margin of Safety for bolts on antenna structure:

STATUS	INPUT	NAME	OUTPUT	UNITS	COMMENT
		A_C	1.275E-1	in^2	Cross sect. Area of equiv. cylinder
	.6	Dw		in	Diameter of bolt head (washer)
	.5	Dh		in	Diameter of hole
	1.7	Dj		in	Diameter of joint
		T	4.583E-1	in	Total thickness of joint between head
		K_B	9009360	lb/in	Stiffness of the bolt
	29100000	E_B		lb/in^2	Modulus of elasticity of bolt
	1.419E-1	A_B		in^2	Tensile Stress area of bolt
	4.583E-1	L_B		in	Length of the bolt
		K_J	2809710.1	lb/in	Stiffness of joint
	10100000	E_C		lb/in^2	Modulus of elasticity of aluminum
					Mass of antenna parts
		M_pla	1.77	lb	Mass of baseplate
	.25	t_pla		in	Thickness of baseplate
	8.5	l_pla		in	Length of baseplate
	8.5	w_pla		in	width of baseplate
	.098	rho_pla		lb/in^3	Density of bsaseplate
		M_con	1.464	lb	Mass of Delrin Cone
	6	D_bas		in	Diameter at base of cone
	.625	D_top		in	Diameter at top of cone
	3	h_bas		in	Height of base cone
	3.125E-1	h_top		in	Height of cut-off (top) cone
	2.688	h_con		in	Height of Delrin cone
	5.182E-2	rho_con		lb/in^3	Density of antenna rod
		M_rod	1.02	lb	Mass of antenna rod
	.625	D_rod		in	Diameter of antenna rod
	12.05	h_rod		in	Height of antenna rod
	.276	rho_rod		lb/in^3	weight density of antenna rod
		M_nut	1.793E-1	lb	Mass of nut
	1	D_nut		in	Diameter of nut
	.5	h_nut		in	height of nut
		M_cap	2.168E-1	lb	Mass of antenna cap
	4	D_cap		in	Diameter of antenna cap
	6.25E-2	t_cap		in	Thickness of antenna cap
	.276	rho_cap		lb/in^3	weight density of cap
		M_ant	2.941	lb	Mass of antenna assembly (w/o plate)
		M_a_p	4.711	lb	Mass of antenna and plate
		M_ro1	3.76E-2	lb	Mass of roll pin along x axis
		y_BAR	4.818	in	CG of antenna assembly (minus plate)
		y_bar	2.96	in	CG of antenna assembly plus baseplate
	-.125	y_pla		in	CG pos. of plate
		y_con	.998	in	CG position of cone
		y_rod	7.1	in	CG position of rod
		y_nut	13.375	in	CG position of nut
	13.625	y_cap		in	CG position of antenna cap
	1.613	y_ro1		in	CG position of x roll pin
	2.15	y_ro2		in	CG position of y roll pin
	.25	D_ro		in	Diameter of roll pins
	.276	rho_ro		lb/in^3	density of roll pins
		M_ro2	2.303E-2	lb	Mass of y roll pin

STATUS	INPUT	NAME	OUTPUT	UNIT	COMMENT
		F_e	11.777	lb	Applied External load
		F_eb	8.977	lb	Portion of load carried by bolt
		F_ej	2.8	lb	Portion of load carried by joint
	10	gfat			gravity factor
	4	n_bolt			number of bolts
		F_p	2766.27	lb	Preload in bolt
		F_ty	13480.5	lb	Tensile yield force
	95000	sig_ty		lb/in^2	AMS 5734 (A286 Alloy, p. 6-5)
		F_tu	19866	lb	Ultimate Tensile force
	140000	sig_tu		lb/in^2	AMS 5734 (A286 Alloy, p. 6-5)
	91000	tau_su		lb/in^2	AMS 5734 (A286 Alloy, p. 6-5)
		F_se	33.309	lb	External shear load (hand)
	.31	u		.	Coefficient of friction
		F_te	43.242	lb	External tensile load (hand)
		f_t	218.972	lb	Tensile load in bolt including FS
	1.3	FSp			preload Factor of Safety (1.3)
	2	FSe			External load Factor of Safety (2.0)
		f_s	66.619	lb	Shear load in bolt including FS
	19494.5	factor			Preload torque factor (to force)
	.2	K			Torque coefficient
	.5	D_nom		in	nominal bolt diameter
		Tor	276.627	lb-in	torque
		F_g	47.107	lb	resultant force of gravity
		F_s	66.619	lb	Total shear force
		R1x	31.465	lb	Z Dir force due to x loading
		L_tnut	3.606	in	Length from CG to nut
		R2x	31.465	lb	Z Dir force due to x loading (pin 2)
		R1z	11.777	lb	Z Dir force due to z loading
	2.55	L_tpr		in	Length to nut in x, y dir
	0	R1y		lb	Z Dir force due to y loading
L	-58.76	Yshear		lb	shear in y dir (hand)
L	58.93	Zshear		lb	shear in z dir (hand)
	2	FS			Factor of Safety (per Bolted Joint HBK)
		MS_y	52.87		Margin of safety on yield (hand)
		MS_u	85.796		Margin of safety against ult (hand)
L	. .	F_pmin	117.729	lb	minimum preload (hand)
L		F_pmax	8762.325	lb	Maximum preload
L		F_pmini	282.35	lb	minimum preload (Images)
		f_ti	456.197	lb	tensile force incl FS (Images)
L		F_si	83.219	lb	External shear load (Images)
L	58.471	F_tei		lb	External tensile load (Images)
		f_si	166.439	lb	tensile force incl. FS (Images)
L		F_sei	83.219	lb	External shear load (Images)
L		MS_yi	23.625		Margin of safety on yield (Images)
L		MS_ui	39.909		Margin of safety against ult (Images)

APPENDIX D

STRUCTURAL MATERIAL PROPERTIES

ALUMINUM 6061-T6

("Military Standardization Handbook", 1983)

Density (ρ, lb./in^3)	.098
Young's Modulus (E, psi):	9.9×10^6
Poisson's Ratio (dimensionless):	.33
Yield Strength (σ_y, psi)	36×10^3
Ultimate Tensile Strength (σ_u, psi)	42×10^3

DELRIN (Acetal)

("Almac for Plastics")

Density (ρ, lb./in^3):	.0513
Young's Modulus (E, psi):	410×10^3
Poisson's Ratio (dimensionless):	.35
Yield Strength (σ_y, psi)	8×10^3
Ultimate Tensile Strength (σ_u, psi)	10×10^3

17-7ph STAINLESS STEEL (Rod = AMS 5644, Plate = MILS 25043)

("Military Standardization Handbook", 1983)

Density (ρ, lb./in^3):	.276
Young's Modulus (E, psi):	29×10^6
Poisson's Ratio (dimensionless):	.28
Yield Strength (σ_y, psi)	140×10^3
Ultimate Tensile Strength (σ_u, psi)	170×10^3

APPENDIX E

ANTENNA WEIGHT AND COG LOCATIONS

COMPONENT	WEIGHT (lb.)	Z LOCATION (IN)
BASE-PLATE	1.77	-.125
DELRIN CONE	1.464	.998
ANTENNA ROD	.999	6.17
NUT	.067	13.25
CAP	.216	13.625
X ROLL PIN	.038	1.613
Y ROLL PIN	.023	2.15
ASSEMBLY (W/O PLATE)	2.94	4.82
ASSEMBLY (W PLATE)	4.71	3.83

APPENDIX F - DIMENSIONED DRAWINGS

8.50

6.80

1.70

1.70" RADIUS 4X

8.50

6.80

1.70

2.40

6.10
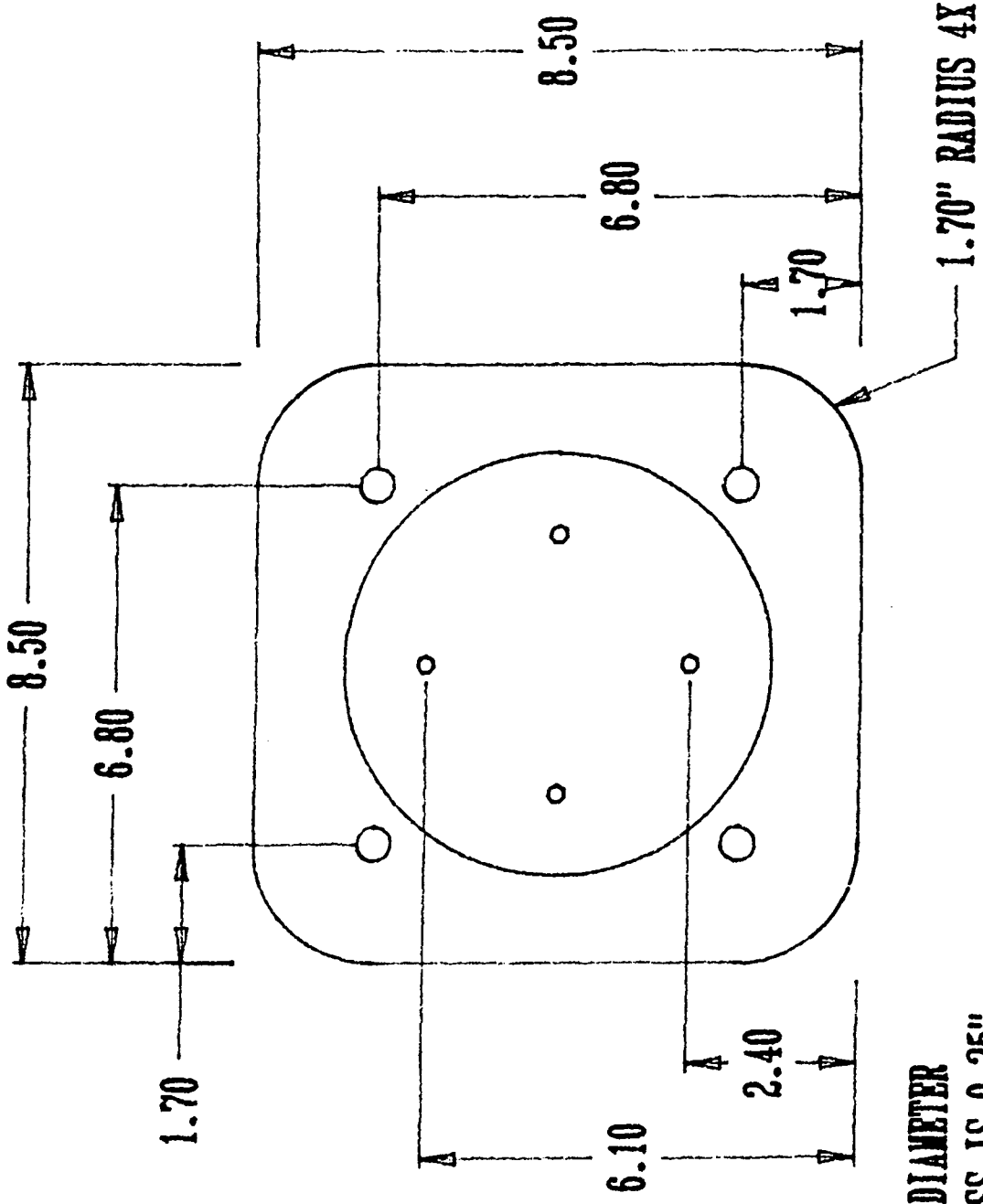
A. 4 HOLES 0.5" DIAMETER
B. PLATE THICKNESS IS 0.25"
C. MAT'L: 6061-T6 AL
D. 4 HOLES COUNTER-
   SUNK IN BOTTOM 0.25" DIA

Aluminum antenna baseplate (antplat.prt)
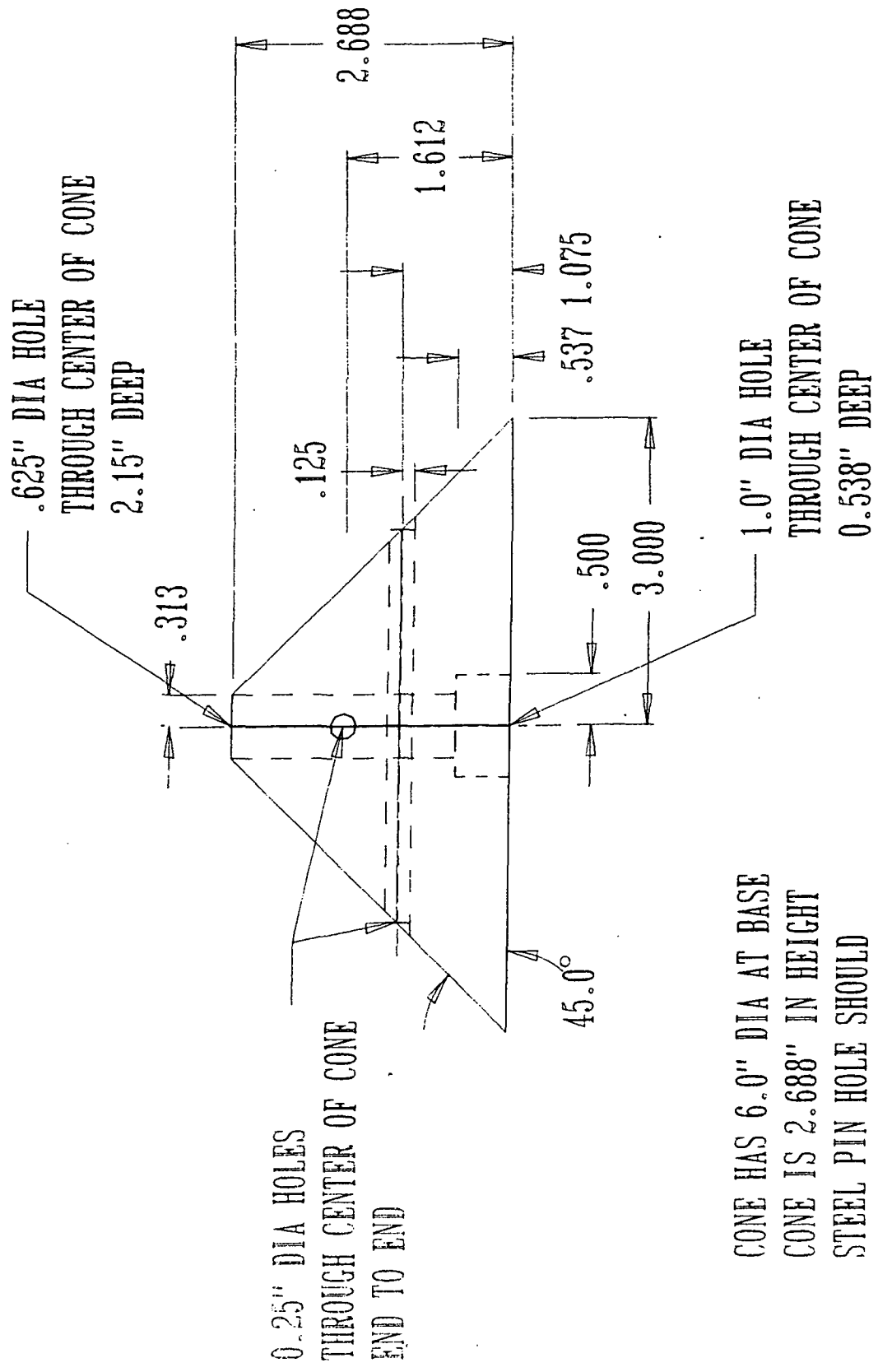
.625" DIA HOLE
THROUGH CENTER OF CONE
2.15" DEEP

.313

.125

.537 1.075

2.688

1.612

.500

3.000

45.0°

0.25" DIA HOLES
THROUGH CENTER OF CONE
END TO END

1.0" DIA HOLE
THROUGH CENTER OF CONE
0.538" DEEP

CONE HAS 6.0" DIA AT BASE
CONE IS 2.688" IN HEIGHT
STEEL PIN HOLE SHOULD
BE 0.25" IN DIA.

Delrin conical antenna support (antcon.prt)

5/8" DIA
UNC THREAD
(11 THREADS/IN)
0.5" LONG

ϕ.625
DIA OF ROD

17-7ph AMS 5644
STAINLESS STEEL
ANTENNA ROD

2 HOLES
.25" DIAM
AT .538"
AND 1.075"
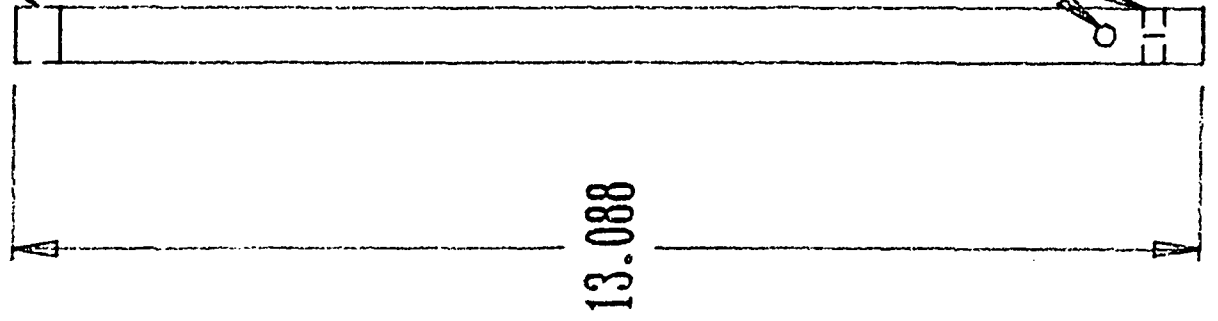
13.088

Stainless steel antenna rod (antrod.prt)
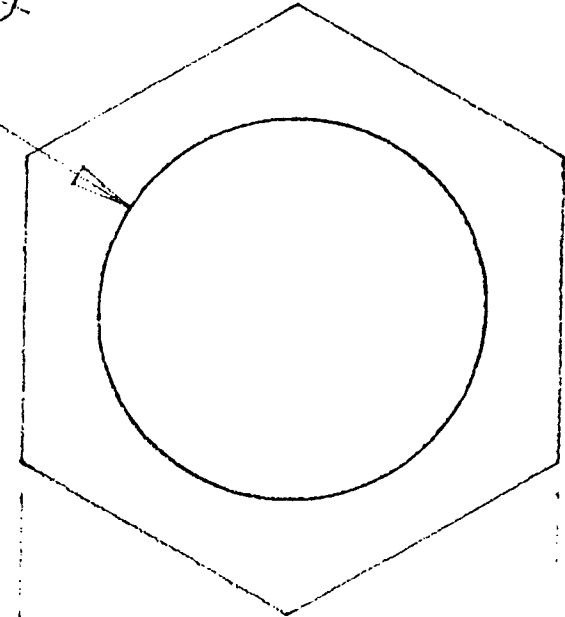
STAINLESS STEEL NUT
MARINE GRADE AISI 316
0.50" LONG
5/8" UNC THREAD
(11 THREADS/IN)

Ø.625

.433

.866

Stainless steel course thread antenna nut (antnut.prt)

Ø4.00
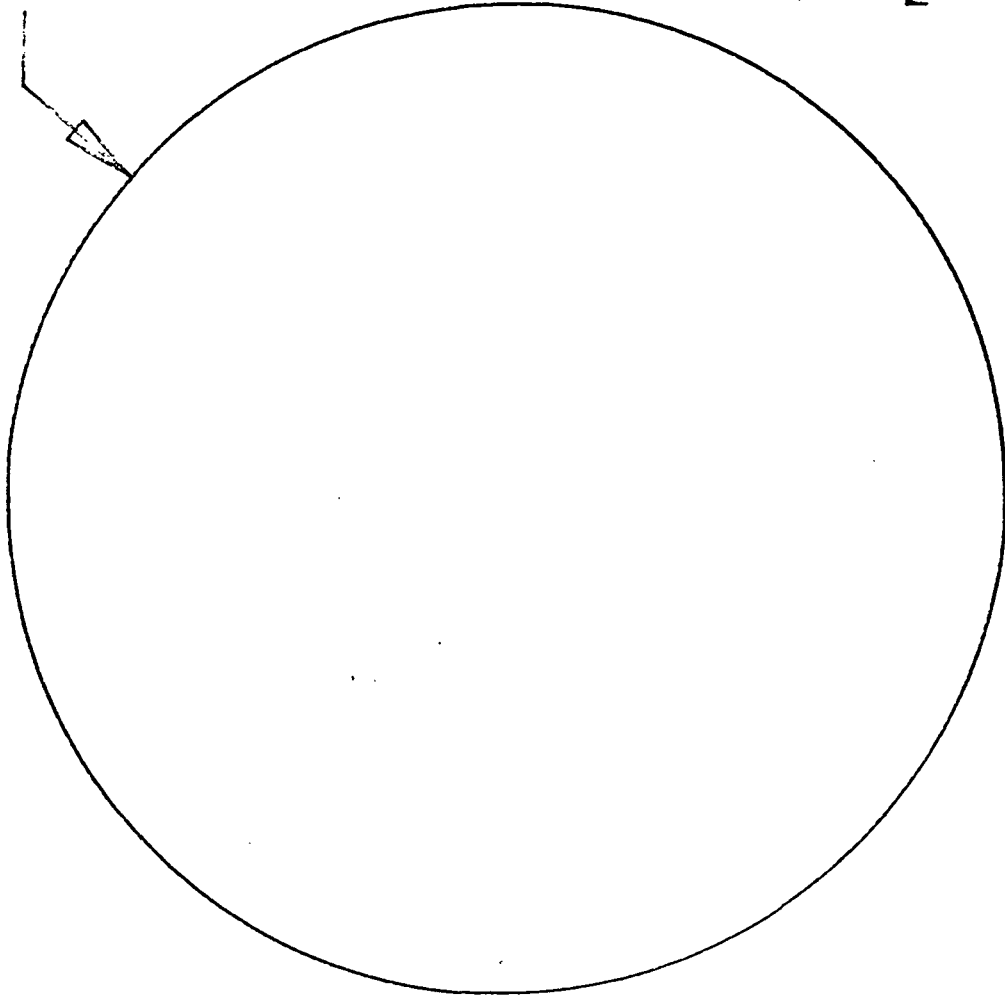
1/16" THICK
T17-7PH MILS 25043
STAINLESS STEEL

Stainless steel antenna cap (antcap.prt)
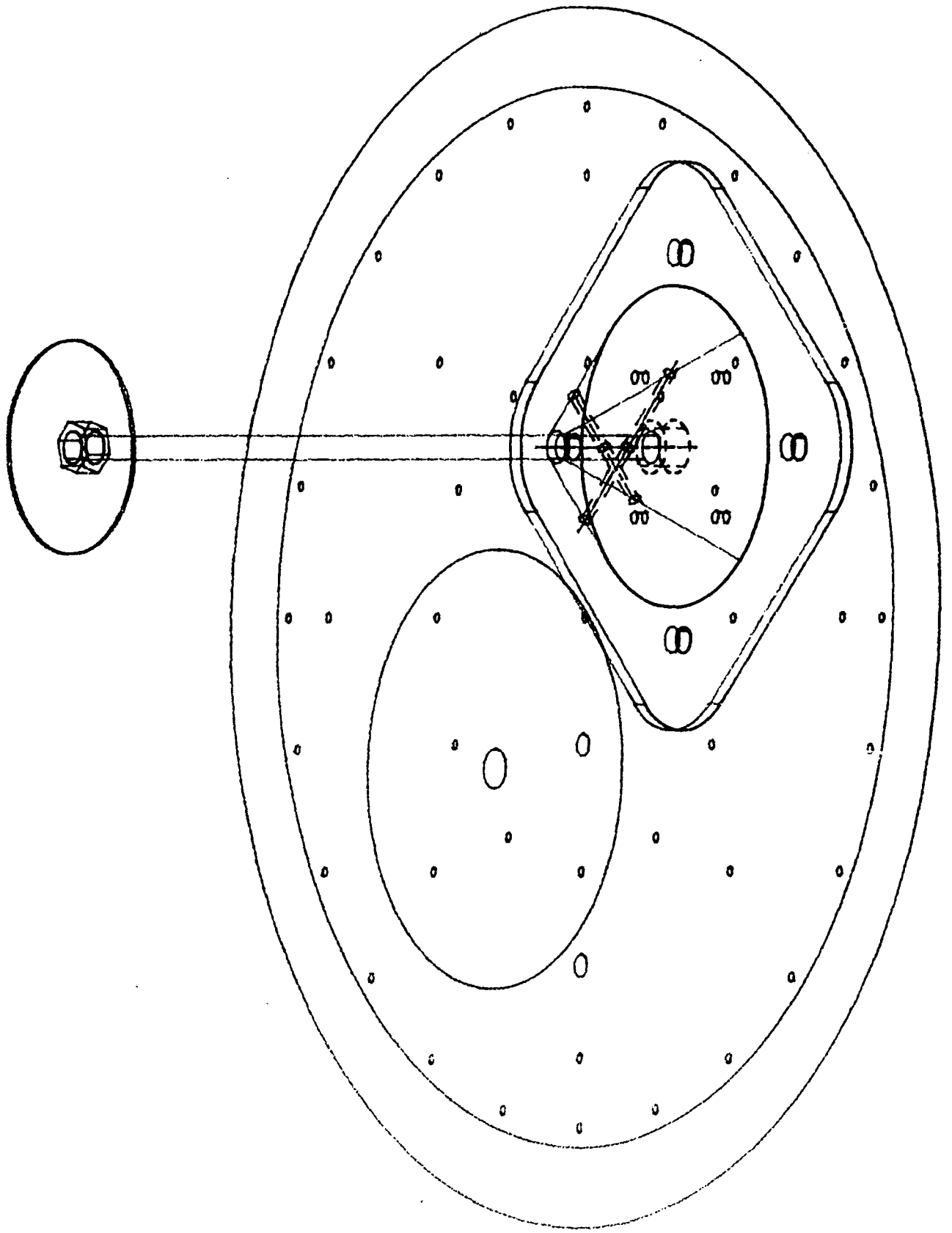
GASCan mounting plate with placement of antenna

MGI Endplate

Note: Plate is 0.25 in. thick
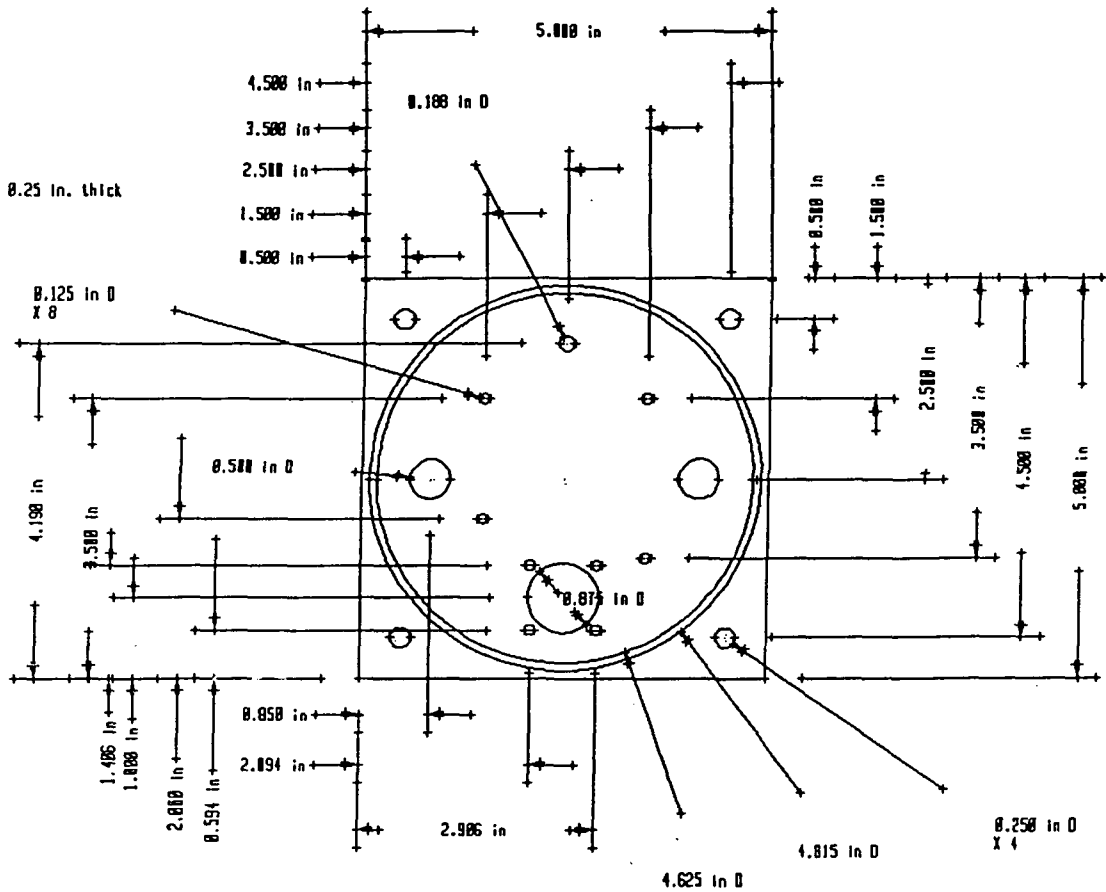
MGI Heat Flux Gauge Holding Block

0.125 in D
X 4

0.250 in D

0.375 in D

0.500 in

0.125 in

0.500 in

1.000 in

0.125 in

1.000 in

0.938 in

0.750 in

0.844 in

0.469 in

Ø.125 in D

Ø.500 in

J-Cell Battery Box

Note: All holes 0.25 in diameter
All angles 120 deg

8.500 in

5.750 in

8.250 in

7.250 in

5.500 in

3.250 in

3.250 in

8.750 in

0.516 in

1.516 in

2.316 in

3.316 in

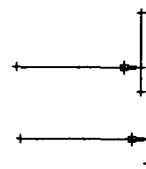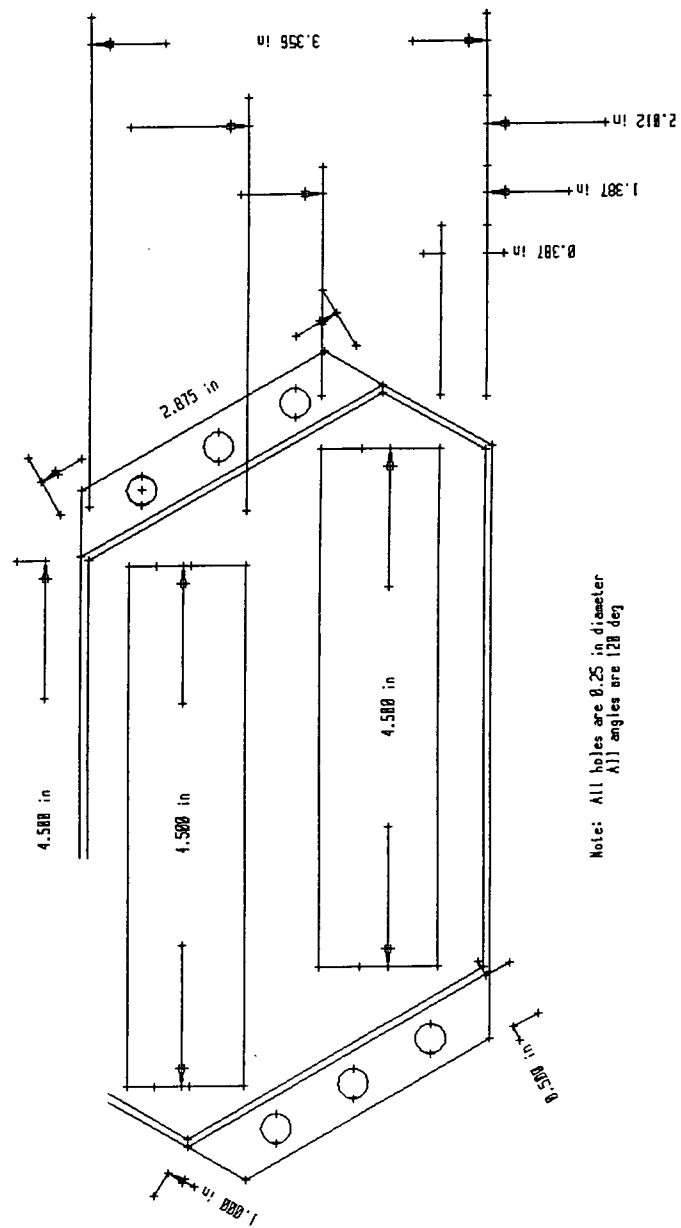4.016 in

5.016 in

5.629 in
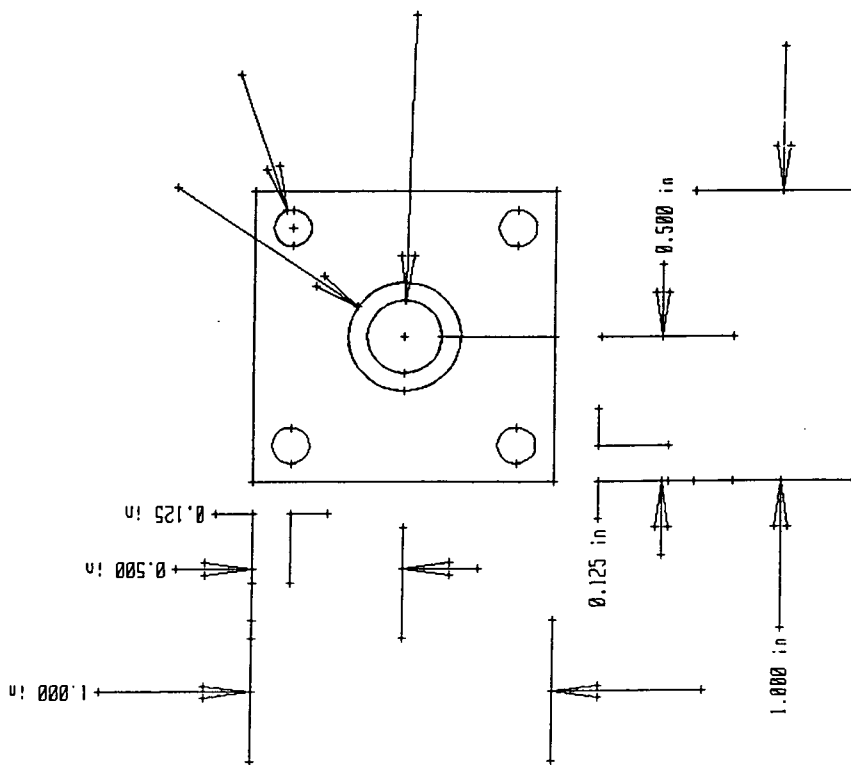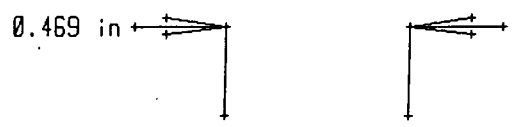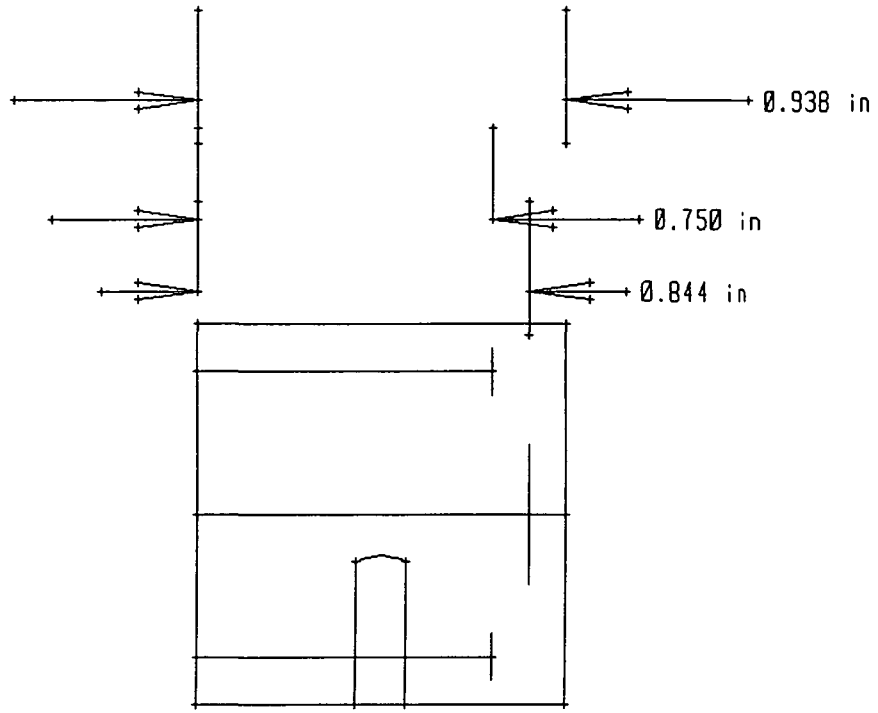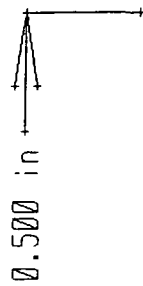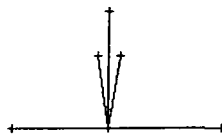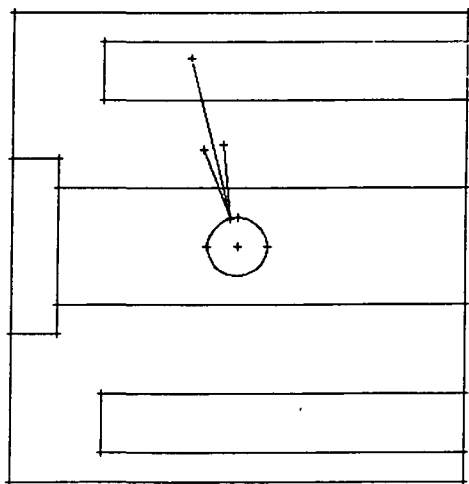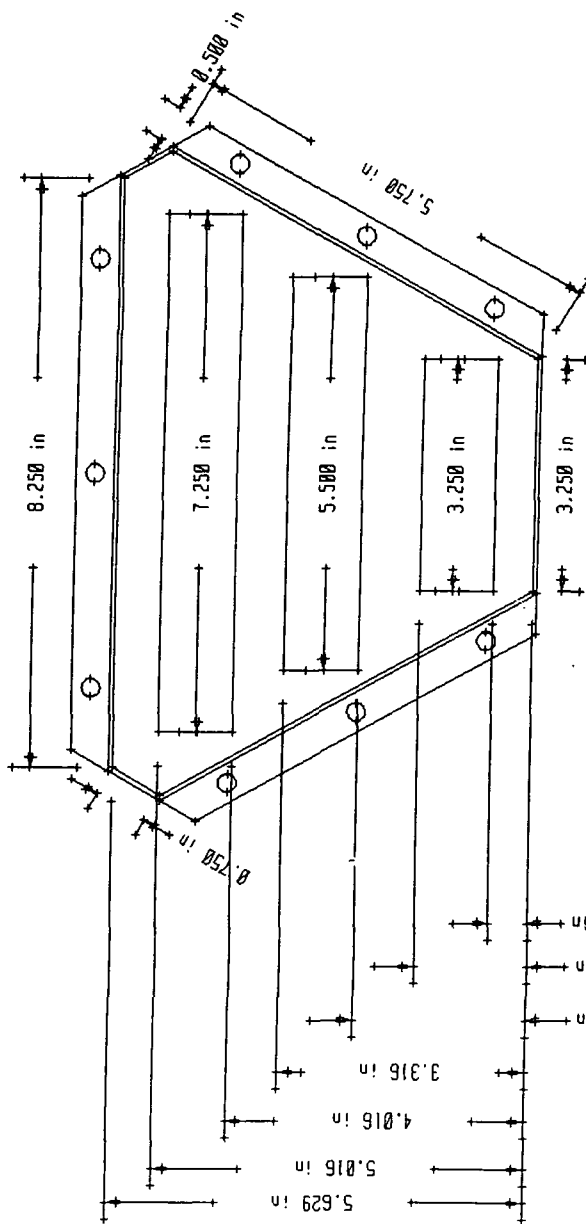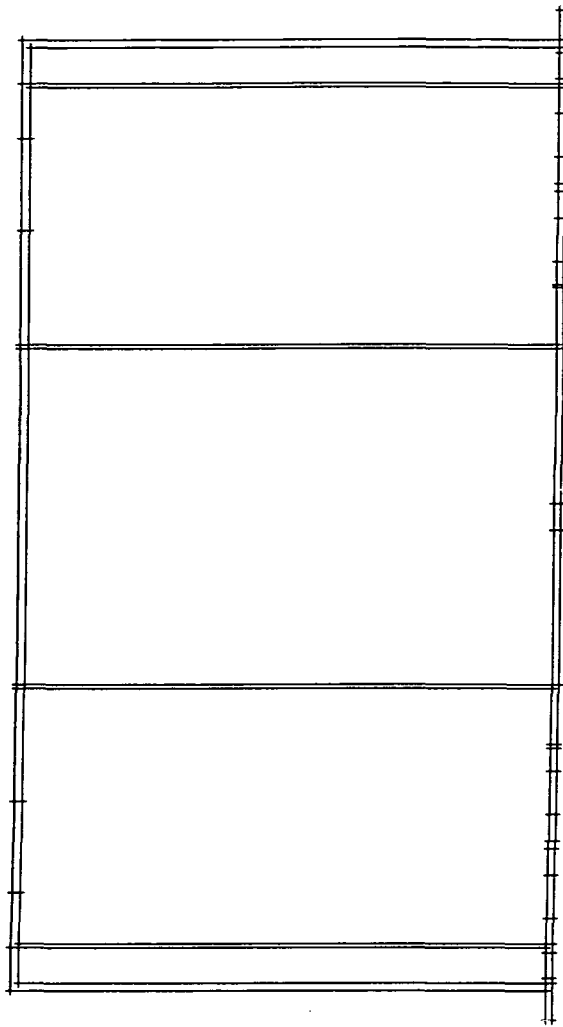
0.063 in

5.000 in

5.062 in

X-Cell Battery Box

3.356 in

2.812 in

1.381 in

0.381 in

2.875 in

4.500 in

4.500 in

4.500 in

Note: All holes are 0.25 in diameter
All angles are 120 deg

0.500 in

1.000 in

0.063 in

2.938 in

3.000 in

Battery Box Enclosure

16.817 in

16.317 in

7.656 in

0.500 in

2.625 in D

120.000 deg

7.973 in

8.262 in

9.718 in

10.000 in

120.000 deg

4.999 in

9.713 in

10.000 in

8.250 in D
X 18

8.157 in

Note: Plate is 0.25 in. thick

7.973 in

8.262 in

5.875 in

5.625 in

18.264 in

14.133 in

4.131 in
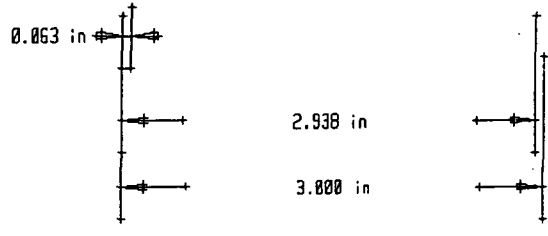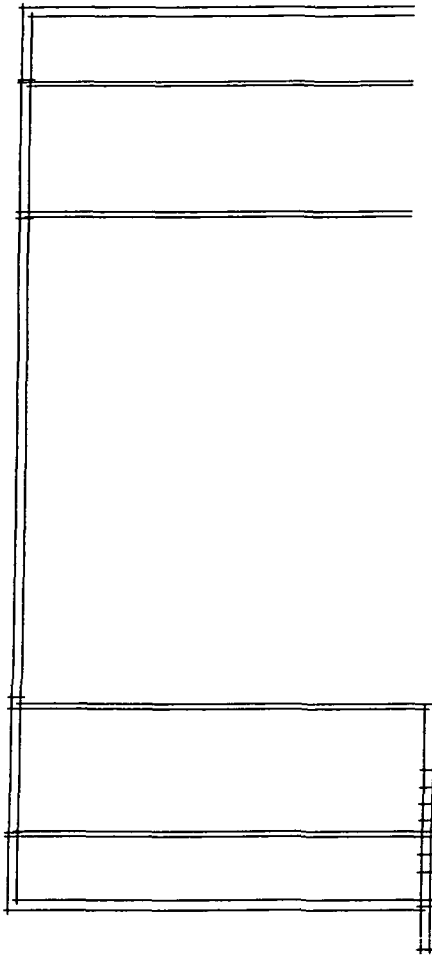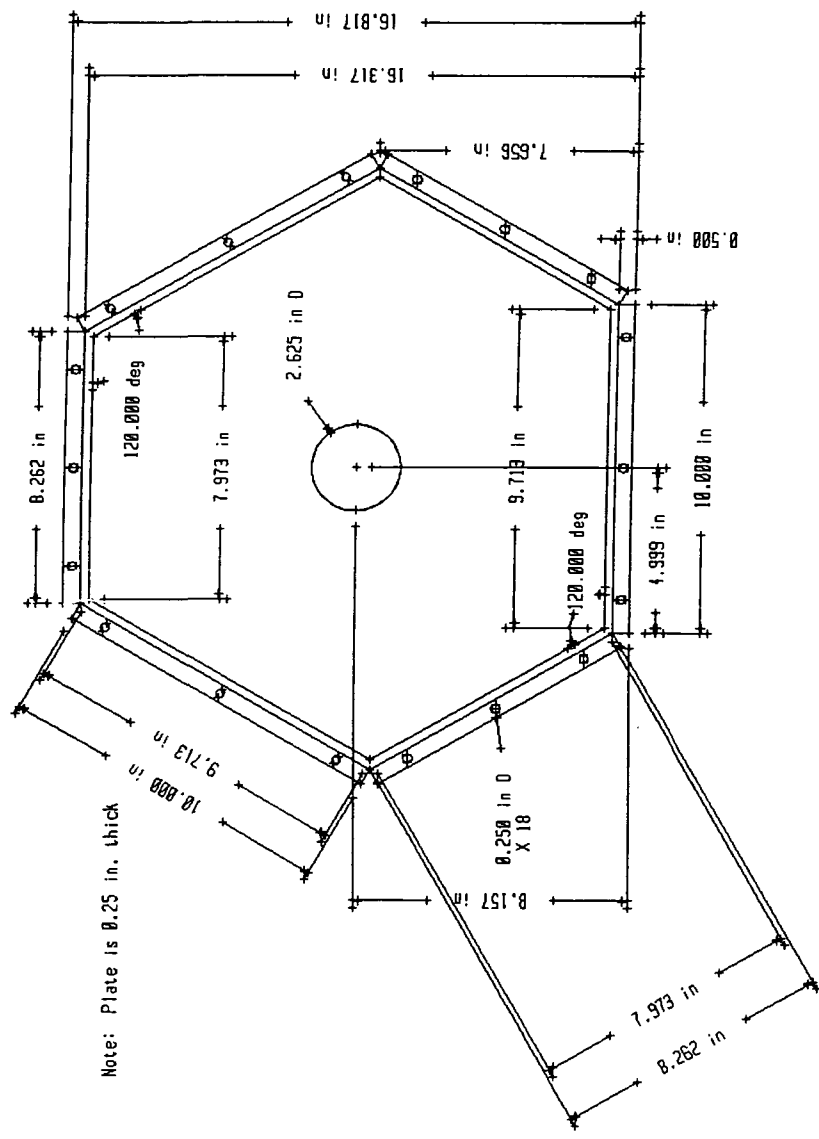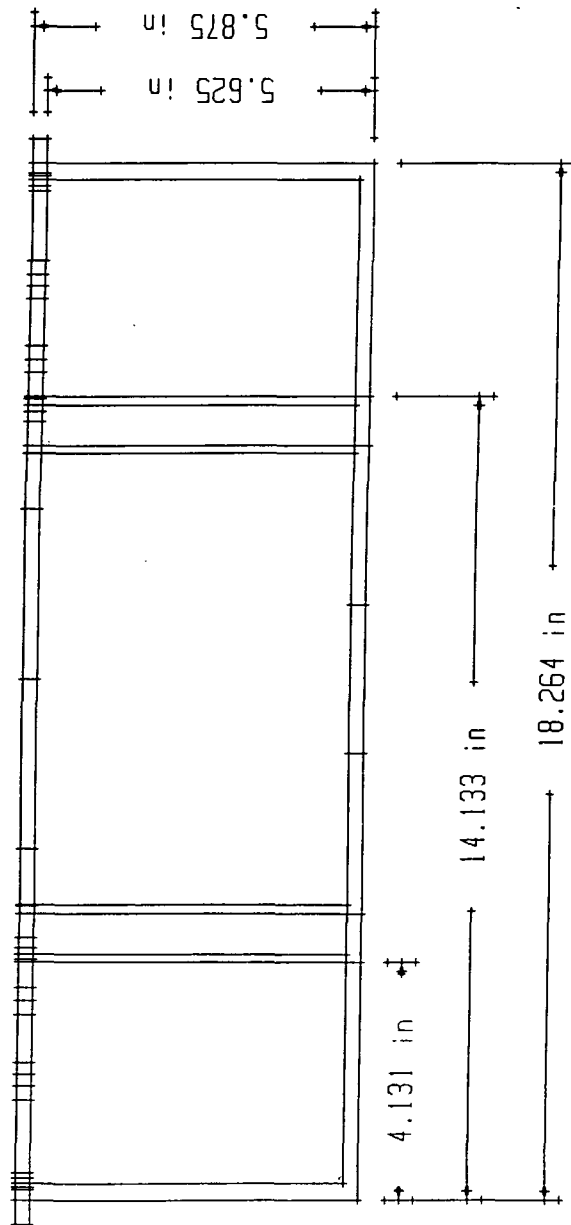
Lateral Support Bumper - Internal Wedge
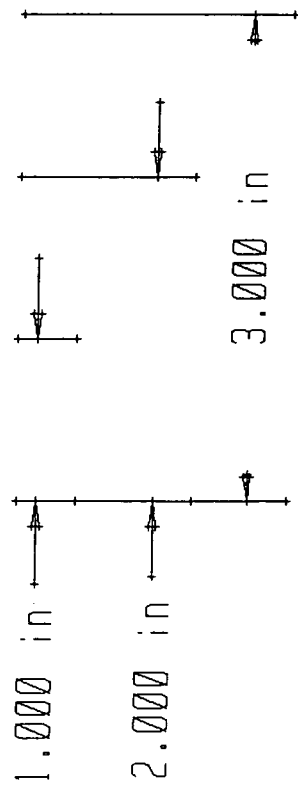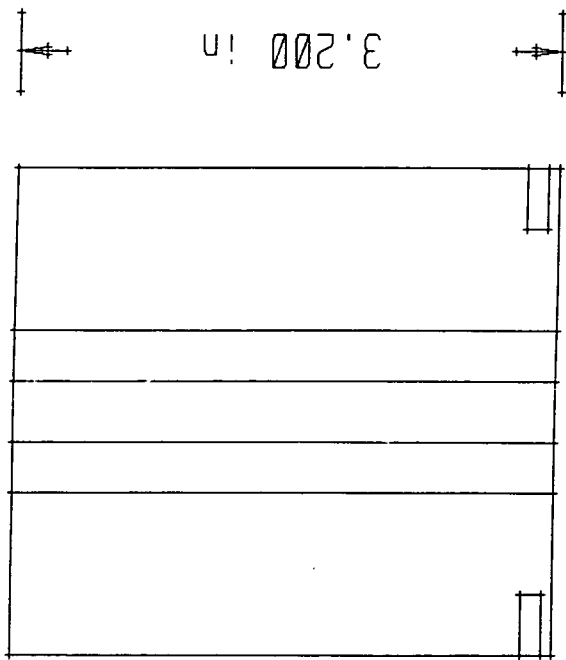
3.200 in

3.000 in

1.000 in

2.000 in

1.125 in

1.000 in

0.375 in D

3.000 in

1.000 in

2.000 in

3.200 in

1.000 in

Ø.500 in

Ø.875 in
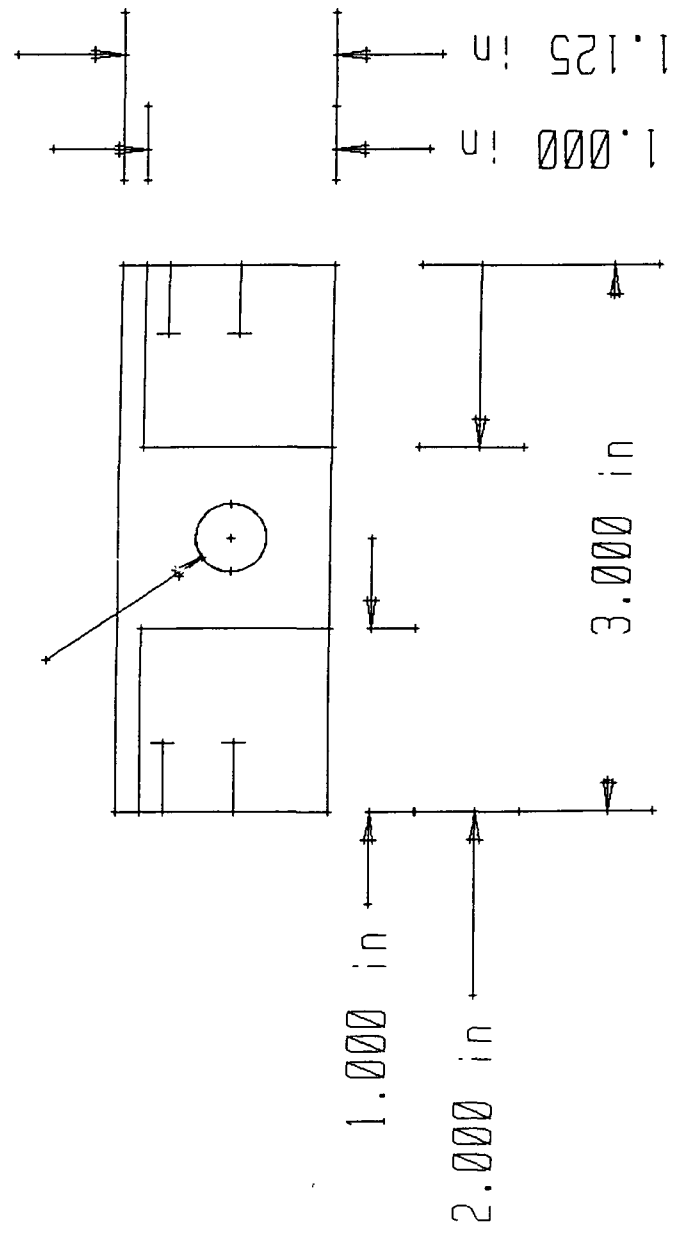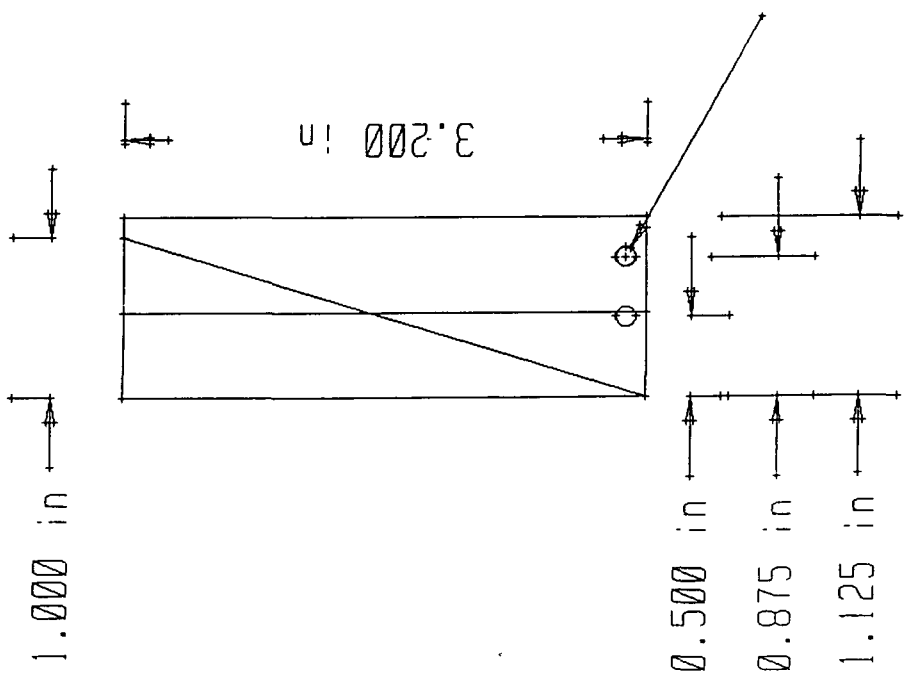
1.125 in

Ø.125 in D
X 4, Ø.375 in. depth

Lateral Support Bumper - Bumper Pad

4.000 in
3.750 in
3.500 in

2.500 in

1.500 in
0.500 in

0.250 in

0.203 in
0.500 in
0.657 in
0.777 in
1.254 in
1.373 in
1.500 in

20.000 in D

2.622 in

0.676 in

3.200 in

4.200 in
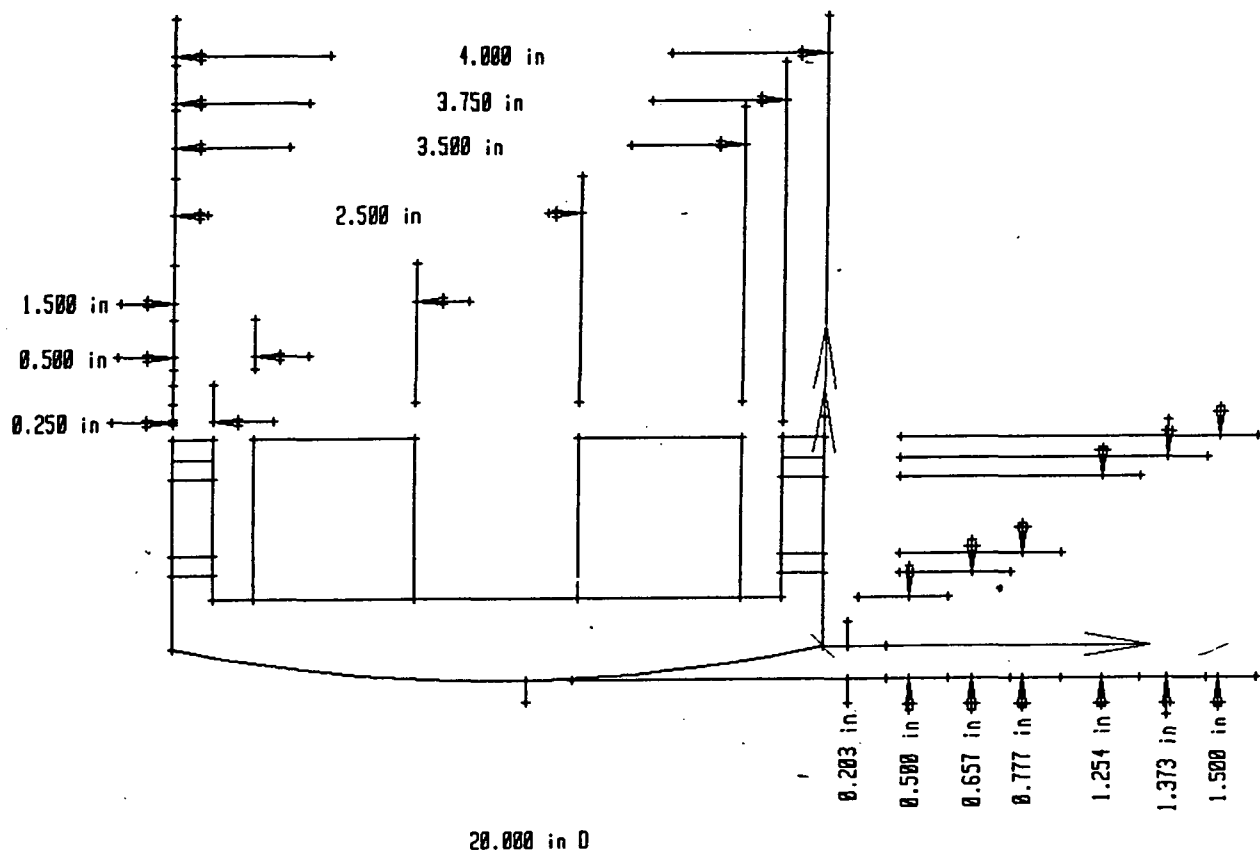
72.646 deg
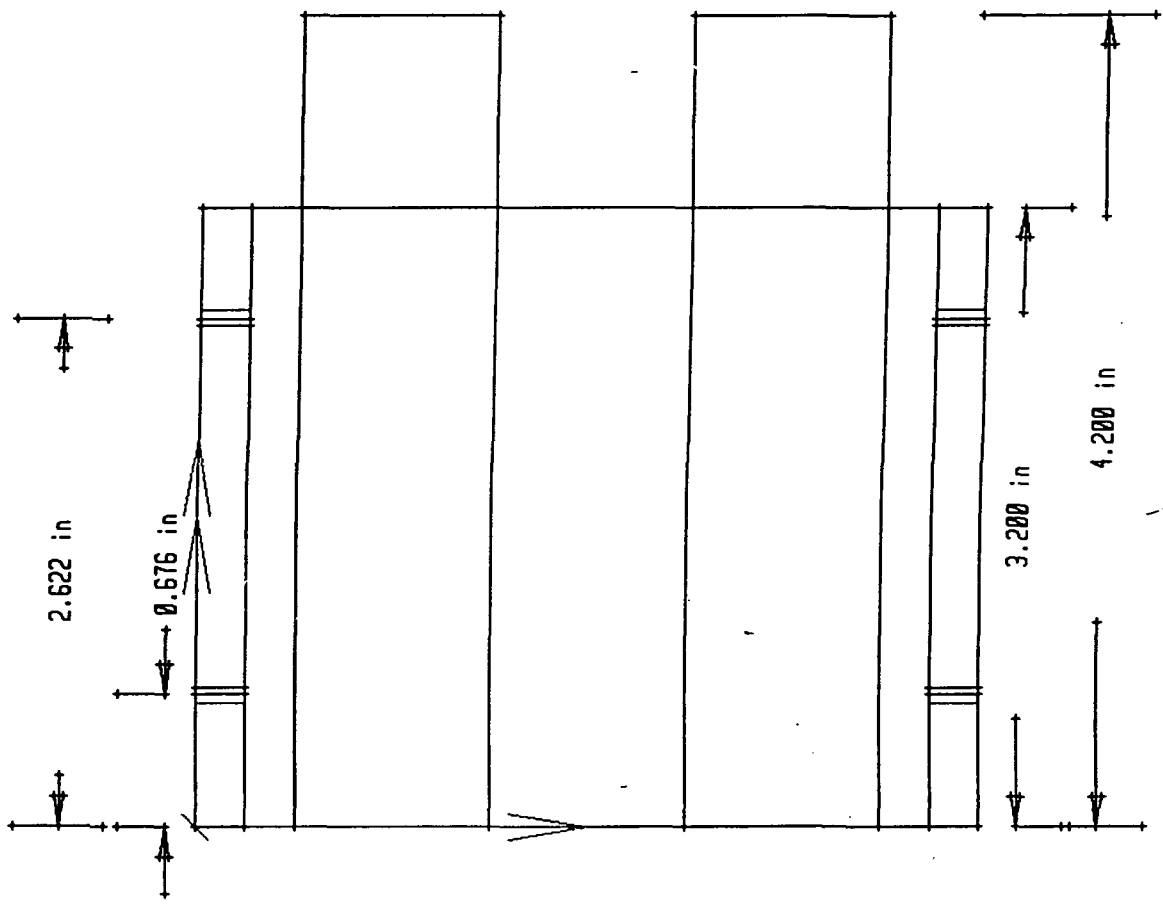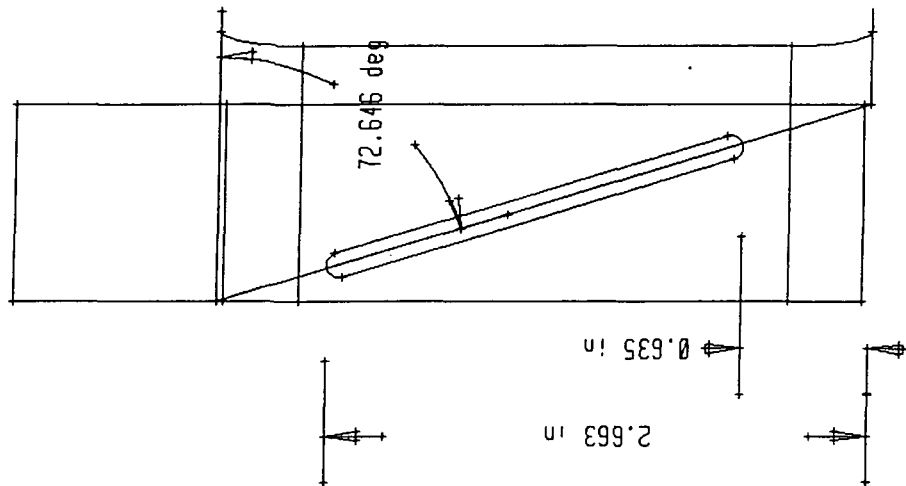
0.635 in.

2.663 in.

Slot is 2.125 in. long
0.125 in. width

Lateral Support Bumper - Mounting Bracket

3.262 in

2.512 in

0.750 in

0.062 in

3.438 in

3.500 in

4.250 in

0.375 in

0.438 in

0.250 in D

X 4

3.262 in

0.757 in

0.187 in
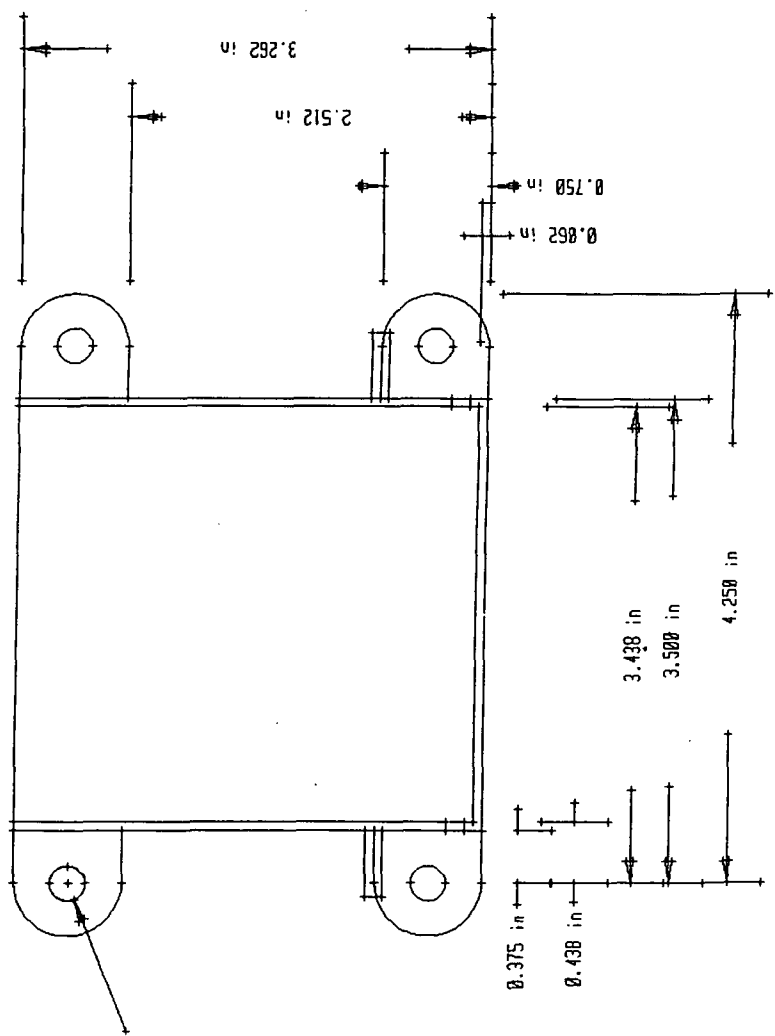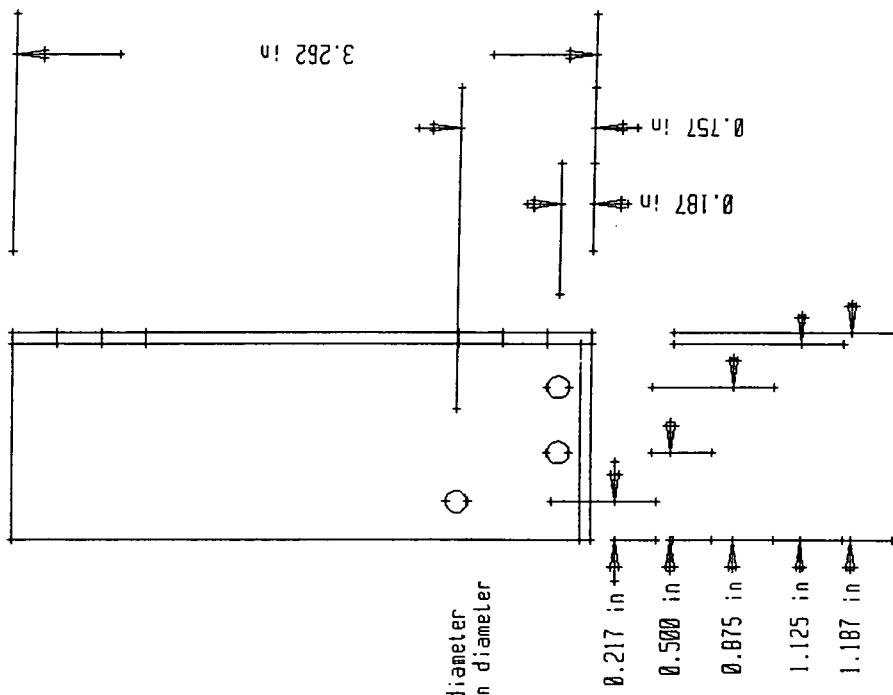
Peg is 0.125 in diameter
holes (X 2) 0.125 in diameter

0.217 in

0.500 in

0.875 in

1.125 in

1.187 in

Ø.813 in

Ø.75Ø in

Ø.277 in
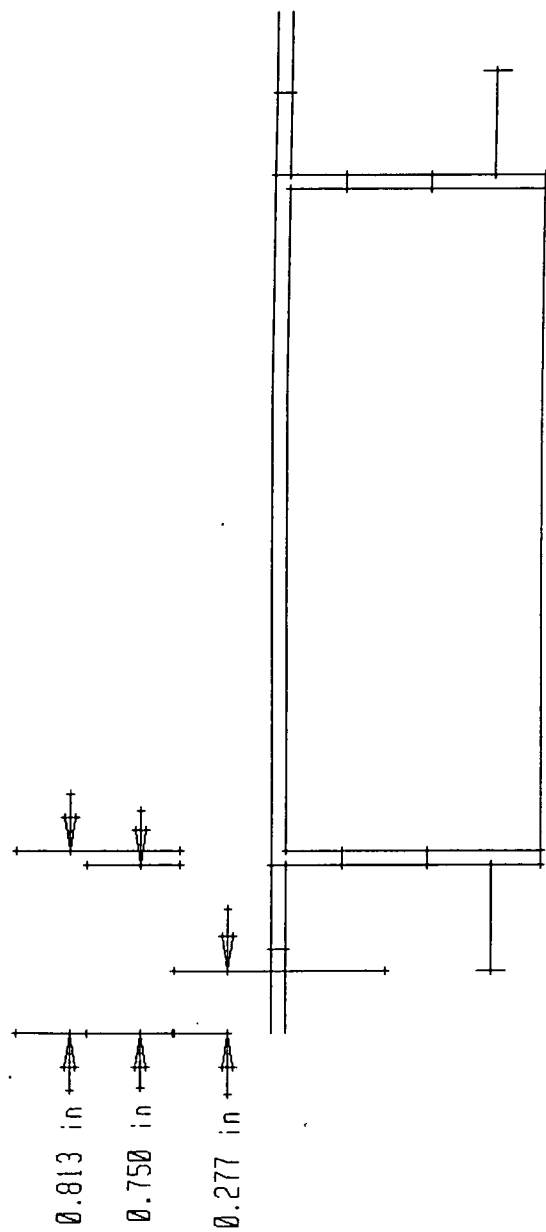
APPENDIX G

Materials List and Purchase Information

Distributor	Materials	Price List
AAA Metals Co., Inc.	MIL-S-25043 17-7ph sheet 5" X 5"	70.00
Hanson Commerce Ctr 68 Industrial Blvd. Hanson, MA 02341 (800)531-9500	AMS 5644 rod O.D. 0.625" X 15"	87.00
American Steel and Aluminum Co. Norwood, MA (800)232-8140	AISI 1010 sheet 0.0625" X 48" X 36"	85.00
City Welding & Fabrication 16 Southbridge St. Worcester, MA 01609 (508) 791-1100	Welding of 4 MGI canisters and antenna plate Welding of Tri-Wall Welding of x- and j- cell battery boxes	160.00 100.00 80.00
Dillsburg Aeroplane Works 114 Sawmill Rd. Dillsburg, PA 17019 (717)432-4589	Al 2024-T6 bar 1.5" X 4" X 30" Al 6061-T6 plate 0.25" X 48" X 50" Al 6061-T6 plate 0.25" X 6.0" X 25" Al 6061-T6 plate 0.75" X 6.0" X 72" Al 6061-T6 pipe O.D. 0.50" wall 0.120"	96.50 320.00 26.67 90.00 1.60
Industrial Suppliers of Worcester 212 Summer St. Worcester, MA 01604 (508) 757-5606	9/16 - 18 Male (VCR) tap 1/4 - 18 Male NPT tap 1/4 - 18 Male NPS tap	17.00 11.00 18.00

(

MSC Industrial Supply Co. 151 Sunnyside Blvd. Plainview, NY 11803-1592 (617) 938-8600	two (2) 3/32", 3/16" shank double end mills, 2 flute two (2) jewelers saws 1" X 0.020"	21.00 38.67
New England Knife and Steel Products Co. Inc. 6 Burton St. Worcester, MA 01607 (508) 753-2895	4140 H.T. 5/8" X 6" X 30"	150.00
Plastics Unlimited, Inc. 80 Winter St. Worcester, MA 01609-2280 (508) 752-7842	Delrin rod O.D. 6" X 12"	150.00

Total Expenditures   **$1,540.00**

C-3.

APPENDIX H

Current Component Weight Breakdown Sheet

Component	Quantity	Weight (lbf)
IPPE	1	4.8
MGI canisters	4	23.6
Fluid cylinder	1	5.9
Camera	1	1.8
RFF Platform and shaft	1	14.0
Pump, mirror and piping	*1*	*8.0*
Fluid, wiring and plumbing	*1*	*15.0*
Battery box sealed enclosure	1	13.3
X-cell battery cage	2	2.2
J-cell battery cage	3	8.2
X- and J-cell batteries	27 J, 12X	59.7
Power Distribution	1	5.0
Tri-wall	3	7.8
Midplate	1	7.4
ISS shaft	1	1.3
RFF shaft	1	3.0
ISS support legs	3	9.0
Bumper assembly	3	6.9
Antenna	1	5.0
TOTAL WEIGHT		201.9
ALLOWABLE WEIGHT		200.0

APPENDIX I

List of Useful Contacts:

Bagley, Jim, Con-Am Inspection, Auburn, MA. Phone: (508) 832-5500. Certified Aluminum Weld Inspector.

Billings, Todd. WPI Washburn Shops. Phone: X5230. Consult for all machining.

Beaupre, Andy. WPI Robotics Lab. Phone: X5122, 5633. Consult for all CNC work.

Curci, Paul. City Welding and Fabrication, Worcester, MA. Phone: (508) 791-1100. Certified Welder.

Derosier, Steve. WPI Higgins Machine Shop. Phone: X5219. Consult for machining.

Gale, John (Joe). WPI Washburn Shops. Phone: X5230, 5236. Consult for machining.

Knapp, Charles, Goddard Space Flight Center, Greenbelt, MD. Phone: (301) 286-0720, Fax: (301) 286-1694. WPI primary contact for the GASCan project.

McKeogh, Ruth. ME Dept. Secretary. Phone: X5872. Consult for student accounts and purchase orders.

Muganda, Donald, Reviewer for GASCan Payloads. Phone: (301) 572-1407. Specifications for welding requirements of parts used on GAS Canisters.

Peden, Mark, Hernandez Engineering, Inc., Goddard Space Flight Center, Greenbelt, MD. Phone: (301) 286-7501. Best person to contact for questions on safety.

APPENDIX J

TK Solver Rule Sheet for Bolt Program for MGI, ISS

;material properties
Fsu=sigma_us*Ab
Ftu=sigma_ut*Ab
Fty=sigma_vt*Ab

;bolt stiffness
Kb=(Eb*Ab)/L
Ab=.25*Pi()*Db^2

;joint stiffness
Kj=(Em*Ac)/T
Ac=(Pi()/4)*((((3*Db+.577*T)^2)/4)-Db^2)

;preload force
Fp_max=.65*Fty

Fp_min=Fse/.3 + (Kj/(Kj+Kb))*Fe

;critical load to avoid separation
Fec=Fp_min*(1+(Kb/Kj))

;torque/preload relation
Torq= Fp_min*K*Db

;margin of safety for tension and shear
MSy=1/((((ft/Fty)^2+(fs/(.55*Fty))^2)^.5)-1
MSu=1/((((ft/Ftu)^2+(fs/(Fsu))^2)^.5)-1

ft=(FSe)*(Fp_min)+(FSe)*(fk)*(Fe)+Ft
fk=1/(1+Kj/Kb)
fs=FSe*Fse
Fse=.3*(Fp_min-(Kj/(Kj+Kb))*Fe)

TK Solver Variable Sheet for MGI, ISS

input	variable	output	units	Description
	Kb	1,963,495	lb./in	bolt stiffness
	Kj	3,253,442	lb./in	joint stiffness
3E7	Eb		psi	Young's Modulus bolt
1E7	Em		psi	Young's Modulus material
.75	L		in	bolt length
.5	T		in	joint thickness
15	Fe		lb.	external force (tension)
.2	K			torque coefficient
.25	Db		in	nominal bolt diameter
0	Ft		lb.	thermal force
85,000	sigma_u		psi	ultimate shear strength
130,000	sigma_u		psi	ultimate tensile strength
85,000	sigma_y		psi	tensile yield strength
	Fsu	4,172.428	lb.	shear ultimate load for bolt
	Ftu	6,381.36	lb.	tensile ultimate load for bolt
	Fty	4,172.428	lb.	tensile yield load for bolt
1.3	FSp			factor of safety on preload - confidence
2	FSey			yield factor of safety on external load
2.6	FSeu			ultimate factor of safety on external
2	FSe			yield or ultimate FOS on external load
	Ac	0.163	in²	effective joint area
	Ab	0.049	in²	cross-sectional bolt area
	Fp_max	2712.078	lb.	preload max
	Fp_min	432.68779	lb.	preload min
	Fec	693.821	lb.	force to joint critical separation
	Torq	21.634	lb.-in	applied torque
	MSy	5.655		margin of safety tension and shear (yield)
	MSu	3.211		margin of safety tension and shear (ultimate)
	ft	876.667	lb.	tensile load in bolt
	fs	254	lb.	shear load in bolt including FSe
	fk	0.376	lb.	fraction of external load carried by bolt
127	Fse		lb.	Shear force external

APPENDIX K

Program to determine the tilt at various critical radii

Variables:

 i,j,k,l - loop counters

 n - counts the number of critical radii that are found by the program

 v1 - Velocity for free vortex

 v2 - Velocity of forced vortex

 V2old - previous value of v2

 circ - circulation

 LOOPB - Critical radius

 LOOPD - Angular velocity of the platform

 GRAV - Artificial gravity level

 DIFF - Pressure difference

angular velocity is varied from 1 to 5000

Circulation is varied from .18 to .38 ft^2/s

Equations:

Critical radius = Percentage * .166667 ft

Platform angular velocity = Sqrt(Gravity/ Radius of the platform)

v1= circulation / (2*Pi*critical radius)

v2=angular velocity*critical radius

Pressure difference = absolute value (platform angular velocity * circulation*

       LOG(container radius/critical radius)/(artificial gravity*Pi)

```
main()
 {
#include <stdio.h>
#include <math.h>
#define PI 3.141592654


int i,j,k,l;
float n,v1,v2, v2old;
float circ, LOOPB, LOOPD, GRAV, DIFF;

        for(i=0;i<=20;i++) /*loop to define circulation*/
                {
                circ=.18+i*.01;
                printf("The circulation is: %f\n", (.18+i*.01));
                for(j=10;j<=400;j++) /*loop to define critical radius*/
                        {
```

```c
                    LOOPB = .001* j  * .166667;
                    v1=((.18+i*.01)/(2*3.14159*j*.001*.166667));
                    /* Loop to define platform angular velocity */
                    for (k=2;k<4; k=k+2)
                                {
                    GRAV = k/10.0*32.17;
                    LOOPD= (sqrt(GRAV/.807813));
                    for(l=0;l<=21200;l=l+100) /*loop to define fluid angular
velocity*/
                                        {
                    v2old=v2*1.0;
                    v2=(j*.001*.166667*l);
                    if(v2>=v1&& v2old<=v1)
                                            {
                                            printf("Critical Radius: %Ff\n",
j*.001*.166667);

                                            DIFF

        =abs((LOOPD*circ*log(.166667/LOOPB))/(GRAV*PI));
                                            printf("%f\n",DIFF*12.0/(GRAV));
                                            n=n+1.0;
                                            }

                                        }
                                    }
                                }


                        }

printf("The number of possible critical radii are: %f\n",n);

}
```

Appendix L

CNC Boss Code and Machining Methodology

Bumper bracket outside bumper

CNC:
Tool 1 = 1 inch bit
Tool 2 = 1/4 inch bit
Tool 3 = 1/8 inch bit

Code:
INSIDE FACE
Cutting depth = .05 inches
# of passes = 20

```
N10G0G90X0.00Y0.00Z0.25T1F20M6
N20X2.0Y0.00
N30G1Z-1.0
N40Y4.3
N50Z0.25
N70G0G90X0.00Y0.00
N80T2M6
N90X0.375Y0.00
N100G1Z-1.0
N110Y4.3
N120Z0.25
N130G0G90X3.625
N140G1Z-1.0
N150Y0.00
N16000.25
N170G0G90X0.00Y0.00
N180M2
```

OUTSID0E FACE
Cutting depth per pass = .05 inches
# of passes = 10

```
N10G0G90X0.00Y0.00Z0.25T1F20M6
N20Y3.7
N30G1Z-0.5
N40X4.0
N50Z0.25
N60G0G90X0.00Y0.00
N70M2
```

LEFT SIDE

```
Cutting depth per pass = .05 inches
# of passes = 10
N10G0G90X0.00Y0.00Z0.25T1M6
N20Y3.7
N30G1Z-0.5
N40X1.5
N50Z0.25
N60G0G90X0.00Y0.00
N70T3M6
# of passes = 5
N80X0.717Y0.676
N90G1Z-.25
N100X1.314Y2.622
N110Z0.25
N120G0G90X0.00Y0.00
N130M2
```

RIGHT SIDE
```
Cutting depth per pass = .05 inches
# of passes = 10
N10G0G90X0.00Y0.00Z0.25T1M6
N20Y3.7
N30G1Z-0.5
N40X1.5
N50Z0.25
N60G0G90X0.00Y0.00
N70T3M6
N80X1.314Y0.676
N90G1Z-.25
N100X0.717Y2.622
N110Z0.25
N120G0G90X0.00Y0.00
N130M2
```

OUTER FACE

To finish the outer face, the outside diameter of 20 inches must be ground down using a belt sander.

Bumper bracket inside wedge

TOOl=1 INCH BIT

Fixture stock in milling machine at 17.3 degrees and mill both faces.

Cutting depth =.05 inches.
# of passes = 19

Drill
3/8th's inch bit
1 hole drilled lengthwise through the piece. 1.5 inches from either side, .625 inches in height from bottom (uncut side).

1/8th inch bit
two holes drilled at the sides at the wide end of the wedges

1 hole drilled 0.25 inches from flat (uncut) side, one at 0.625 inches from flat side. Both cut to a depth of 0.375 inches. Repeat for other side.

TOO1=1 INCH BIT

Fixture stock in milling machine at 17.3 degrees and mill both faces.
Cutting depth =.05 inches.
# of passes = 19

Drill
3/8th's inch bit
1 hole drilled lengthwise through the piece. 1.5 inches from either side, .625 inches in height from bottom (uncut side).

1/8th inch bit
two holes drilled at the sides at the wide end of the wedges

1 hole drilled 0.25 inches from flat (uncut) side, one at 0.625 inches from flat side. Both cut to a depth of 0.375 inches. Repeat for other side.

APPENDIX M

HAND CALCULATIONS

From Smith(1994), the range of Froude numbers which produced vorticies from a mere dimple to a fully formed air core was .2 to .4. By substituting this range into the definition for the Froude Number:

$$Fr_H = \frac{V_{out}}{\sqrt{gH}} = \frac{4Q}{\pi d^2 \sqrt{gH}}$$

where

V_{out} stands for the velocity of the fluid at the outlet

d stands for the drain diameter

Q stands for the flowrate

g stands for the gravity level

H stands for the fluid height

And given
 d = .013 ft
 H = 4.91 ft
 G = 32.17 ft/s^2

the minimum and maximum flowrates at 1 G can be found.

@ Fr = .2

$$Fr = \frac{4Q}{\pi d^2 \sqrt{gH}} = \frac{4Q}{\pi (.013)^2 \sqrt{(32.17)(.4091)}} = .2$$

Q = 9.63x 10^{-5} ft^3/s = 0.043 GPM - This is the minimum flowrate

@ Fr = .4

$$Fr = \frac{4Q}{\pi d^2 \sqrt{gH}} = \frac{4Q}{\pi (.013)^2 \sqrt{(32.17)(.4091)}} = .4$$

Q = 1.93x 10^{-4} ft^3/s = 0.086 GPM - This is the maximum flowrate

Given these flowrates, the Reynolds number can be calculated.

$$Re = \frac{4Q}{\pi d \nu}$$

Where ν is the kinematic viscosity

Given $\nu = 1.1$ Cst $= 1.183 \times 10^{-6}$ ft²/s

At the minimum flowrate

$$Re = \frac{4Q}{\pi d \nu} = \frac{4(9.63 \times 10^{-5})}{\pi(.013)(1.183 \times 10^{-6})}$$

Re = 7992

At the maximum flowrate
Re = 15978

Setting the minimum and maximum flowrates @ 1 G as the minimum and maximum flowrates for the experiment, the Froude numbers at different gravity levels and flowrates can be calculated. For example, using the definition for the Froude number and setting the flowrate to the minimum and the gravity level to .2 G's

$$Fr = \frac{4Q}{\pi d^2 \sqrt{gH}} = \frac{4(9.63 \times 10^{-5})}{\pi(.013)^2 \sqrt{(.2)(32.17)(.4091)}} = .447$$

The angular velocity of the platform can be calculated by using the equation

$$g = \omega^2 R$$

where

g stands for the gravity level
ω stands for the platform angular velocity
R stands for the platform radius

@ .2 Gs the angular velocity is

$$\omega^2 = \frac{g}{R} = \frac{.2(32.17)}{.8203} = 7.84$$

$\omega = 2.822$ rad/s

To determine the fluid angular velocity, the equation for the critical radius is used:

$$r_c = \sqrt{\frac{\Gamma}{2\pi\Omega}}$$

Where:

Γ denotes the circulation

Ω denotes the angular velocity of the fluid.

For

a circulation of .18 ft^2/s

a critical radius of 1% of the container radius = .01 * .166667 = .016667

$$\Omega = \frac{\Gamma}{2\pi r_c^2} = \frac{.18}{2\pi(.016667)^2} = 10312 \ \text{rad/s}$$

APPENDIX N

ULTRASONIC FLOW MEASUREMENT EQUIPMENT INFORMATION

Equipment list

Model 6860 Ultrasonic Flowmeter

2 Model A311S 10 MHz ultrasonic transducers

2 Model A303S 1 MHz ultrasonic transducers.

The 10 MHz ultrasonic transducers which were purchased for the Rotational Fluid Flow experiment are unusable with the 6860 ultrasonic flowmeter, since the 6860 can only handle transducers in the 1 - 5 MHz range. The 1 MHz model A303S transducers may be suitable for use with the 6860 flowmeter, however the programming information that Smith(1994) used in his PT-860 portable ultrasonic flowmeter is required to properly set up the 6860 ultrasonic flowmeter. If this information cannot be obtained then it will be necessary to purchase new transducers.

All of the above equipment was made by:

> Panametrics Corp.
> 221 Crescent St.
> Waltham, Ma.
> Tel: 800-225-8330
>   617-899-2740
> Fax: 617-899-1552

A representative of Panametrics PCI division recommended a pair of CPT transducers, model number C-PT-10-N-P-00-0, as a substitute for the 1 MHz transducers. However, due to their $895 cost, it is recommended that the Model A303s transducers be used.

The Panametrics contact is:

Rory McMahon
Panametrics PCI division
Tel: 800-833-9438, ext. 338.

APPENDIX O

RFF PURCHASE INFORMATION

There are a number of things that still need to be purchased for the Rotational Fluid Flow experiment. They include:

Dow Corning 200 Silicon Oil (1.1 Cst)	$52/quart	WM. F. NYE. INC. P.O. Box G-927 New Bedford, MA. 02742 Tel: 617-555-7212 Fairhaven office Tel: 508-996-6721
Slip Rings and brush blocks	PN WSD-1750-6 220 volts, 15 amps Refurbished: $860 New: $1,515	Wendon Co. 203-348-6271

The slip rings will cost less if the present ones are sent back to be refurbished.

The following need to be purchased, however, no information has been obtained

1/4 in I.D. aluminum tubing

Hermetic seal with 5 connectors.

Wiring

Minor parts for Assembly

Mirror bracket materials